49/2/2017
ISSN 1338-3523
ISSN 0369-2086

Mineralia Slovaca

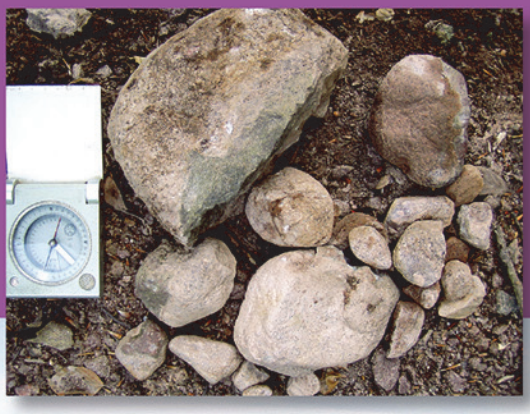

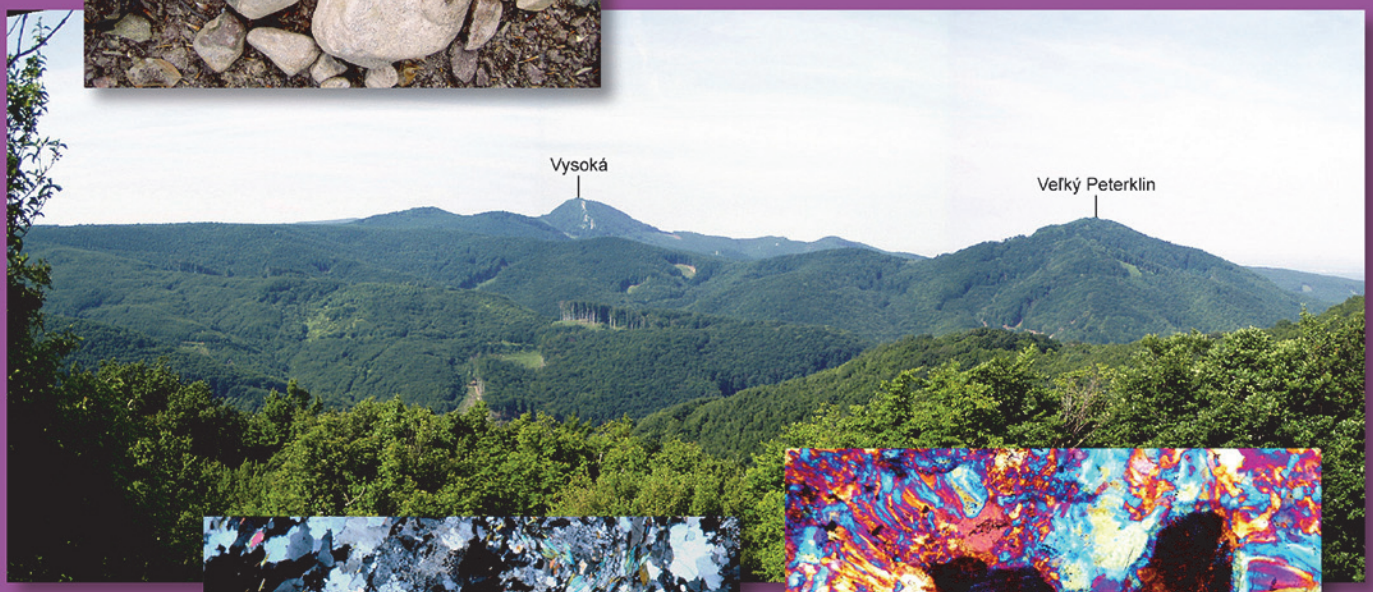

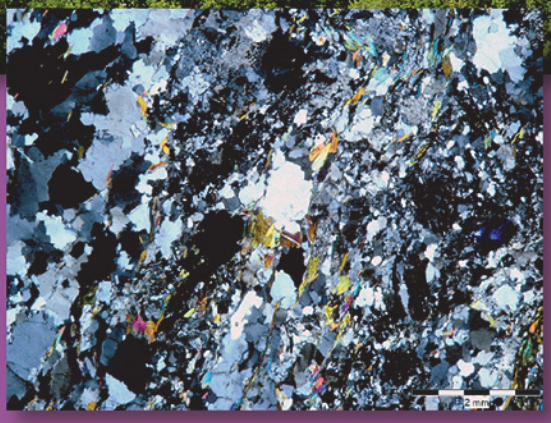

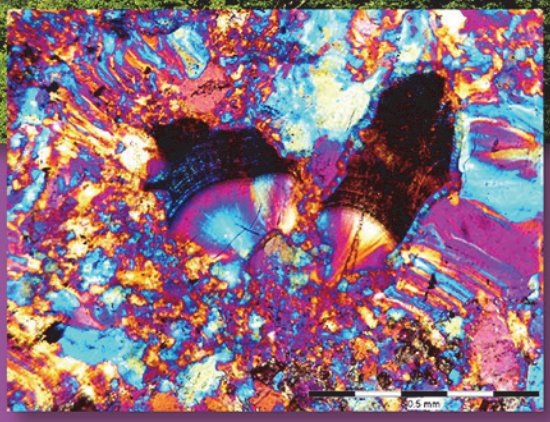

Štátny geologický ústav Dionýza Štúra Bratislava

Mineralia Slovaca

Časopis pre regionálnu a environmentálnu geológiu
a aktivity Slovenskej geologickej spoločnosti a geologických asociácií

PREDSEDA VYDAVATEĽSKEJ RADY – CHAIRMAN OF EDITORIAL BOARD

BRANISLAV ŽEC
Štátny geologický ústav Dionýza Štúra Bratislava

VEDECKÝ REDAKTOR – SCIENTIFIC EDITOR

ZOLTÁN NÉMETH
Štátny geologický ústav Dionýza Štúra
Regionálne centrum Košice
Jesenského 8, 040 01 Košice
zoltan.nemeth@geology.sk

REDAKČNÁ RADA – EDITORIAL BOARD

Igor Broska, Ústav vied o Zemi SAV Bratislava
Klement Fordinál, Štátny geologický ústav D. Štúra Bratislava
Vlasta Jánová, Ministerstvo životného prostredia SR Bratislava
Martin Kováčik, Štátny geologický ústav D. Štúra Bratislava
Peter Malík, Štátny geologický ústav D. Štúra Bratislava
Jozef Michalík, Ústav vied o Zemi SAV Bratislava
Ľubomír Petro, Štátny geologický ústav D. Štúra Košice
Dušan Plašienka, Prírodovedecká fakulta UK Bratislava
Marián Putiš, Prírodovedecká fakulta UK Bratislava
Igor Slaninka, Štátny geologický ústav D. Štúra Bratislava
Ján Soták, Ústav vied o Zemi Banská Bystrica
Ladislav Šimon, Štátny geologický ústav D. Štúra Bratislava
Pavel Uher, Prírodovedecká fakulta UK Bratislava

REDAKCIA – EDITORIAL STAFF

Vedúci oddelenia vydavateľstva ŠGÚDŠ a propagácie – Head of the Department of ŠGÚDŠ Publishers and Promotion

LADISLAV MARTINSKÝ
ladislav.martinsky@geology.sk

Jazykoví redaktori – Lingual editors

Janka Hrtusová – Zoltán Németh
janka.hrtusova@geology.sk

Grafická úprava a technické spracovanie – DTP processing

Slávka Žideková
slavka.zidekova@geology.sk

Mineralia Slovaca (Web ISSN 1338-3523, ISSN 0369-2086), EV 3534/09, vychádza dvakrát ročne. Vydavateľ a tlač: Štátny geologický ústav Dionýza Štúra, Mlynská dolina 1, 817 04 Bratislava, IČO 31 753 604. Dátum vydania čísla 49/2/2017: december 2017.
Predplatné v roku 2018 vrátane DPH, poštovného a balného pre jednotlivcov 16,50 €, pre členov SGS a geologických asociácií 15,40 €, pre organizácie v SR 22,00 €. Cena jednotlivého čísla pri osobnom nákupe v predajniach ŠGÚDŠ v Bratislave a v Košiciach je 5,50 € vrátane DPH. Časopis možno objednať v redakcii a v knižnici regionálneho centra v Košiciach.
Adresa redakcie: Štátny geologický ústav D. Štúra – RC Košice (Mineralia Slovaca), Jesenského 8, 040 01 Košice. Telefón: 055/625 00 43; fax: 055/625 00 44, e-mail: mineralia.slovaca@geology.sk, e-mail knižnica: secretary.ke@geology.sk

Mineralia Slovaca (Web ISSN 1338-3523, ISSN 0369-2086) is published twice a year by the State Geological Institute of Dionýz Štúr Bratislava, Slovak Republic. The date of issuing of the number 49/2/2017: December 2017.
Subscription for the whole 2018 calendar year (two numbers of the journal): 33.00 € (Europe), 45.00 € (besides Europe), including VAT, postage and packing cost. Claims for nonreceipt of any issue will be filled gratis.
Order send to address of the Editorial office: Štátny geologický ústav D. Štúra – RC Košice (Library), Jesenského 8, SK-040 01 Košice, Slovak Republic. Phone: +421/55/625 00 43; fax: +421/55/625 00 44, e-mail: mineralia.slovaca@geology.sk, library: secretary.ke@geology.sk

© Štátny geologický ústav Dionýza Štúra Bratislava

www.geology.sk/mineralia

Mineralia Slovaca 49 (2017) • 2

Obsah – Content

PÔVODNÉ ČLÁNKY – ORIGINAL PAPERS

Dyda, M., Ružička, P. & Hain, M.
Crystal size distribution (CSD) of titanite inclusions in grossular from a calc-silicate rock in the Malé Karpaty Mts., Slovakia
Distribúcia kryštálových veľkostí (CSD) titanitových inklúzií v grosulári z vápenato-silikátovej horniny Malých Karpát, Slovensko 113

Kováčik, M. & Olšavský, M.
Obliakový materiál vrchnopaleozoických sedimentov hronika v Malých Karpatoch: petrogenetické a proveniencné otázky
Pebble-material of Hronic Upper Paleozoic sediments in the Malé Karpaty Mts. (Western Carpathians): petrogenetic and provenance aspects 125

Žecová, K.
Paleoecology of calcareous nannofossils from Paleogene formations of the Magura Unit in the Western Carpathians
Paleoekológia vápnitých nanofosílií z paleogénnych súvrství magurskej jednotky Západných Karpát 141

Gaál, Ľ., Németh, Z., Bella, P. & Koděra, P.
Caves in magnesite – a rare phenomenon of karstification: The case study from Slovakia
Jaskyne v magnezitoch – vzácny fenomén krasovatenia: príkladová štúdia zo Slovenska 157

Polák, Ľ., Vlasáč, J., Vrtiška, L. & Mikuš, T.
Cryptomelane, $K(Mn^{4+}_7Mn^{3+})O_{16}$, from the Dúbravica-Zolnica Fe deposit (North Veporic Unit, Slovak Republic)
Kryptomelán $K(Mn^{4+}_7Mn^{3+})O_{16}$ z Fe ložiska Dúbravica-Zolnica (severné veporikum) 169

Štyriaková, I., Bekéniová, A. & Štyriaková, D.
The quality improvement of non-metallic raw materials by bioleaching
Zlepšovanie kvality nerudných surovín biolúhovaním 177

OBÁLKA: 1 – Pohľad z hrebeňa Vápennej na horizont s vyčnievajúcim masívom Vysoká (k. 754) a Veľký Peterklin (k. 587, vpravo), podľa ktorého sú pomenované peterklinské vrstvy malužinského súvrstvia (malokarpatský perm hronika). Foto: M. Olšavský. 2 – Obliakový materiál tvorený najmä mylonitizovanými granitoidmi pochádzajúci z polymiktného zlepenca peterklinských vrstiev (lokalita jjz. od k. Klokoč). Foto: M. Olšavský. 3 – Mikroskopická snímka obliaka diaftoretického leukokratného granitu (skrížené nikoly). Foto: M. Kováčik. 4 – Mikrofotografia chalcedónových radiálnych útvarov s (+) charakterom minerálu (v strede) na styku s tmavohnedým ankeritom poukazuje na zrudnenie viazané na vrchnokarbónsku epochu (skrížené nikoly, sadrovcová doštička). Foto: M. Kováčik. Ďalšie podrobnosti o danej problematike poskytuje článok autorov Kováčik a Olšavský v tomto čísle časopisu.

COVER: 1 – View from the Vápenná mountain ridge towards horizon with dominating massifs of Vysoká (e. p. 754 m) and Veľký Peterklin (e. p. 587 m, on the right), the latter giving the name to the Peterklin Beds conglomerates of Permian Malužiná Fm. (Hronic Unit of the Malé Karpaty Mts.). Photo: M. Olšavský. 2 – The pebble-material consisting predominantly of mylonitized granitoids derived from the polymict conglomerate of the Peterklin Beds (localized to SSW from e. p. Klokoč). Photo: M. Olšavský. 3 – Microphoto of diapthorized leucocrate granite pebble (crossed nicols). Photo: M. Kováčik. 4 – The microphoto of the chalcedony radial forms (in the middle) with (+) optic sign, coexisting with ankerite, points to Late Carboniferous minerallization period (crossed nicols with inserted gypsum plate). Photo: M. Kováčik. Further details about this topic are presented in the paper by Kováčik and Olšavský in this issue of the journal.

Mineralia Slovaca, 49 (2017), 113 – 123
Web ISSN 1338-3523, ISSN 0369-2086

Crystal size distribution (CSD) of titanite inclusions in grossular from a calc-silicate rock in the Malé Karpaty Mts., Slovakia

MARIAN DYDA[1], PETER RUŽIČKA[1] and MIROSLAV HAIN[2]

[1]Department of mineralogy and petrology, Faculty of Natural Science, Comenius University, Mlynská dolina, 842 15 Bratislava, Slovakia, dyda.marian@gmail.com
[2]Institute of Measurement Science, Slovak Academy of Sciences, Dúbravská cesta 9, 841 04 Bratislava, Slovakia, umerhain@savba.sk

Abstract: Titanite inclusions ($L \approx$ 10-60 μm) regularly dispersed in a grossular porphyroblast (V = 0.068 cm^3) from calc-silicate rock have been studied using the X-ray high resolution micro-tomography (*Nanotom 180*). This advanced methodical approach allowed the direct acquiring of the titanite crystal size distribution CSD and its numerical assessment that formed 3D visualization and a stereological basis for detailed analysis. The data for titanite nucleation rate ($J' \approx 5.6 \times 10^{-6}$ cm^{3}s^{-1}), average growth rate ($G' \approx$ 1.4 x 10-12 cm s^{-1}) and residence time ($\tau \approx$ 4-84 yr) have been acquired. Crystallization of titanite inclusions was relative swift and in a short time span. The calculation of isobaric mineral equilibria indicates that garnets grew in an equilibrium calc-silicate assemblage of grossular + calcite + phlogopite + tremolite + quartz at pressure P ~ 300 MPa, temperature of T ~ 500-550 °C and fluid composition of $X_{CO2} < 0.25$. These conditions are related neither to a long-term regional, neither to short-lived contact-metamorphic conditions, but to regional-periplutonic metamorphism along granitic plutons.

Key words: crystal size distribution, titanite, 3D X-ray CT, grossular, residence time, growth rate

Graphical abstract

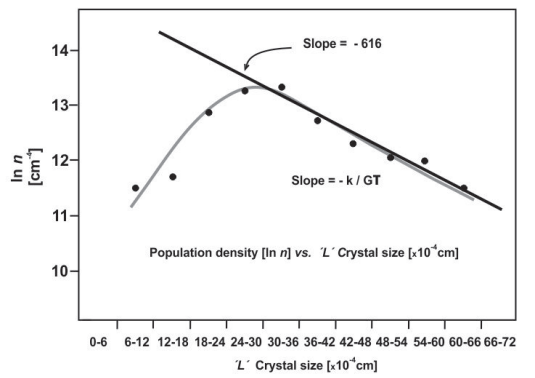

Highlights

- The calculated slope and intercept of the crystal size distribution (CSD) plot suggest the higher nucleation rates for the studied titanite inclusions in grossular from calc-silicate rocks and shorter growth, but not such as for typical contact metamorhism.
- The different forms of CSD in contact and regional metamorphic rocks are consequences of different thermal histories of two metamorphic environments.

Introduction

Magmatic and metamorphic rock textures can indicate the mode and rate of crystallization as the crystal arrangement and crystal size is a direct documentation of the crystallization path at which a particular rock developed. Numerical crystal size data yield thus a more complex insight into a rock thermal evolution through quantitative textural data. And though many rock texture forming processes have been successfully duplicated in laboratories, detailed kinetic inconsistencies still persist.

A fundamental observation is that grain size variations throughout a particular rock are small. This indicates that crystallization process did not vary significantly. However, the combination of heating and cooling history of a metamorphic rock during progressive and regressive stages remains a pertaining problem. The relation between temperature, recrystallization including mixed fluid transportation in an open system is however considerably complex.

Crystal size is the product of some mean growth rate and growth residence time. If the number of crystals per unit size in rock sample is plotted versus their representative sizes in a semilogaritmic fasion, many rock samples show a remarkable smooth, often linear trends with negative slopes (see e.g. Marsh, 1988).

The theory of crystal size distribution (CSD) developed by Randolph and Larson (1971) in chemical engineering enables these data to be interpreted to yield quantitative information on crystal growth rate, nucleation rate and nucleation density. Consequently, the CSD theory was applied to igneous and metamorphic rocks (Kretz, 1966; Cashman & Marsh, 1984; Cashman & Ferry, 1988) and

developed to a very effective petrographic method (see e.g. Peterson, 1996; Higgins, 2000; Zeh & Millar, 2001; Higgins, 2002; Eberl et al., 2002; Petrík et al., 2003; Zeh, 2004; Higgins, 2006). CSD studies thus became a tool through which crystallization can be studied in a complex system with minimum assumptions.

X-ray computed micro-tomography (CT) is a powerful, non-destructive method to investigate small objects, minerals and rocks' textures in three dimensions. Particular phases are distinguished in X-ray tomography on the basis of their linear attenuation coefficient. This depends directly on the electron density of the mineral, the effective atomic structure of the mineral, and the energy of the incoming X-ray beam. The data collected is a serie of closely spaced 2D slices through the object can be constructed to produce a 3D image. The modern range of X-ray micro-tomography instruments have resolutions in the range of 7–30 μm with sample sizes of ~ 7 cm by ~ 3 cm diameter (see e.g.: Zeh, 2004; Jerram et al., 2009; Putiš et al., 2011; Vojtko et al., 2011; Ružička et al., 2013; Dyda et al., 2014).

The acquired 3D data provides a valuable information on titanite shape, number and volume which has been used to characterize the titanite inclusion population in the grossular garnet. Both, 2D and 3D textural studies using CSD textural analysis techniques are successfully tested on complex rock textures, and prove to be a useful technique in specific quantification of mineral phases in rock analysis.

Geology of the studied area

The pre-Alpine basement of the Western Carpathians is represented mainly by medium to high-graded paragneisses, orthogneisses, amphibolites and other metamorphic rock complexes which were later intruded by granitoidic rocks of Variscan age. These high-grade polymetamorphic rocks are found in the „core mountains" which exhibit the crystalline core, specific tectonic features and tectonical overprinting by Mesozoic events.

The Malé Karpaty Mts. are the westernmost and outermost core mountains (Fig. 1.) and they possess some distinctive features in comparison with other Western Carpathians core mountains. Malé Karpaty Mts. play a specific and important role in the Eastern Alpine and Western Carpathian relationship as they bear some typical geological features of both mountain systems but they have a prevailing Carpathian influence (Maheľ, 1983).

The sedimentary overburden was metamorphosed to greenschists facies before the granitoidic rocks intrusion and the periplutonic processes became dominant in some areas. The Variscan postkinematic granitoidic rocks are the predominant constituent of the Malé Karpaty Mts. crystalline complex. They form two separate granitoid massifs, the Bratislava (S-type) and Modra (I-type affinity) massif (Cambel & Vilinovič, 1987) separated by a 4-8 km wide zone of schists.

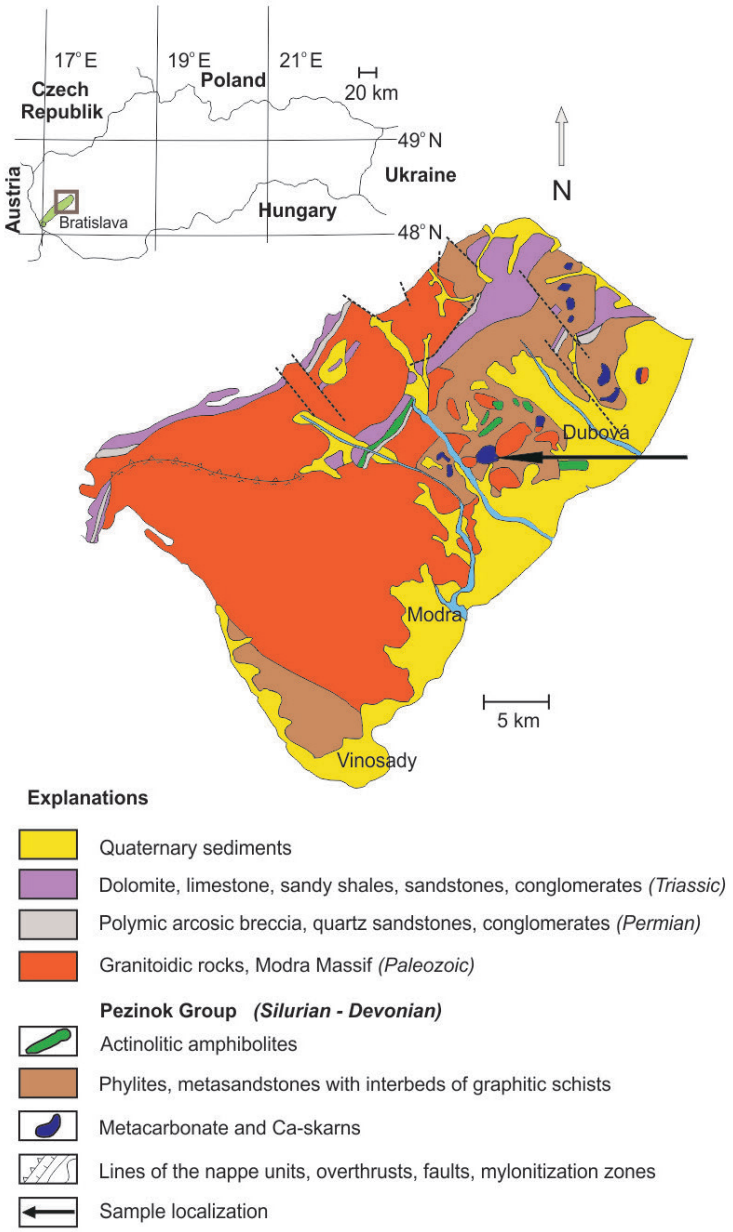

Fig. 1. The occurrence of the studied calc-silicate rock, Dolinkovský vrch, in the crystalline complex of the Malé Karpaty Mts. Scatch is based on the geological map of Maheľ and Cambel (1972).

The age data based on the Rb-Sr isochrone gives for granodiorite of Modra massive 327 ± 18 m.y. (Cambel et al., 1990) and age acquired by U-Pb method 320 m.y. (Shcherbak et al., 1988). These age determinations are considered to be the age of Modra granodiorite massif intrusion and have been later confirmed by Kohút et al. (2009).

Metamorphic zonation is connected with granitoidic intrusion (Cambel, 1954; Šímová & Šamajová, 1979; Cambel et al., 1989). The spatial relationship and metamorphic zonality exists in some areas only as rudimentary remnants. At other places the complete metamorphic zonality has been preserved (Dyda & Miklóš, 1993; Dyda, 1997). Metamorphic zones documenting the intrusive character of Modra granodiorite are lithologically complex and have been described by Cambel (1958) as the Harmonia serie. Its periplutonic zones are relatively narrow ~50-100 m, (Kováčik in Maglay et al., 2011).

Complex tectonic structures of the mountains reflect their complicated development which started hundreds of kilometers southwards and rests of Variscan mountains were overridden by Paleo-Alpine nappe piles. Their structures were modified by back-thrusts and transpressional tectonics (Putiš, 1987, 1991; Plašienka, 1989; Plašienka et al., 1991). Due to the tectonic disturbances of the Variscan orogen it is still unclear whether the crystalline complexes in some „core mountains“are in autochthonous position (see Maglay et al., 2011; Polák et al., 2012).

Grossular garnet, enriched in Cr and V, with diopside, albite, K-feldspar, titanite and clinozoisite in Ca-skarn near Dubová, Malé Karpaty Mts., was studied by Uher et al. (2015).

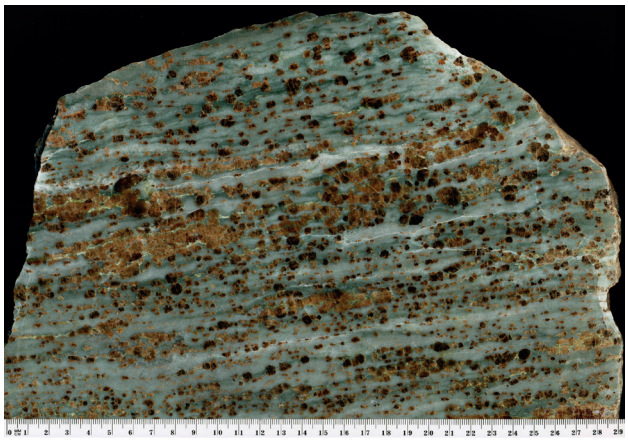

Fig. 2. Hand specimen of the studied layered calc-silicate rock. Grossular garnets are accumulated probably according to the preffered chemical composition of the sedimentary protolith.

Mineral assemblage of the grossular bearing calc-silicate rock

The mineral assemblage of the studied calc-silicate rock (Fig. 2.): grossular (Grs), tremolite (Tr), phlogopite (Phl), calcite (Cal) and quartz (Qtz) is given in the terms of the following mass - balance reactions of mixed fluid phase equilibria:

$6Cal + 5Phl + 24Qtz = 3Tr + 5Kfs + 2H_2O + 6CO_2$ I.

$5Dol + 8Qtz + H_2O = Tr + 3Cal + 7CO_2$ II.

$Tr + 3Cal + 2Qtz = 5Di + H_2O + 3CO_2$ III.

$2Czo + 3Qtz + 5Cal = 3Grs + H_2O + 5CO_2$ IV.

$Qtz + Cal = Wo + CO_2$ V.

$2Czo + CO_2 = Cal + 3An + H_2O$ VI.

with the following metamorphic reaction thermo-data taken from Holland and Powell (2011):

ΔH [kJ]	ΔS [J K^{-1}]	ΔV [kJbar^{-1}]	
617.14	1288.6	-15.14	[I'.]
476.43	1024.2	-11.98	[II'.]
324.32	207.9	-10.79	[III'.]
448.97	860.3	-14.93	[IV'.]
91.90	162.2	-1.96	[V'.]
38.07	74.7	6.81	[VI'.]

Choosing the isobaric approach to the mineral-fluid equilibria calculation, the monovariant equilibrium temperature for a particular reaction has been assessed according to the formulation given by Kretz (1994):

$$T = \frac{\Delta H + (P-1).\Delta V_S}{\Delta S - R\left(n \ln\left(x_i P - 1\right)\right).\varphi_i + \left(m \ln\left(x_j P - 1\right)\right).\varphi_j} \quad [1.]$$

where x_i, x_j is the mole fraction of fluid component in fluid mixture and φ_i, φ_j is the fugacity coefficient of component i, j at chosen temperature and pressure, *n* and *m* stand for number of moles of fluid species in the reaction.

The iterative calculation of the isobaric monovariant curves determines thus the limited divariant field of the studied mineral assemblage.

Presence of zoizite in a calc-silicate rock is an X_{CO2} limit indicator that represents the maximum mole fraction of CO_2 (X_{CO2}) in equilibrium metamorphic fluid (Fig.3). Calculated monovariant curve [VI.] is valid for equilibrium coexistence of calcite and zoizite. Maximum X_{CO2} at which zoizite is stable is at ~ 520 °C and ~ 0.4 X_{CO2}. From this simplified restriction steams that studied mineral assemblage was formed at $X_{CO2} < 0.4$ at maximum pressure

of 300 MPa. Tremolite divariant stability field is restricted by monovariant curves [I.] and [III.]. It has a wider temperature extent and the maximum temperature of coexistence of tremolite with zoizite in the divariant zoizite stability field is ~ 550 °C. Intersection of monovariant lines [III.] and [IV.] at temperature ~ 550 °C determines the maximum temperature of Gros + Tr + Czo equilibrium coexistence. This assemblage remains stable at lower temperatures and at lower CO_2 content $X_{CO2} \approx 0.25$ in metamorphic fluid. In the studied assemblage Gros + Cal + Tr + Phl + Qtz (striped area) the higher temperature phases as diopside and wolastonite were absent and the temperature in the this periplutonic zone not exceeded ~ 550 °C and 300 MPa at fluid composition $X_{CO2} < 0.25$.

Monovariant curves are calculated for pure solid phases. Thus in the first approximation the equilibrium temperature for the reaction (I.) is calculated using the chosen fluid composition: $X_{H2O} = 0.25$, $X_{CO2} = 0.75$ and with fugacity coefficints for water $\varphi H_2O = 1$ and carbon dioxide $\varphi CO_2 = 1$. The obtained temperature is 440 °C. For this temperature 440 °C and pressure are tabulated values for $\varphi H_2O = 0.293$ and for $\varphi CO_2 = 7.307$. Substituting these values in the above formula we repeat the calculation getting 520 °C. And, iteratively, for this temperature and pressure the tabulated values for φH_2O and φCO_2 are used for next calculation obtaining finally 524 °C. As the repeated calculation yields practically the same number, we consider the resulting value to be the equilibrium temperature. Calculated isobaric mineral equilibrium indicates that univariant mineral assemblage Phl + Qtz + Cal + Kfs + Tr occuring at temperature ~ 524 °C may coexists with metamorphic fluid of composition $X_{H2O} = 0.25$, $X_{CO2} = 0.75$;

For many metamorphic equilibria calculations involving H_2O and CO_2, the fugacity coefficints for water and carbon dioxide may be acquired from tables e.g. of Burnham et al.,1969; Helgeson & Kirkham, 1974, for H_2O and for CO_2 from Takenouchi & Kennedy, 1964; Mel'nik, 1972, or by using a computer program of Belonoshko et al., (1992).

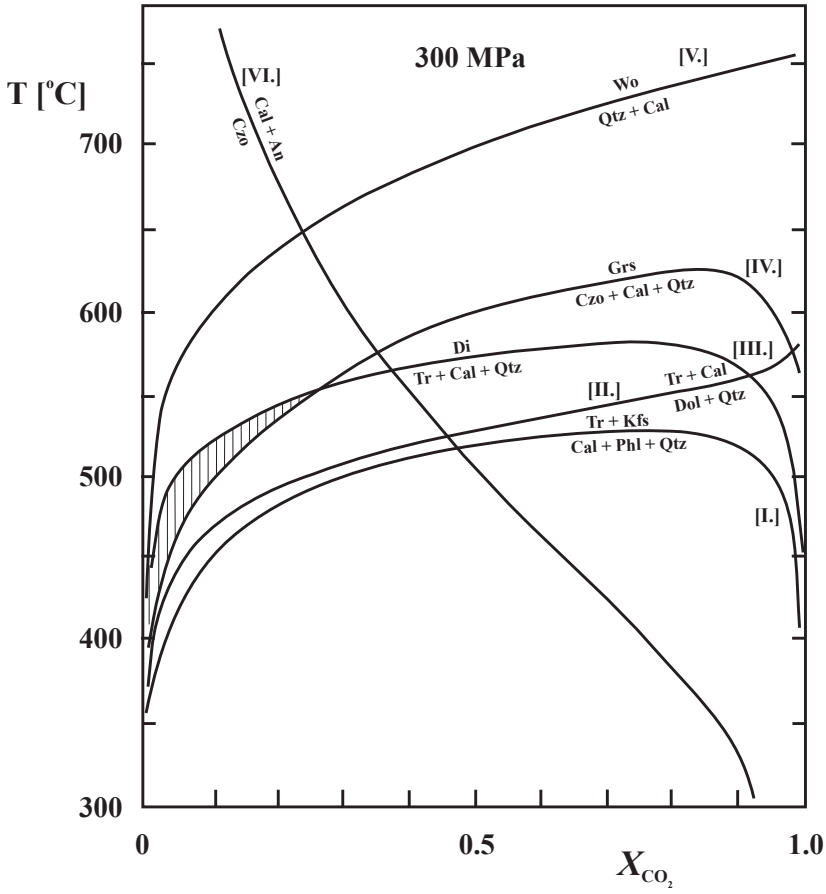

Fig. 3. Schematic isobaric T – X_{CO2} diagram determines the mineral equilibria pertinent to the studied mineral assemblage. The shaded area indicates the fluid composition with which the stable mineral assemblage was in equilibrium. Topologies of the isobaric univariant curves are calculated using the internally consistent thermodynamic dataset of Holland and Powell (2011).

Titanite inclusions in grossular

The growth rate of minerals in most magmatic and metamorphic rocks is approximately constant at 10^{-10} to 5 x10^{-11} cm/sec and these rates are consistent with many crystal size measurements. Growth rate is generally increasing with increasing of effective overstepping of metamorphic reaction (ΔT) as it is predicted from many kinetic crystallization models (Kretz, 1966; Jones et al., 1972; Kirkpatric, 1976; Waters & Lovegrove, 2002; Zieg & Marsh, 2002; Kile & Eberl, 2003). This is consistent with many tectonic interpretations of undercooling processes in magmatic systems and/or overheating and cooling during metamorphic crystallization. In samples, where deformation or annealing does not appear, to have been important, the processes were mostly temperature and time dependent and size distribution was controlled by the rate of heating of the host rocks during metamorphism and by relative rates of crystal nucleation and growth.

Size distribution is in many cases typically bell-shaped with maximum number of crystals at intermediate size, where the right hand part of the distribution curve is approximately linear. Therefore, certain generalization about the development of the titanite population

can be made from the linear correlation between crystal sizes and their population density. Nucleation rate depends significantly on the type of metamorphic regime. High nucleation rates occur during contact metamorphic conditions whereas the high-grade regional metamorphism is represented by slow rate of nucleation. The observed trend thus suggests that nucleation rate changes with regime of metamorphism: rate during contact metamorphism > rate during lowgrade regional metamorphism > rate during high grade regional metamorphism (Cashman & Ferry, 1988).

Tiny idioblastic titanite inclusions ($L \approx$ 10-60 µm) are regularly dispersed in garnet porphyroblast ($V = 0.068$ cm^3) as determined using the X-ray high-resolution microtomography (Fig. 4) that allowed the direct acquiring of the titanite crystal size distribution (CSD) as seen in Fig. 5. Such a numerical assessment formed a stereological basis for detailed analysis of number, shape and size of titanite inclusions (Fig. 6).

However, in calc-silicate rock matrix minerals (calcite + tremolite + quartz), titanite crystals have been only seldom identified microscopically. It is presumed that the

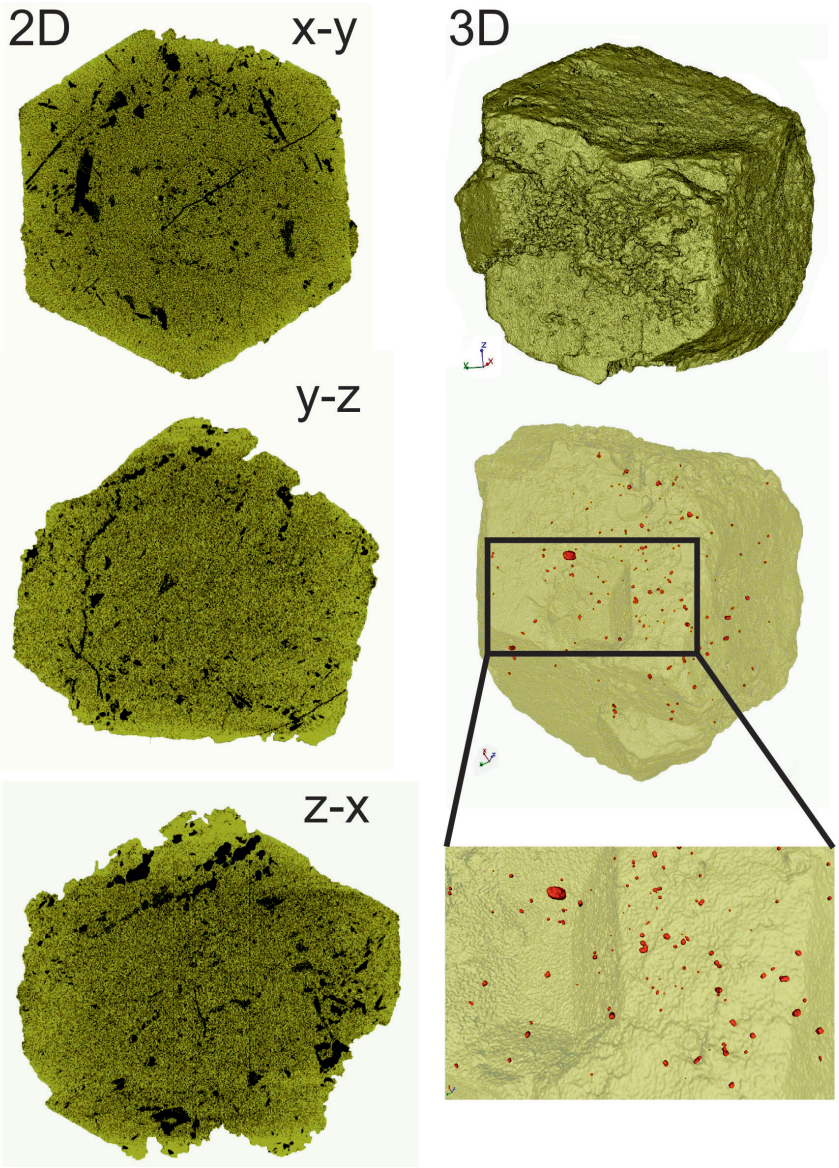

Fig. 4. The 3D distribution of titanite inclusions (red-brown) in grosssular is obtained by X-ray computer tomography (*Nanotom 180*). Volume of crystal containing 116 inclusions is 0.068 cm^3. This is an ideal technique to obtain a 3D image of an object. It creates a series of closely spaced 2 D images that are produced by the attenuation of X-ray passing through the object. The sections are then combined to create a 3D image. Minerals must have different X-ray attenuation coefficient to be distinguished by this CT image technique. Despite these new and expensive techniques the standard 2-D sections methods are likely to continue for gaining the data for *ln* (*n*) versus *L* plot construction (see e.g. Castro et al., 2003).

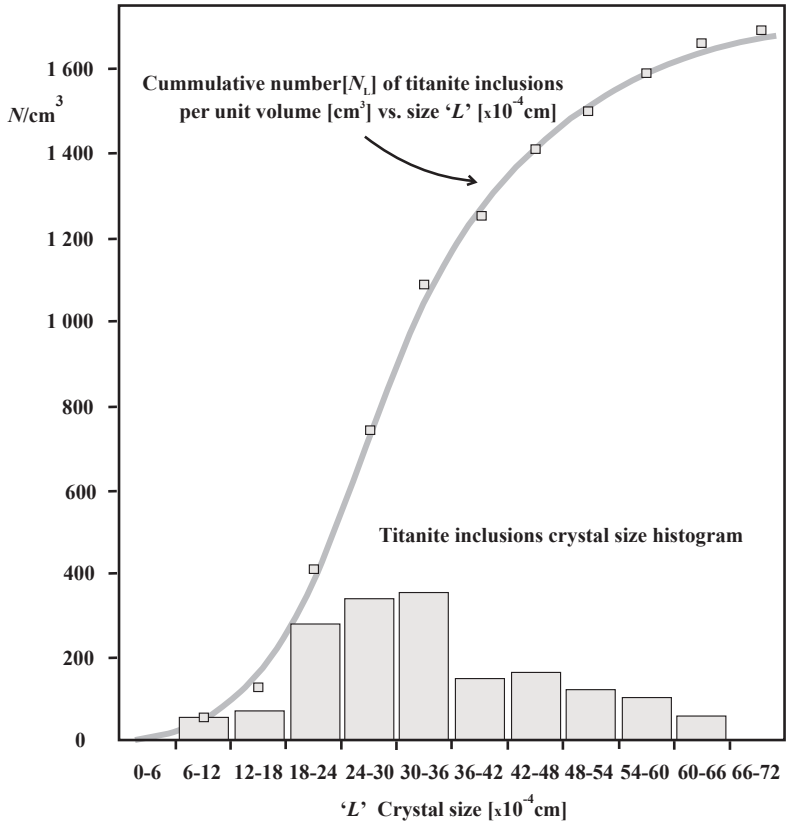

Fig. 5. Crystal size frequency histogram of titanite inclusions in grossular is quasi bell-shaped and documents the increase of nucleation at a constant growth rate that presumes a crystal independent growth, similar to behavior of other silicate minerals.
In normal (Gauss) distribution, the frequency distribution curve is symetrical to aritmetical mean ($\overline{x}$). The class size intervals are chosen in such a way that in the size intervals $\overline{x}$ - 2σ to $\overline{x}$ + 2σ are grouped ~ 95 % of all acquired size data. The extent of class intervals – h is then given: $h = (X_{max} - X_{min}) / m$, where X_{max} is the maximal value in the set, X_{min} is the minimal value, m is number of classes. First and last size class is usually left open.

protolith contained some detritic sedimentary Ti minerals as e.g. ilmenite, titanomagnetite, leucoxene, etc. which could have been partly transformed during increase of metamorphic temperature by metamorphic reactions into idioblastic shapes of titanite. These may have served later as the potential places for garnet heterogeneous nucleation and growth.

CSD of tiny titanite inclusions in grossular present the normal, Gauss' distribution patterns (Fig. 5) indicating thus that the conservation of number and shape of the formed CSD, after the crystallization remained unchanged. This figure shows that studied titanite distribution in grossular was not changed due to final contact metamorphism and formation of diopside and wollastonite.

The cummulative curve of acquired data rises steeply and then flattens (Fig. 5). When these data are converted to number of crystals per unit volume, these trends are enhanced. Important is the cumulative CSD presentation through the plot ln(n) versus "L". This plot is then used to linearize crystal size distribution (see e.g. Marsh, 1988; Cashman & Marsh, 1988; Eberl et al., 2002). The constructed plot, ln (n) vs. "L" from the acquired data (Fig. 6) was then used to calculate the least-squares line and its slope that has been determined to be $b = -616$ cm^{-1}.

According to Marsh (1988), it is convenient to deal with a cumulative distribution which can be derived from the histogram function n (L):

$$N(L) = \int_0^L n(L)\,dL \qquad [2.]$$

N (L) is thus a function describing the total number of crystal of size L and smaller (number of crystals per unit volume). N(L) is also a simpler and more certain measurement in that progressively increasing sum. Stable population density n (L) is defined as the slope of cumulative number curve at any given size class. The n (L) is the number of crystals per unit length (L) and per unit volume:

$$n(L) = \frac{dN(L)}{dL} \qquad [3.]$$

The function n (L) is defined as the population density of crystals in any size range divided by the size interval

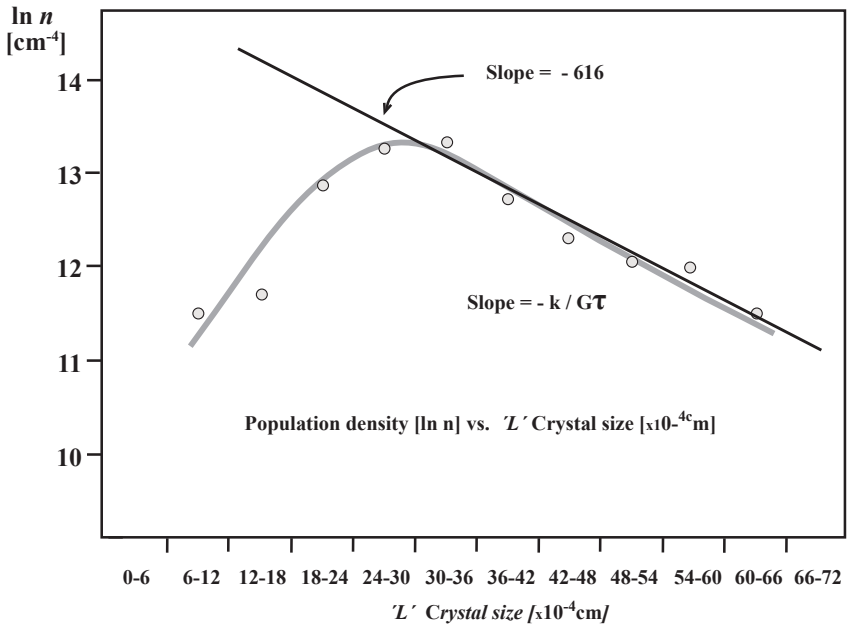

Fig. 6. The correlation of *ln* (*n*) vs. *L* in the diagram has the function $n = n^0 e^{-Lb}$ where n^0 is the intercept at $L = 0$ and *b* is the linear equation constant describing the slope of the curve. In CSD theory the *G* is the growth rate and τ is the effective residence time of the titanite population growth in the sample. Slope describes the comparative parameter of the measured CSD indicating that titanite inclusions must have been grown within a very short time interval. Population density (*n*) is the number of crystals in any size range divided by the size interval.

and on the plot of cumulative number of crystals against size (*L*) that gives the slope of the curve. In a typical crystal size distribution, ln (*n*) versus (*L*) the slope of the line is determined by the relation

$$slope = \frac{-k}{G\tau} \qquad [4.]$$

where *k* is the constant, *G* is the growth rate and τ is the residence time.

Tab. 1
Calculated data for titanite inclusions nucleation and growth.

Intercept	Slope	Nucleation rate [J', N° cm^3 s^{-1}]	Average growth rate [G', cm s^{-1}]	Residence time [τ, yr]
ln 15.50	–616	5.61 x 10^{-6}	1.04 x 10^{-12}	49
W & W (1984)	T [°C]	ΔT [°C]	ΔS_R [J/mol/deg]	τ [years]
	520	1 – 10	5 – 80	4 – 84

Discusion and conclusions

Crystal size histogram of titanite inclusions is bell-shaped with the maximum number of crystals at intermediate sizes (Fig. 5). This distribution shape is similar to many others CSD data which represent crystal distribution in most contact metamorphic rocks. However, the residence time for nucleation and growth of mineral phases along the contacts with granitic plutons emplaced in upper crust can be very similar. This size distribution suggests that titanite inclusions in the studied sample grew under conditions of continuous nucleation and growth and we could determine their growth characteristics and their crystallization residence time.

Walther and Wood (1984) proposed a general Arrhenius relation between temperature and growth rate of many silicate minerals. This empirical relation has been successfully applied to the crystallization of minerals at higher temperatures. On the basis of the formulated relations among reaction entropy (ΔS_R) of the reaction under given *T* and *P* and the equilibrium temperature overstepping (ΔT), the presupposed growth rate and crystallization residence time may be approximated. In many cases the reaction overstep and extent of disequilibrium can be assessed (Waters & Lovegrove, 2002; Zeh & Holness, 2003).

The exact value of ΔS_R for titanite forming reaction is unknown. A lower limit for ΔS_R is probably ~ 5 J/mol/deg, what is a typical value for polymorphic transformations (e.g. andaluzite → sillimanite, calcite → aragonite). ΔS_R ~ 80 J/mol/deg stands for most metamorphic reaction and may be taken as the higher limit. Accepting these ΔS_R limits and the ΔT extent, the residence time may be bracketed τ ≈ 4 – 84 years (Tab. 1).

The nucleation and growth of titanite inclusions was swift and the CSD data show (Tab. 1) that titanite inclu-

sions have been grown within a short period of time. The calculated value obtained for average nucleation rate was as $J' = 5.61 \times 10^{-6}$ N° $cm^3 s^{-1}$, and average growth rate $G' = 1.04 \times 10^{-12}$ cm s^{-1}, giving thus the crystallisation residence time for titanite inclusions in garnet at $\tau \approx 49$ yr., what is consistent with the other CSD data on titanite nucleation and growth in metamorphic environment (see e.g. Zeh, 2004).

These obtained residence time data are consistent e.g. with growth time for magnetite in rock between 0.03 – 32 years or 210 years for a growth of 0.05 cm pyroxene from contact aureole studied by Joesten (1983).

Histogram Fig. 5 shows a quasi normal distribution of crystal sizes. This indicates that post crystallization processes did not modify the original size distribution after crystallization has been completed. In some specific cases the increase of grain size occurs upon annealing. Crystals will coarsen by the transfer of matter from small to large crystals. The process is driven by resulting overall reduction of the total specific surface free energy at the crystal-matrix contact interfaces. Ostwald ripening is characterized by simultaneous growth and resorption of crystals in the same matrix and the system is not in thermodynamic equilibrium until all precipitated material is gathered in one crystal of each mineral present. While this never occurs in nature, the local equilibrium is reached when all crystals are approximately of the same size (Kretz, 1994; Waters & Lovegrove, 2002; Eberl et al., 2002). Such a process of Ostwald ripening is recognized to occur due to diffusion trough matrix. However, the high diffusion coefficient of grossular in post-crystallization conditions (T < 520 °C) could have hindered the possible annealing and/or riping of titanite inclusions during post peak-metamorphic cooling.

Titanite inclusions in grossular from the studied calc-silicate rock offered CSD data which suggest their continuous nucleation and growth. The calculated slope and intercept (see Tab. 1) of the CSD plot (Fig. 6) suggest, in comparison with other titanite growth rate estimates, that the growth rate for studied titanites was short and nucleation rates were high, but no so high as for typical contact metamorphosis. There is no evidence for further modification of the CSD after the initial period of crystal nucleation and growth has been completed.

Finally, the different forms of CSD in contact and regional metamorphic rocks are natural consequences of the differences in thermal history of two metamorphic environments. Regional metamorphism involves high temperature followed by prolonged cooling at high to moderate temperatures. CSD initially produced by continuous nucleation and growth at, or near thermal peak of regional metamorphism may later be significantly modified by annealing processes during prolonged cooling. Studied sample involved crystallization temperatures ~ 500 - 550 °C for a short period of time and CSD characteristics of continuous nucleation and growth of the studied titanite remained unmodified. This implies that the choice of studied specimen was outside of an immediate contact with granitic apophyses and does not represent a typical hornfels.

Variscan metamorphism of paragneises in the Malé Karpaty Mts. involved, however, higher periplutonic recrystallization peak temperatures and pressures 570 - 650 °C, 350 - 610 MPa (Dyda, 2000), followed by tectonic uplift and cooling to moderate temperatures. The CSD of garnets initially produced by continuous nucleation and growth at, or near thermal peak of metamorphism were later significantly modified by annealing during prolonged cooling and exhumation at various calculated cooling rates, verifying thus the different uplift conditions of individual tectonic blocks during final stages of the Variscan orogenic events.

Acknowledgement:

Authors express their thanks to Prof. M. Putiš, Dr. I. Petrík and Dr. M. Kováčik for their very constructive scientific remarks and suggestions, which improved the primary manuscript. This work was supported by the Slovak Research and Development Agency under the contract N°. APVV-0546-11; APVV-15-0050.

References

Belonoshko, A. B., Shi, P. & Saxena, S., 1992: SUPERFLUID: A FORTRAN-77 program for calculation of Gibbs free energy and volume of C-O-S-N-Ar mixtures. *Comput. Geosci., 18, 1 267 – 1 269.*

Burnham, C.W., Holloway, J. R. & Davis, N. F., 1969: Thermodynamic properties of water to 1000 °C and 10 000 bars. *Geol. Soc. Amer. Spec. Paper, 132, 1 – 96.*

Cambel, B., 1954: Geologicko-petrografické problémy severovýchodnej časti kryštalinika Malých Karpát. *Geol. Práce, Zoš., 36, 3 – 74.*

Cambel, B. & Vilinovič, V., 1987: Geochemistry and petrology of the granitoid rocks of the Malé Karpaty Mts. *Bratislava, Veda, Vyd. Slov. Akad. Vied, 247 p.*

Cambel, B., Bagdasarian, G. P., Veselský, J. & Gukasian, R. Ch., 1980: To the problem of interpretation of nuclear-geochronological data on the age of basement rocks of the Western Carpathians. *Geol. Zbor., Geol. carpath., 31, 27 – 47.*

Cambel, B., Korikovsky, S. P., Miklóš, J. & Boronikhin, V. A., 1989: Calc-silicate rockes (erlans and Ca-skarns) in the Malé Karpaty Mts. region. *Geol. Zbor. Geol. carpath., 40, 3, 281 – 304.*

Cambel, B., Kráľ, J. & Burchart, J., 1990: Izotopová geochronológia kryštalinika Západných Karpát. *Bratislava, Veda, Vyd. Slov. Akad. Vied, 183 p.*

Cashman, K. V. & Ferry, J. M., 1988: Crystal size distribution (CSD) in rocks and the kinetics and dynamics of crystallization. *Contr. Mineral. Petrol., 89, 401 – 415.*

Cashman, K. V. & Marsh, B. D., 1984: Crystal size spectra and kineticks of crystal growth in magmas: II. Application. *Geol. Soc. Amer. Bull., 16, 465.*

Cashman, K. V. & Marsh, B. D., 1988: Crystal size distribution (CSD) in rocks and the kinetics and dynamics of crystalli-

zation. II. Makaopuhi lava lake. *Contr. Mineral. Petrol.*, *99, 292 – 302.*

Castro, J. M., Cashman, K. V. & Manga, M., 2003: A technique for measuring 3D crystal size distribution of prismatic microlites in obsidian. *Amer. Mineralogist*, *88, 1 230 – 1 240.*

Dyda, M., 1997: Disturbance of the Variscan metamorphic complex indicated by mineral reactions, P-T data and crystal size of garnets (Malé Karpaty Mts.). *In: Grecula, P., Hovorka, D. & Putiš, M., 1997: Geological Evolution of the Western Carpathians. Bratislava, Geocomplex, 333 – 342.*

Dyda, M., 2000: Exhumation and cooling rates of the Variscan basement metamorphic complex inferred from petrological data (Malé Karpaty Mts.). *Slovak Geol. Mag.*, *6, 293 – 297.*

Dyda, M. & Miklóš, J., 1993: Periplutonické zóny bratislavského granitoidného masívu (Malé Karpaty): rekryštalizácia, dehydratačné a objemové zmeny. *Miner. Slov., 25, 93 – 103.*

Dyda, M., Ružička, P. & Hain, M., 2014: Crystal size distribution (CSD) of titanite inclusions in grossular from the calc-silicate skarn in Malé Karpaty Mts., Slovakia. *Congress of the Carpathian-Balkan Geological Association, Tirana. Bul. Shkenc. Gjeol., 2, Sp. Iss., 180.*

Eberl, D. D., Drits, V. A. & Srodon, J., 1998: Deducing growth mechanism for minerals from the shapes of crystal size distribution. *Amer. J. Sci., 298, 499 – 533.*

Eberl, D. D., Kile, D. E. & Drits, V. A., 2002: On geological interpretations of crystal size distributions: constant vs. proportionated growth. *Amer. Mineralogist, 87, 1 235 – 1 241.*

Helgeson, H. C. & Kirkham, G. H., 1974: Theoretical prediction of the thermodynamic behaviour of aqueous electrolytes at high pressures and temperatures: I. Summary of the thermodynamic electrostatic properties of the solvents. *Amer. J. Sci., 274, 1 089 – 1 198.*

Higgins, M. D., 2000: Measurement of crystal size distribution. *Amer. Mineralogist, 79, 113 – 119.*

Higgins, M. D., 2002: Closure in crystal size distributions (CSD), verification of CSD calculations, and the significance of CSD fans. *Amer. Mineralogist, 87, 171 – 175.*

Higgins, M. D., 2006: Quantitative textural measurement in igneous and metamorphic petrology. *Cambridge University Press, 265 p.*

Holland, T. J. B. & Powell, R. 1985: An internall consistent thermodynamic dataset with uncertainties and correlations: Data and results. *J. Metamorph. Geol., 3, 343 – 370.*

Holland, T. J. B. & Powell, R., 1990: An enlarged and updated internally consistent thermodynamic dataset with uncertainties and correlations: the system K_2O-Na_2O-CaO-MgO-MnO-FeO-Fe_2O_3-Al_2O_3-TiO_2-SiO_2-C-H_2-O_2. *J. Metamorph. Geol., 8, 89 – 124.*

Holland, T. J. B. & Powell, R., 2011: An improved and extended internally consistent thermodynamic dataset for phases of petrological interest, involving a new equations of state for solids. *J. Metamorph. Geol., 29, 333 – 383.*

Jerram, D. A., Mock, A., Davis, G. R., Field, M., & Brown R. J., 2009: 3D crystal size distributions: A case study on quantifying olivine populations in kimberlites. *Lithos, 112S, 223 – 235.*

Joesten, R., 1983: Grain growth and grain – boundary diffusion in quartz from the Christmass Mountains (Texas) contact aureole. *Amer. J. Sci., 283 A, 233 – 254.*

Jones, K. A., Morgan, G. J. & Galwey, A. K., 1972: The significance of the size distribution function of crystals formed in metamorphic reactions. *Chem. Geol., 9, 137 – 143.*

Kile, D. E. & Eberl, D. D., 2003: On the origin of size-dependent and size-independent crystal growth: influence of advection and diffusion. *Amer. Mineralogist*, 88, *1 514 – 1 521.*

Kirkpatrik, R. J., 1976: Towards a kinetic model for magma crystallization. *J. geophys. Res., 81, 2 565 – 2 571.*

Kohút, M., Uher, P., Putiš, M., Ondrejka, M., Sergeev, S., Larionov, A. & Paderin, I., 2009: SHRIMP U-Th-Pb zircon dating of the granitoid massifs in the Malé Karpaty Mountains (Western Carpathians): evidence of Messo-Hercynian succesive S- to I-type granitic magmatism. *Geol. Carpath., 60, 5, 345 – 350.*

Kretz, R., 1966: Grain size distribution for certain metamorphic minerals in relation to nucleation to nucleation and growth. *J. Geol.*, *74, 147 – 173.*

Kretz, R., 1994: Metamorphic crystallization. *John Wiley, 507 p.*

Maglay, J., Pristaš, J., Nagy, A., Fordinál, K., Elečko, M., Havrila, M., Buček, S., Kováčik, M., Hók, J., Baráth, I., Kubeš, P., Kucharič, Ľ., Malík, P., Klukanová, A., Liščák, P., Ondrášik, M., Zuberec, J., Baláž, P., Čurlík, J. & Šefčík, P., 2011: Vysvetlivky ku geologickej mape Podunajskej nížiny-Trnavskej pahorkatiny 1 : 50 000. *Bratislava, Št. Geol. Úst. D. Štúra, 322 s.*

Maheľ, M., 1983: Beziehung Westenkarpaten-Ostalpen, Position des Ubergangs – Abschnittes, Deviner Karpaten. *Geol. Zbor. Geol. carpath.*, *34, 131 – 149.*

Maheľ, M. & Cambel., B., 1972: Geologická mapa Malých Karpát. *Bratislava, Geol. Úst. D. Štúra.*

Marsh, B, D., 1988: Crystal size distribution (CSD) in rocks and the kinetics and dynamics of crystallization. *Contr. Mineral. Petrol.*, *99, 277 – 291.*

Melnik, Yu., 1972: Thermodynamic parameters of compressed gasses and metamorphic reactions involving water and carbon dioxide. *Geochem. Int., 9, 419 – 426.*

Norton, D. & Knight, J., 1977: Transport phenomena in hydrothermal systems: cooling plutons. *Amer. J. Sci., 277, 937 – 981.*

Peterson, T. D., 1996: A refined technique for measuring crystal size distributions in thin section. *Contr. Mineral. Petrol., 124, 395 – 405.*

Petrík, I., Nabelek, P. I., Janák, M. & Plašienka, D., 2003: Conditions of formation and crystallization kinetics of highly oxidised pseudotachylytes from High Tatras (Slovakia). *J. Petrol., 44, 5, 901 – 927.*

Plašienka, D., 1989: Štruktúrny vývoj tatrika Malých Karpát. *Miner. Slov., 21, 538.*

Plašienka, D., Michalík, J., Kováč, M., Gross, P. & Putiš, M., 1991: Paleotectonic evolution of the Malé Karpaty Mts. – An overview. *Geol. Carpath.*, *42, 195 – 208.*

Polák, M. (ed.), Plašienka, D., Kohút, M., Putiš, M., Bezák, V., Maglay, J., Olšavský, M., Havrila, M., Buček, S., Elečko, M., Fordinál, K., Nagy, A., Hraško, Ľ., Németh, Z., Malík, P., Liščák, P., Madarás, J., Slavkay, M., Kubeš, P., Kucharič, Ľ., Boorová, D., Zlinská, A., Siráňová, Z. & Žecová, K., 2012: Vysvetlivky ku geologickej mape Malých Karpát 1 : 50 000. *Bratislava, Št. Geol. Úst. D. Štúra, 287 s.*

Putiš, M., 1987: Geológia a tektonika juhozápadnej a severnej časti kryštalinika Malých Karpát. *Miner. Slov.*, *19, 135 – 157.*

Putiš, M., 1991: Tectonic styles and Late Variscan-Alpine evolution of the Tatric-Veporic crystalline basement in the Western Carpathians. *Zbl. Geol. Paläont., H.1, 181 – 204.*

Putiš, M., Radvanec, M., Hain, M., Koller, F., Koppa, M. & Snárska, B., 2011: 3-D analysis of perovskite in serpentinite (Dobšiná quarry) by X-ray micro-tomography. In: Ondrejka, M., Šarinová, K. (eds.): Proceedings of the Petros Symposium. *Bratislava, Comenius University Press, pp. 33 – 37.*

Randolph, A. D. & Larson, M. A., 1971: Theory of Particulate Processes. *New York, Academic Press, 251 pp.*

Ružička, P., Hain, M., Bačík, P., Milovská, S. & Juhász, P., 2013: 3D distribúcia titánových inklúzií v granáte z lokality Modra-Harmónia (Malé Karpaty, Slovensko). *Bull. mineral-petrolog. Odd. Nár. Muz. (Praha), 21, 2, 131 – 142.*

Shcherbak, N. P., Bartnicky, E. N., Mickevich, N. Y., Stepanyuk, L. M., Cambel, B. & Grecula, P., 1988: U-Pb radiometric zircon age determination from the Modra granodiorite of the Malé Karpaty Mts. and a porfyroid of the lower Paleozoic of the Spišsko-gemerské Rudohorie Mts. (Western Carpathians). *Geol. Zbor. Geol. carpath., 39, 427 – 436* (in Russian).

Šímová, M. & Šamajová, E., 1979: Prejavy kontaktnej metamorfózy v oblasti Dolinkovského vrchu v Malých Karpatoch. *In: Sympózium o petrogenéze a geochémii geologických procesov. Bratislava, Veda, 223 – 229.*

Takenouchi, S. & Kennedy, G. C., 1964: The binary system H_2O–CO_2 at high temperature and pressure. *Amer. J. Sci., 262, 1 055 – 1 074.*

Uher, P., Ružička, P. & Bilohuščin, V., 2015: Chrómom a vanádom obohatený grossulár zo skarnu Dubová v Malých Karpatoch (Slovensko). *Bull. mineral.-petrolog. Odd. Nár. Muz. (Praha), 23, 1, 19 – 25.*

Vojtko, P., Broska, I., Ševčík, R. & Hain, M., 2011: Distribúcia Fe-Ti oxidov v mineráloch a horninách: predbežné výsledky z počítačovej mikrotomografie. *In: Hain, M., Karovič, K., Jerz, J. (eds.): Použitie moderných nedeštruktívnych meracích metód vo výskume nových materiálov v rámci centra excelentnosti CEKOMAT. Zborník z konferencie. Bratislava, Ústav merania SAV, 37 – 40*

Waters, D. J. & Lovegrove, D. P., 2002: Assessing the extent of disequilibrium and overstepping of prograde metamorphic reactions in metapelites from the Bushveld Complex aureole, South Africa. *J. Metamorphic Geol., 20, 135 – 149.*

Walther, J. V. & Wood, B. J., 1984: Rate and mechanism in prograde metamorphism. *Contr. Mineral. Petrol., 88, 246 – 259.*

Waters, D. J. & Lovegrove, D. P., 2002: Assessing the extent of disequilibrium and overstepping of prograde metamorphic reactions in metapelites from the Bushveld Complex aureole, South Africa. *J. Metamorph. Geol., 20, 135 – 149.*

Zeh, A. & Holness, M., 2003: The effect of reaction overstep on garnet microtextures in metapelitic rocks of the Ilesha Schist Belt, SW Nigeria. *J. Petrology, 44, 967 – 994.*

Zeh, A. & Millar, I. L., 2001: Metamorphic evolution of garnet–epidote–biotite gneiss from the Moine Supergroup, Scotland, and geotectonic implications. *J. Petrology, 42, 529 – 554.*

Zeh, A., 2004: Crystal size distribution (CSD) and textural evolution of accessory apatite, titanite and allanite during four stages of metamorphism: and example from Moine Supergroup, Scotland. *J. Petrology, 45, 2 101 – 2 132.*

Zieg, M J. & Marsh, B. D., 2002: Crystal size distributions and scaling laws in the quantification of igneous textures. *J. Petrology, 43, 85 – 101.*

Distribúcia kryštálových veľkostí (CSD) titanitových inklúzií v grosulári z vápenato-silikátovej horniny Malých Karpát, Slovensko

Merania distribúcie kryštálových veľkostí (CSD) v malom objeme hornín sú skôr ojedinelé a v rozmeroch ~ 0,07 cm^3 sa zatiaľ nerealizovali. Bežný metodický prístup hodnotenia CSD je založený hlavne na 2D meraniach a transformácia 2D hodnôt do 3D údajov je spojená so značnými komplikáciami a numerickými úpravami.

Na röntgenovom mikrotomografe Nanotom 180 sa stereologickým zobrazením získalo 116 titanitových inklúzií, rovnomerne rozptýlených v objeme grosuláru (obr. 4). Ich početnosť, veľkosť ($L \approx 10 – 60$ µm) a rovnomerná distribúcia umožnili uplatniť numerické metodiky CSD (obr. 6) a získať tak charakteristiky definujúce nukleačnú rýchlosť ($J' \approx 5{,}6 \times 10^{-6}$ $cm^3 . s^{-1}$), rýchlosť kryštálového rastu ($G' \approx 1{,}4 \times 10 – 12$ cm . s^{-1}) aj rezidenčný čas kryštalizácie ($\tau \approx 4 – 84$ *rok*) titanitových inklúzií.

Látková bilancia progresívnej reakcie vytvárajúcej titanitové inklúzie nebola špecifikovaná a hodnota entropickej zmeny (ΔS_R) pri reakcii vytvárajúcej titanit nie je známa. Spodný limit ΔS_R je pravdepodobne ~ 5 J/mol/deg, čo je typická hodnota pre polymorfné transformácie (napr. andaluzit → sillimanit, kalcit → aragonit). Entropická zmena ΔS_R ~ 80 J/mol/deg je platná pri mnohých metamorfných reakciách a môže sa považovať za horný limit.

Akceptovaním týchto limitov ΔS_R a teploty ΔT môže byť potom rezidenčný čas rastu rámcovo vymedzený rozsahom $\tau \approx 4 – 84$ rokov (tab. 1). Nukleácia a rast idioblastických titanitových inklúzií v takmer homogénnom granáte boli rýchle a trvali krátky časový interval, čo je konzistentné s inými údajmi o nukleácii a raste titanitových inklúzií v metamorfnom prostredí (napr. Castro et al., 2003; Zeh, 2004). Rezidenčné časy rastu korešpondujú napr. s časom rastu magnetitu v rohovcoch (0,03 – 32 rokov) a tiež s rastom 0,05 cm pyroxénu v kontaktnej aureole (≈ 210 rokov; Joesten, 1983).

Granáty kryštalizovali ako rovnovážna súčasť progresívnej minerálnej asociácie grosulár + kalcit + flogopit + tremolit + kremeň pri teplote (T ~ 500 – 550 °C) a tlaku (P ~ 300 MPa), vymedzených monovariantnými krivka-

mi určujúcimi divariantné pole tejto asociácie. Minerálna asociácia bola určovaná intruzívnym magmatickým telesom aj zložením metamorfného fluida, keď vysoký obsah H_2O (X_{CO2} < 0,2) vyjadruje intenzívny periplutonický vplyv magmatických fluíd na minerálnu asociáciu.

Periplutonická kontaktná kryštalizácia granátu zrejme kopírovala pôvodné litologické zloženie sedimentárneho komplexného karbonátového protolitu. Porfyroblasty grosuláru majú zachovaný idioblastický vývoj a sú bez sekundárnych retrográdnych aj deformačných znakov. Vývoj titanitových inklúzií bol progresívny, jednoetapový a nepodliehal neskorším zmenám, ktoré by modifikovali pôvodnú distribúciu kryštálových veľkostí. Veľkosť titanitových inklúzií má normálnu, Gaussovu distribúciu kryštálových veľkostí a minimálnu tendenciu k lognormálnej distribúcii. To potvrdzuje minimálnu zmenu počtu a tvaru kryštálov po skončení kryštalizácie a počas neskoršieho chladnutia, keď v procese Ostwaldovho zrenia sa hmota menej stabilných, menších kryštálov transferuje na väčšie, stabilnejšie kryštály.

Progresívna minerálna reakcia vytvárajúca titanitové inklúzie nebola definovaná. Je však pravdepodobné, že čiastočnými reaktantmi boli pôvodné Fe-Ti minerály v protolite (napr. ilmenit, titanomagnetit, leukoxén), ktoré mohli pri rozklade zároveň podmieňovať heterogénnu nukleáciu granátov aj titanitových inklúzií. V matrixe horniny bol však titanit mikroskopicky identifikovaný len zriedkavo. Rast inklúzií a grosuláru mohol byť synchrónny. To by však vyžadovalo definíciu progresívnej metamorfnej reakcie na hmotnostnej bilančnej báze, keď by titanit aj grosulár boli reakčnými produktmi takejto reakcie. Vypočítaná dĺžka rezidenčného času rastu titanitových inklúzií je so zreteľom na metamorfné podmienky relatívne krátka.

Variská periplutonická zonálnosť v Malých Karpatoch je na mnohých miestach významne porušená, fragmentovaná alpínskou tektonogenézou a niektoré horninové bloky nemusia priestorovo zapadať do predpokladanej metamorfnej zonálnosti. Podmienenosť periplutonických kontaktných premien, ich intenzita a rozsah sú potom určované najmä vzdialenosťou od tepelného zdroja. V špecifických metamorfných horninových blokoch má potom numerické hodnotenie CSD najmä všeobecný komparatívny petrologický význam.

Doručené / Received: 27. 4. 2017
Prijaté na publikovanie / Accepted: 19. 12. 2017

Mineralia Slovaca, 49 (2017), 125 – 140
Web ISSN 1338-3523, ISSN 0369-2086

Obliakový materiál vrchnopaleozoických sedimentov hronika v Malých Karpatoch: petrogenetické a proveniencné otázky

MARTIN KOVÁČIK a MÁRIO OLŠAVSKÝ

Štátny geologický ústav D. Štúra, Mlynská dolina 1, 817 04 Bratislava;
mato.kovacik@geology.sk; mario.olsavsky@geology.sk

Pebble-material of Hronic Upper Paleozoic sediments in the Malé Karpaty Mts. (Western Carpathians): petrogenetic and provenance aspects

Abstract: The paper presents the results of petrographic study of the pebbles in Permian Peterklin Beds, belonging to the Malužiná Fm. and locally to the Upper Carboniterous Nižná Boca Fm. of the Hronic Unit in the Malé Karpaty Mts. The pebble material consists of basement rocks – dominantly leucocratic granites and synsedimentary acid volcanics and clastics of intraformation origin. Therefore it is presumed that the source of this material was represented by the basement of the southern parts of that time Tatro-Veporic Unit – the Variscan predecessor of Alpine Tatric and Veporic units. The rocks of the Gemeric Unit provenance were not clearly evidenced in investigated pebbles. Low-grade deformation superimposed upon the basement-rock pebbles indicates a Late-Variscan tectonic event, which occurred approx. inbetween the thermal consolidation of the Variscan granitic massifs and the development of the Upper Paleozoic formations. Mineralization found in chalcedony silicite points to Late Carboniferous low-temperature hydrothermal sulfidic-carbonatic-(phosphatic) metallogenetic period.

Key words: Hronic nappe unit, Upper Paleozoic conglomerates, Late Variscan deformation, provenance, mineralized chalcedony silicite, Malé Karpaty Mts., Western Carpathians

Graphical abstract

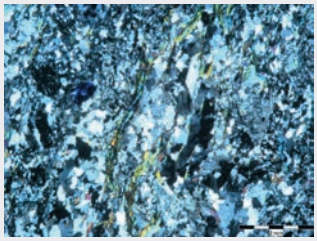

Highlights

- Resistent crystalline pebble material underwent the pre-depositional Late Variscan deformation;
- Gemeric provenance of the pebbles was not proved;
- Low thermal Late-Carboniferous ankerite-sulfide-xenotime mineralization was found in chalcedony silicite.

Úvod

Pri geologickom mapovaní spodnej časti veterlínskeho príkrovu tvoreného ipoltickou skupinou (Olšavský in Polák et al., 2010) bola vyzbieraná kolekcia obliakového materiálu na petrografické štúdium. Polymiktný materiál bol získaný hlavne z permských peterklinských vrstiev a orientačne z vrchnokarbónskeho nižnobocianskeho súvrstvia. Petrograficky sme zhodnotili zhruba 40 vzoriek. Vytypované petrogenetické či štruktúrne prvky boli zdokumentované mikrofotograficky a na elektrónovom mikroanalyzátore Cameca SX 100 (ŠGÚDŠ Bratislava) boli analyzované vybrané minerály a identifikované akcesorické minerály alebo jemnozrnné alteračné fázy. Cieľom práce nie je podať systematickú obliakovú analýzu, je zameraná najmä na fenomény osvetľujúce proveniencné a predvrchnopaleozoické petrogenetické otázky a faktograficky aj interpretačne rozširuje predchádzajúci krátky príspevok autorov Kováčik a Olšavský (2012).

Stručný prehľad doterajších prác

Výskumom proveniencie zdrojových oblastí ipoltickej skupiny (nižnobocianske a malužinské súvrstvie) sa rôzni autori v minulom storočí vo svojich prácach dotkli tejto problematiky skôr okrajovo. Prvé pokusy o zhotovenie obliakovej analýzy prišli s prácami uránového prieskumu (Novotný a Jančok, 1971, s. 45; Novotný, 1972, s. 57). Tu identifikovali petrografické variety a ich približné percentuálne zastúpenie. Pokus o charakterizovanie petrografického zloženia klastického materiálu je možné evidovať v ďalšej dekáde (Vozárová, 1981; Vozárová a Vozár, 1988,

s. 267 – 268). Novšie geochemické/geochronologické štúdie s ohľadom na zdrojovú oblasť boli sústredené na areál Malých Karpát (Vďačný, 2013; Vďačný et al., 2013; Vozárová et al., 2014; Vďačný a Bačík, 2015) a zamerané prevažne na malužinské súvrstvie.

Ako hlavný zdroj sa uvádzajú acidné felzitické plutonické horniny. Menej zastúpené boli nízko až vysoko metamorfované horniny s felzitickými a mafickými vulkanickými horninami (Vďačný, 2013). Materiál bol derivovaný zo zlomovo ohraničeného vyzdvihnutého fundamentu aktívneho kontinentálneho okraja (Vďačný et al., 2013). Boli identifikované viaceré potenciálne zdrojové oblasti: variské magmatity ohraničené subdukčnou zónou ako hlavný zdroj, acidné metavulkanity spojené s nízko metamorfovaným kryštalinickým komplexom a ryolitovo-dacitové synsedimentárne vulkanické centrá v samotnej panve ipoltickej skupiny (Vozárová et al., 2014). V staršom príspevku (Vozárová, 1981, s. 187), týkajúcom sa výlučne nižnobocianskeho súvrstvia, boli na základe petrografickej analýzy doložené tri zdroje: komplex granitoidov, migmatitov a rúl, ako aj komplex epimetamorfovaných hornín a tiež syngenetický dacitovo-andezitový vulkanizmus. V obliakovom materiáli hronického permu Ďurovič (1971) opísal kvarcity, grafitické kvarcity, granitoidné horniny, kremité porfýry, zelené chloriticko-sericitické bridlice, muskovitické svory a pieskovce.

Extraformačný (obliakový) materiál sa nachádza prakticky v celom profile ipoltickej skupiny. V nižnobocianskom súvrství sú prítomné polohy piesčitých zlepencov v asociácii so sľudnatými arkózami. V permských sedimentoch sa zlepence s extraformačným materiálom vyskytujú v štyroch zo šiestich známych litostratigrafických členov malužinského súvrstvia. V Nízkych Tatrách a na Horehroní sú to: bystrianske, kubašské, vysovské a brezovské/stupianske vrstvy (sensu Tulis a Novotný, 1998; Olšavský, 2008). V Malých Karpatoch sú to ich stratigrafické ekvivalenty: žliabocké, peterklinské, klokočské a zámocké vrstvy (Olšavský in Polák et al., 2012).

Vystupovanie obliakového materiálu

Skúmaný polymiktný materiál z ipoltickej skupiny rozšírenej na území Malých Karpát pochádza z dvoch stratigrafických úrovní (obr. 2). V nižnobocianskom súvrství vytvára polohy hrubozrnných sedimentov v podobe sivých, štruktúrne nevytriedených zlepencov, niekedy piesčitých zlepencov s polymiktným materiálom (obr. 3), ktorého klasty dosahujú veľkosť 10 cm. Ide o nepravidelné výskyty v piesčitých hrubozrnných sľudnatých arkózach (ojedinele s polohami prachovcov).

V malužinskom súvrství najhojnejší (najpestrejší) materiál poskytujú peterklinské vrstvy. Prakticky v celom pruhu jeho výskytu (južné svahy Vápennej a Klokoča) sa nachádzajú sedimentárne polohy s hruboklastickým materiálom. Niekoľko lokalít s výskytom zlepencov bolo zaregistrovaných aj v nadložných klokočských vrstvách, kde tvoria len menšie, skôr vzácne akumulácie.

Peterklinské vrstvy sa vyznačujú predovšetkým prítomnosťou hruboklastického polymiktného materiálu,

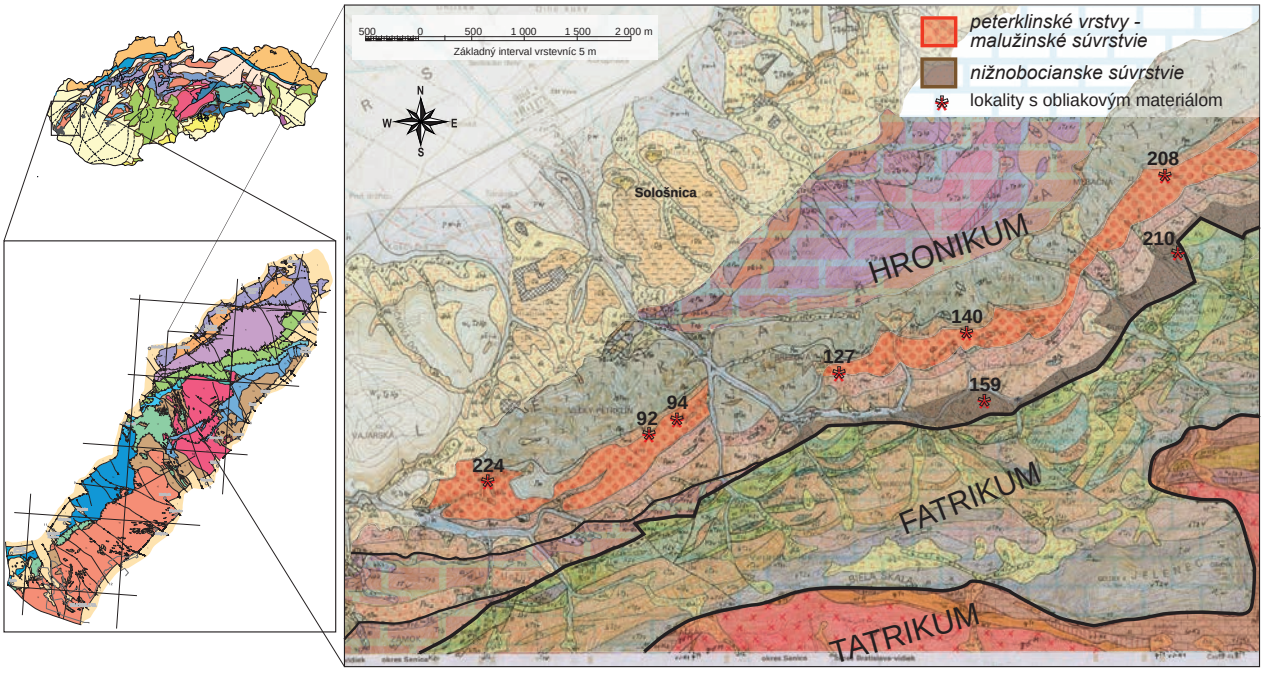

Obr. 1. Situačná mapa výskytov polymiktných zlepencov na liste 1 : 50 000 Sološnica 34-442 (Polák et al., 2010).
Fig. 1. Location of polymict pebble occurrences on the map sheet 1 : 50 000 Sološnica 34-442 (Polák et al., 2010).

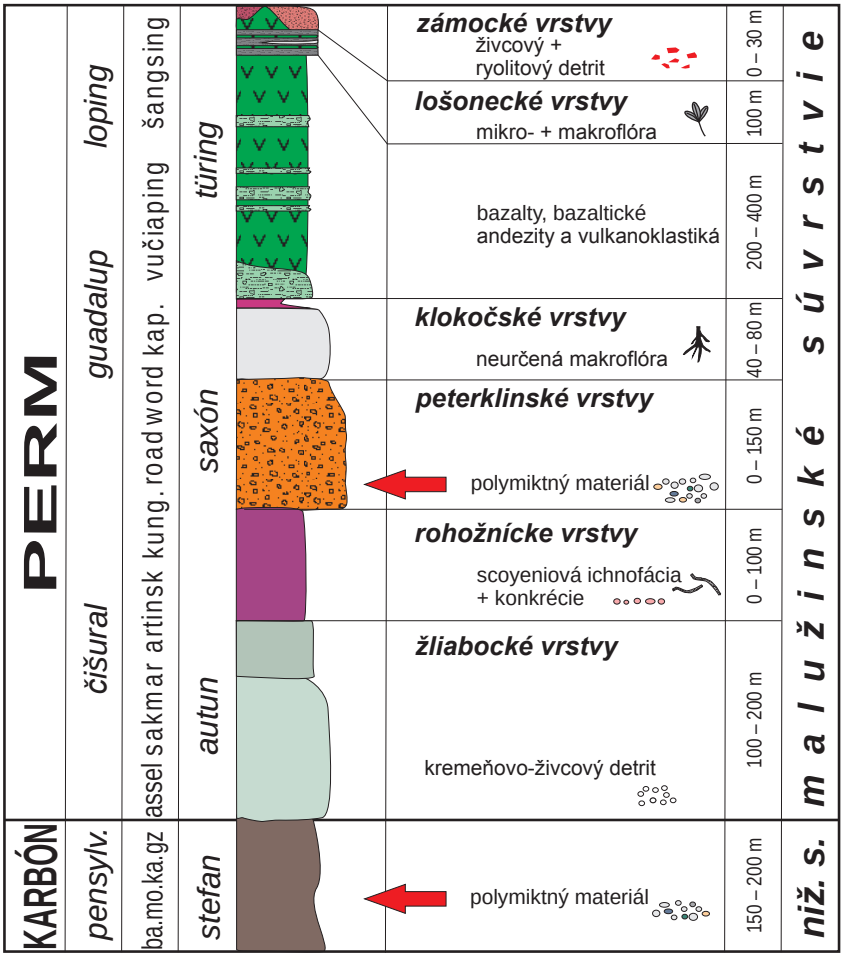

Obr. 2. Litostratigrafická tabuľka ipoltickej skupiny z oblasti Veľký Peterklin – Vápenná – Klokoč.
Fig. 2. Lithostratigraphic column of the Ipoltica Group in the area of Veľký Peterklin – Vápenná – Klokoč.

ktorý je zároveň najhrubšie zrnitý aj v rámci výskytov malužinského súvrstvia v Západných Karpatoch. Obliaky tu dosahujú veľkosť až 30 cm.

Peterklinské vrstvy sú zastúpené predovšetkým drobnozrnnými piesčitými zlepencami a hrubozrnnými arkózovými zlepencami. Väčšie klasty sú spravidla veľmi dobre opracované, priestor medzi nimi je vyplnený drobnozlepencovitým alebo hrubopiesčitým materiálom. Charakteristická je ich mineralogická a štruktúrna nezrelosť. Stratigrafický záznam hruboklastických sedimentov peterklinských vrstiev v malužinskom súvrství z Malých Karpát možno korelovať s depozičnou sekvenciou (DS3) kubašských vrstiev (Tulis a Novotný, 1998; Olšavský, 2008), resp. s bázou II. megacyklu na sv. svahoch Nízkych Tatier (sensu Vozárová a Vozár, 1981).

Dokumentačné body opisovaných vzoriek

Dok. bod 92 (GPS: N 48° 26,664′, E 17°14,338′): *peterklinské vrstvy*, v = 455 m n. m., 480 m na JV od k. Veľký Peterklin, nevýrazný hrebeň smeru VSV – ZJZ, ohyb lesnej cesty, veľmi strmo uložené vrstvy permských hrubozrnných piesčitých až drobnozrnných zlepencov. Vzorky úlomkov hornín z polymiktných variet (metamorfit a tmavá bridlica). Klasty sú veľké až 15 – 20 cm.

D. b. 94 (N 48° 26,770′, E 17° 14,454′): *peterklinské vrstvy*: v = 350 m n. m., 710 m na V od k. Veľký Peterklin, 80 m na Z od k. 361, ľavá strana (v smere toku) bezmennej dolinky zhruba v.-z. smeru, lesná cesta, strmo uložené vrstvy hrubozrnných zlepencov až hrubozrnných pieskovcov, 60 – 80 cm hrubá zlepencová lavica je prekrytá polohou hrubozrnných červenohnedých pieskovcov. Svetloružovkasté zlepence s obliakovým materiálom majú veľkosť do 30 cm.

D. b. 127 (N 48° 26,943′, E 17° 15,765′): *peterklinské vrstvy*, v = 400 m n. m., 500 m na SSV od hájovne Žliabok, nevýrazný hrebeň smeru S – J, ohyb lesnej cesty, piesčité zlepence.

D. b. 140 (N 48° 27,161′, E 17° 16,786′): *peterklinské vrstvy*, v = 440 – 435 m n. m., pravá strana doliny Sološ-

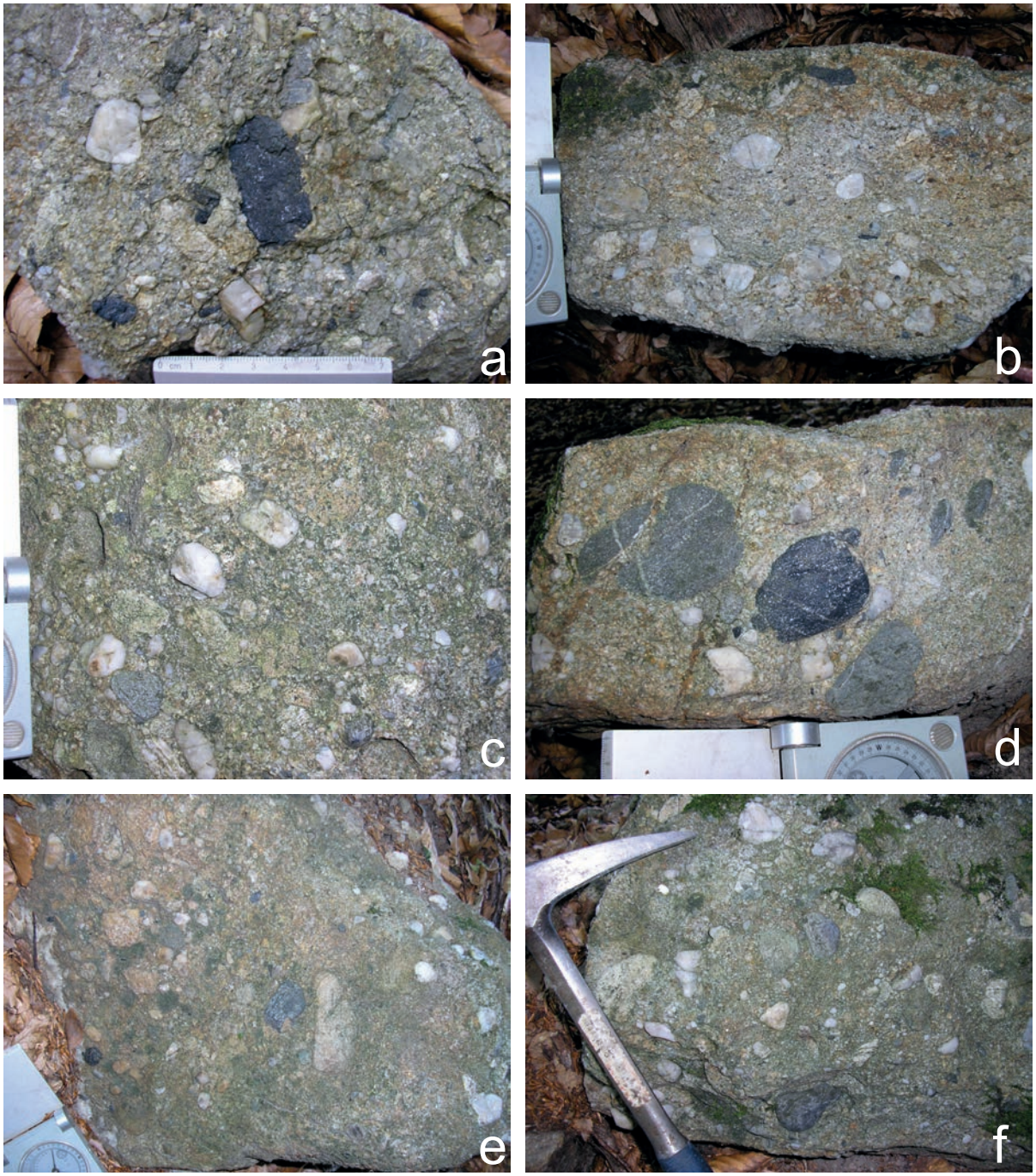

Obr. 3. Nižnobocianske súvrstvie: **a, b, c** – polymiktné zlepence z lokality na ľavej strane doliny Sološnického potoka južne od Horných žliabkov (dokumentačný bod 159); **d, e, f –** zlepence z lokality severne od kóty Mesačná (d. b. 210), úlomky tvorí materiál z kremeňa, rúl, granitoidov a tmavých (meta)sedimentov.
Fig. 3. The Nižná Boca Fm.: **a, b, c** – polymict conglomerates, localized on the left side of the Sološnica creek valley, south of Horné žliabky elevation point (documentation point 159); **d, e, f –** conglomerates built of quartzitic, gneissic, granitic and (meta)sedimentary pebble-material, location e. p. Mesačná (d. p. 210).

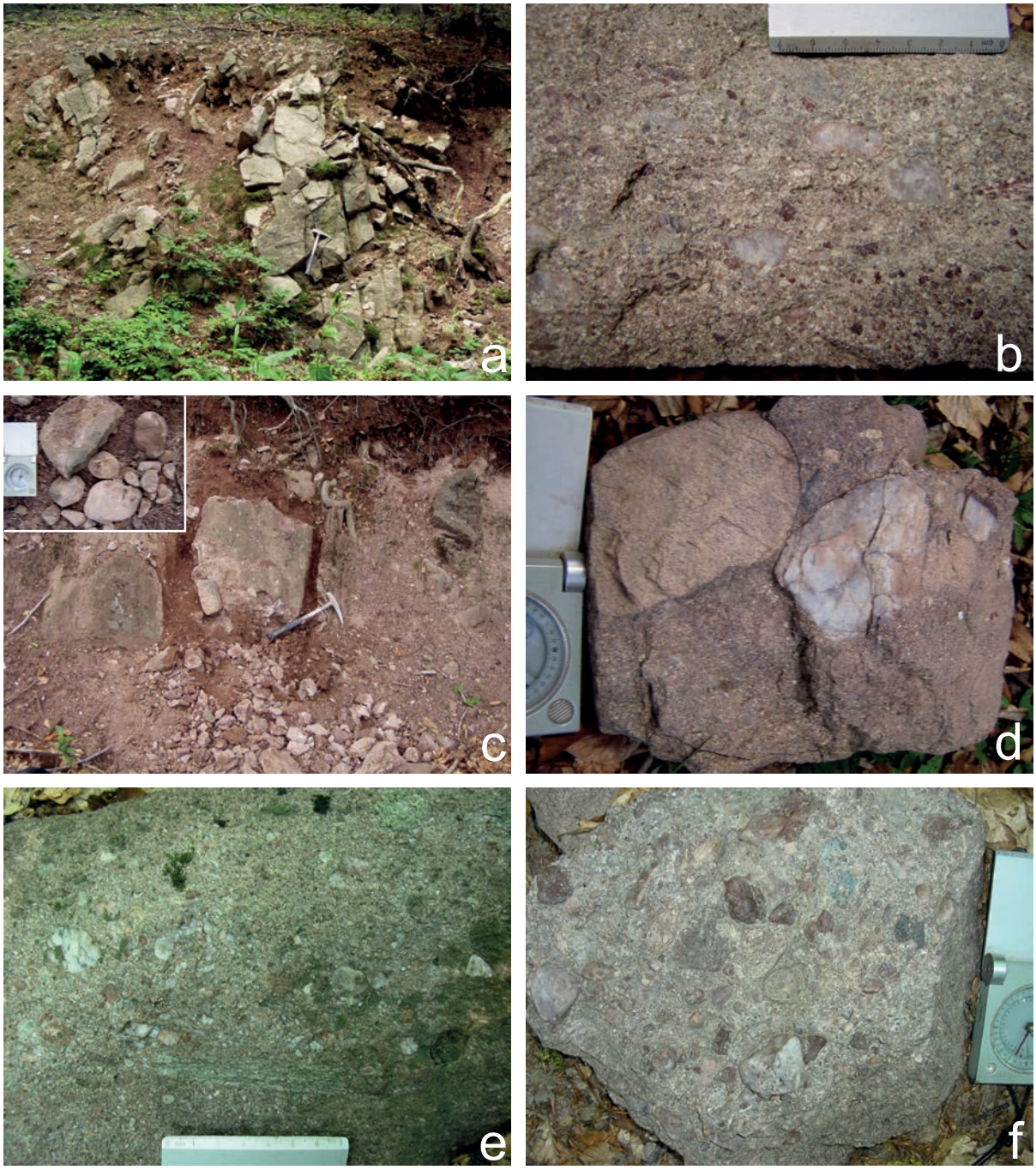

Obr. 4. Peterklinské vrstvy: **a** – strmo sklonené lavice zlepencov v záreze lesnej cesty (dokumentačný bod 92); **b** – detail drobnozrnného zlepenca s väčšími úlomkami kremenných obliakov (d. b. 92); **c** – kolmo vztýčené až mierne preklopené hrubolavicovité zlepence z lokality východne od k. Veľký Peterklin (d. b. 94) obsahujú polymiktný materiál z kryštalinika s klastami do 30 cm; **d** – detail drobnozrnného zlepenca s obliakmi ortoruly a kremeňa (d. b. 94); **e, f** – polymiktné zlepence z lokality jjz. od k. Klokoč (d. b. 208).
Fig. 4. The Peterklin Beds: **a** – deeply dipping conglomerate banks in the forest road rock-cut (documentation point 92); **b** – detailed view on fine-grained conglomerate with larger quartzose pebbles (d. p. 92); **c** – subvertical rudely bedded conglomerates contain polymict crystalline material up to 30 cm in scale, locality east of e. p. Veľký Peterklin (d. p. 94); **d** – detailed view to fine-grained conglomerate with large pebbles of ortogneiss and quartz (d. p. 94); **e, f** – polymict conglomerates localized SSW from e. p. Klokoč (d. p. 208).

nického potoka, Horné žliabky, 200 m na JJZ od k. 547, v ohybe lesnej cesty sa objavujú rozpadavé polymiktné zlepence ružovkastej farby s obliakmi veľkými do 10 cm.

D. b. 159 (N 48° 26,736′, E 17° 16,721′): *nižnobocianske súvrstvie*, v = 380 – 400 m n. m., v sutine sa nachádzajú sivé polymiktné zlepence, zaznamenali sme prítomnosť čiernych úlomkov.

D. b. 208 (N 48° 27.949′, E 17° 18,408′): *peterklinské vrstvy*, v = 485 m n. m., na JJZ od k. Klokoč, bloková sutina na svahu, typické polymiktné zlepence červenohnedých farieb, v okolí vyvetrané klasty obliakov.

D. b. 210 (N 48° 27,564′, E 17° 18,456′): *nižnobocianske súvrstvie*, v = 430 – 435 m n. m., južne od Klokoča, 680 m na S od k. 462 Mesačná, ľavá strana krátkej dolinky smeru S – J, 170 m na SV od k. 433, polymiktné zlepence svetlosivých farieb, piesčité zlepence, netriedený materiál, hrubozrnné arkózy s bielymi živcami + klastická sľuda, v sutine sú typické tmavosivozelené sľudnaté bridlice.

D. b. 224 (N 48° 26,440′, E 17° 13,083′): rozhranie *klokočské/peterklinské vrstvy*, v = 350 m n. m., jz. od k. Veľký Peterklin, 140 m na JJV od k. 408, hrubolavicovité piesčité zlepence, polymiktné zlepence až hrubozrnné pieskovce, ojedinele s klastami do 10 cm.

D. b. 274 (N 48° 28,052′, E 17° 20,482′): *nižnobocianske súvrstvie*, v = 365 m n. m., na miernej elevácii sú v sutine úlomky hrubozrnných arkóz (jeden úlomok s gradačným zvrstvením) a drobnozrnné zlepence, zložené najmä z kremeňa, svetlého živca a úlomkov hornín.

Petrografická charakteristika obliakového materiálu

Formovanie obliakového materiálu je ovplyvnené množstvom činiteľov – zložením zdrojových hornín, charakterom zvetrávania a reliéfu, transportom až po sedimentárno-diagenetické procesy. Skúmaný materiál je viac rezistentný a celkovo dobre opracovaný, svedčiaci o dynamike znosovej oblasti. Exponované prostredie vodných tokov poskytuje horšie podmienky na zachovanie mechanicky menej odolných horninových úlomkov, ako napríklad sľudnatých či ílovitých bridlíc. Pôvod študovaného obliakového materiálu, do ktorého neboli zahrnuté celkovo prevažujúce kremenné obliaky, možno na základe petrografického zhodnotenia zaradiť do týchto základných skupín: *kryštalinika,* pozostávajúceho prevažne z leukokratných granitických hornín, *kyslých vulkanických hornín*, menej zastúpené sú *sedimentárne horniny* klastického pôvodu alebo kremité horniny s nie vždy ujasnenou genézou.

Kryštalinikum

Dominantnú skupinu v študovanom petrografickom materiáli reprezentujú granitické horniny. V závislosti od odchýlok v primárnom minerálnom zložení a štruktúre, ako aj následných deformačných a látkových modifikácií možno spomedzi granitických hornín rozlíšiť viacero variet. Prevažujúci typ predstavujú všesmerné ***muskovitové leukokratné granity,*** kde obvykle prevažuje kremeň nad albitickým plagioklasom. Majú jednoduché minerálne zloženie, zvyčajne obsahujú málo sľúd a v mnohých prípadoch neobsahujú K-živec ani biotit. Prevažuje hypidiomorfná, miestami aj aplitická štruktúra, ojedinele sa objavil pegmatitoidný granit s granofyrickou štruktúrou. Muskovit a albitický plagioklas dosahujú veľkosť v priemere 1,5 – 2 mm, zrná kremeňa bývajú spravidla drobnejšie. V niekoľkých prípadoch je možné pozorovať porfyrický vývoj živcov dosahujúcich veľkosť 5 – 10 mm.

Typy granitov s prevažujúcou jemno- až strednozrnnou homogénnou štruktúrou majú priemernú zrnitosť 0,3 – 0,5 mm. Muskovitický granit (obr. 5a) má v porovnaní s vyhranenejšími leukokratnými typmi vyšší podiel muskovitu (kremeň > plagioklas > muskovit ~ K-živec) a typickú granitickú štruktúru. Podobné štruktúrne črty nesie aj zriedkavý *biotitický granit-granodiorit* s minerálnym zložením kremeň ≥ plagioklas > K-živec > biotit. Zrnitosť týchto hornín dosahuje v priemere 1,5 – 3 mm, s lokálnym vývojom výrastlíc K-živca a plagioklasu. K-živcové výrastlice miestami uzatvárajú plagioklas, samotný K-živec sa však často vyskytuje už len vo forme šachovnicového albitu. Na základe optických prejavov plagioklas vystupuje v dvoch generáciách. Relatívne staršie plagioklasy, na rozdiel od mladších, sa vyznačujú dobre obmedzenými

Obr. 5. Mikrosnímky leukokratných granitov až „ortorúl“ (vľavo neskrížené, vpravo skrížené nikoly): **a** – muskovitický granit – v spodnej časti koncentrácia sericitizovaného plagioklasu, hore mierne deformovaná doména kremeňa s muskovitom (vzorka 127); **b** – duktilne deformovaný leukokratný granit – najlepšie odolávajú premenám výrastlice K-živca (diagonálne orientované, tmavosivé, pri skrížených nikoloch) (vz. 94h); **c** – chloriticko-sericitická pseudomorfóza po granáte (čierne relikty pri skrížených nikoloch) v čiastočne deformovanej kremenno-živcovej hmote (vz. 94c); **d** – pseudomorfóza po granáte zatláčaná sericitom, chloritom a drobnými kryštálmi kremeňa (vz. 140, analýzy zvyškov granátu v tab. 1).

Fig. 5. Microphotographs of leucocrate granites and “ortogneisses” (left – parallel nicols, right – crossed nicols): **a** – muscovite granite – sericitized plagioclases aggregate at the bottom part; upper part shows weakly deformed quartz domain with muscovite (sample 127); **b** – ductile deformation of leucocrate granite – porphyric K-feldspar are the most resistant to deformation (diagonally oriented, dark grey at crossed nicols) (s. 94h); **c** – chlorite-sericite pseudomorph after garnet (black relics at crossed nicols) in partly deformed quartz-feldspar matter (s. 94c); **d** – pseudomorph after garnet replaced by sericite, chlorite and fine quartz crystals (s. 140, for garnet analyses see Tab. 1).

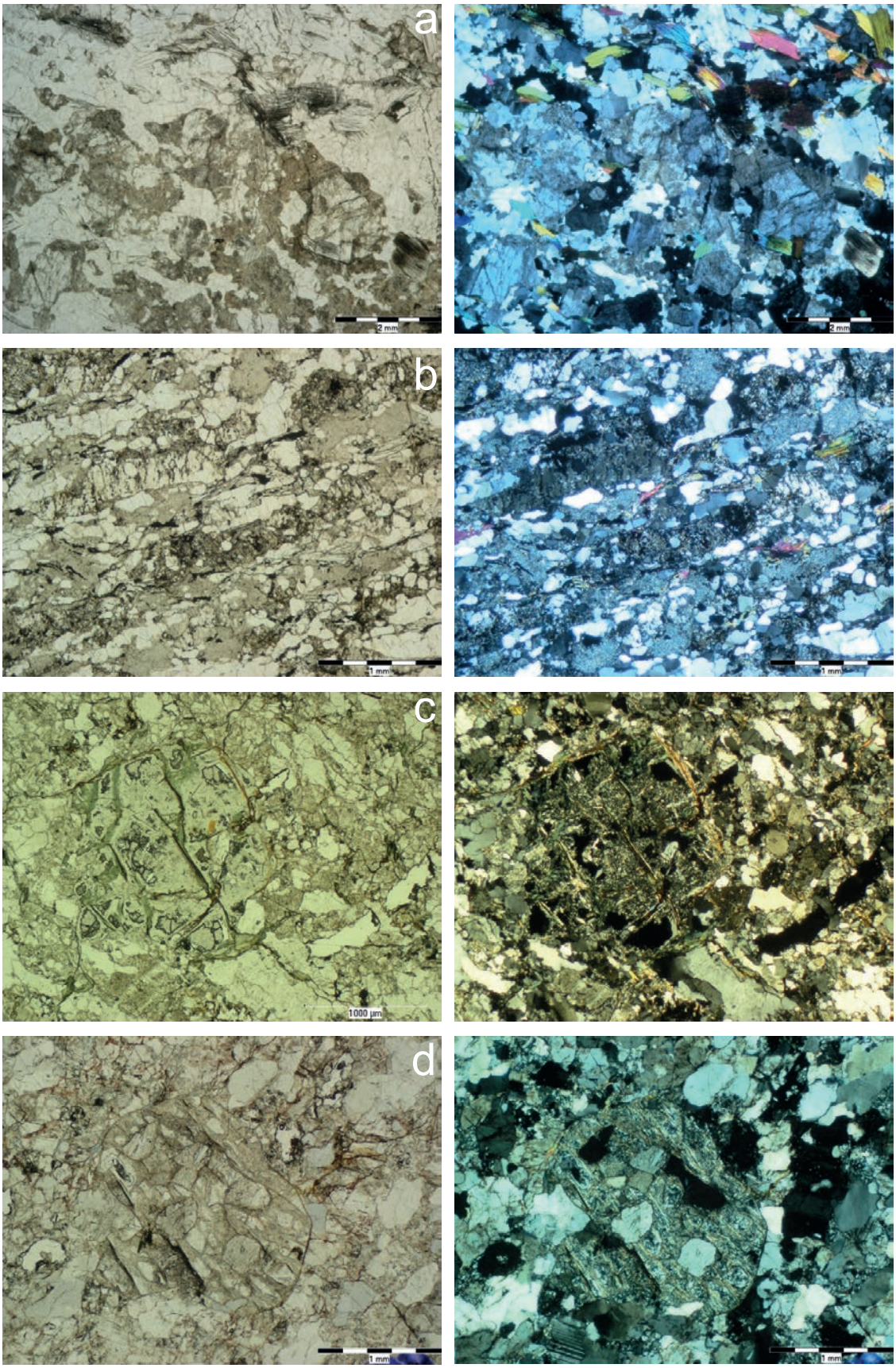
a
2 mm
2 mm
b
1 mm
1 mm
c
1000 µm
d
1 mm
1 mm

kryštálovými tvarmi. Živce, najmä plagioklasy, miestami vytvárajú charakteristické rastové agregáty (obr. 5a).

Skupina ***usmernených granitických hornín*** združuje viacero horninových typov, ktoré majú obdobné minerálne, čiastočne aj mikroštruktúrne parametre ako leukokratné granity. Pomerné minerálne zloženie hornín možno generalizovať takto: kremeň ≥ plagioklas > K-živec >> muskovit, biotit. Celkovo prevažuje hypidiomorfná zrnitosť s premenlivou veľkosťou zrna – niekedy je jemnozrnná (do 0,5 mm) a zároveň homogénna, inokedy je heterogénna, s rozsahom zhruba 0,3 – 2,5 mm. Prerasty živcových zŕn alebo ojedinelé uzavreniny plagioklasu v K-živci naznačujú magmatický pôvod. Plagioklas je zvyčajne sericitizovaný, na rozdiel od menej premeneného K-živca, ktorý býva po okrajoch albitizovaný vo forme „šachovnicového albitu“. Číry albitický plagioklas, asi produkt neskoršej kryštalizácie, nezriedka obsahuje drobný myrmekitický kremeň. V nevýznamnom množstve sú zastúpené sľudy – drobnolupeňový intersticiálny muskovit alebo biotit, spravidla premenený na chlorit.

Tieto horniny (obr. 5b) sa vyznačujú deformáciou sprevádzanou predĺžením kremenných a živcových zŕn za vzniku novotvoreného (rekryštalizovaného) drobného kremeňa a sľudy. Občas pozorujeme druhotne poohýbané výrastlice muskovitových lupeňov. Vytvára sa nepravidelná foliačná stavba s prejavmi deformácie v semiduktilných až duktilných podmienkach, pričom horniny nadobúdajú textúrne znaky pripomínajúce ortoruly. Leukokratná tavenina sa mohla formovať aj v procese injekčnej migmatitizácie v anizotropnom prostredí metamorfného substrátu a môže predstavovať leukosómovú zložku.

Osobitnú skupinu tvoria hrubšie zrnité *leukokratné ruly s granátom*, pričom horniny nesú znaky granitickej magmatickej štruktúry. Granát sa zachováva vo forme hypidiomorfne obmedzených pseudomorfóz veľkých okolo 2 mm a zložených z veľmi jemnozrnného sericitu (obr. 5c, d). Súčasťou pseudomorfóz býva novotvorený kremeň, v niektorých prípadoch tu vznikali aj jemné pukliny vyplnené chloritom – pennínom (tab. 1). Analýza ojedinelých reliktov granátu dokumentuje spessartínovo-almandínové zloženie (obr. 5d, tab. 1) naznačujúce jeho kryštalizáciu z reziduálnych fáz leukokratnej taveniny. Tvorba granátu a vyššieteplotná foliácia nemusia byť v príčinnom vzťahu, keďže existuje množstvo bezgranátových hornín s dobre vyvinutou usmernenou stavbou. Neskorej magmaticko-diferenciačnej genéze týchto hornín môže nasvedčovať aj hojný výskyt xenotímu, nezriedka aj monazitu v asociácii s akcesorickými minerálmi.

Z obliakového materiálu sa nepodarilo s istotou doložiť horniny peliticko-psamitického pôvodu, ktorým dáva zásadnú podobu metamorfné prepracovanie (fylity, svory, pararuly). Silno zbridličnatená jemnozrnná *plagioklasovo-kremitá rula* s muskovitom môže alternatívne predstavovať deformačný produkt aplitoidnej horniny.

Tab. 1

Mikrosondové analýzy zvyškov granátu v sericitovej pseudomorfóze a novotvoreného pennínu v usmernenej leukokratnej „ortorule“ (pozri obr. 5d); posledné 2 analýzy – ankerit asociujúci s chalcedónom (obr. 8).

Microprobe analyses (Cameca SX 100, SGIDS) of relic garnet in sericitized pseudomorph and newly-formed chlorite – pennine in banded leucocrate “orthoneiss” (see Fig. 5d); last analyses – ankerite from chalcedone silicite (Fig. 8).

	Granát		Chlorit	Karbonát	
Vz.	**MK-140**		**MK-140**	**MK-210A**	
SiO_2	37,03	36,82	36,36		
TiO_2	0,02	0,02	0,02		
Al_2O_3	20,58	20,32	32,73		
FeO_{tot}	25,48	29,64	3,29	13,25	14,91
MgO	0,41	0,59	14,12	10,48	9,27
MnO	14,69	10,39	0,04	0,81	0,80
CaO	1,83	1,86	0,09	29,07	28,08
Na_2O	0,06	0,01	0,00		
K_2O	0,01	0,00	0,19		
Total	100,11	99,65	86,84	53,61	53,06
	per 12 O		per 14 O	per 6 O	
Si	3,022	3,024	3,291		
Al IV.					
Al	1,979	1,967	3,492		
Ti	0,001	0,000	0,001		
Cr		0,001			
Mg	0,050	0,072	1,905	1,363	1,453
Fe^{2+}	1,739	2,036	0,249	1,329	1,311
Mn	1,015	0,723	0,003	0,081	0,071
Ca	0,160	0,164	0,009	3,226	3,164
Na					
K			0,022		
alm	58,7	68,0			
spes	34,2	24,1			
gros	5,4	5,5			
py	1,7	2,4			

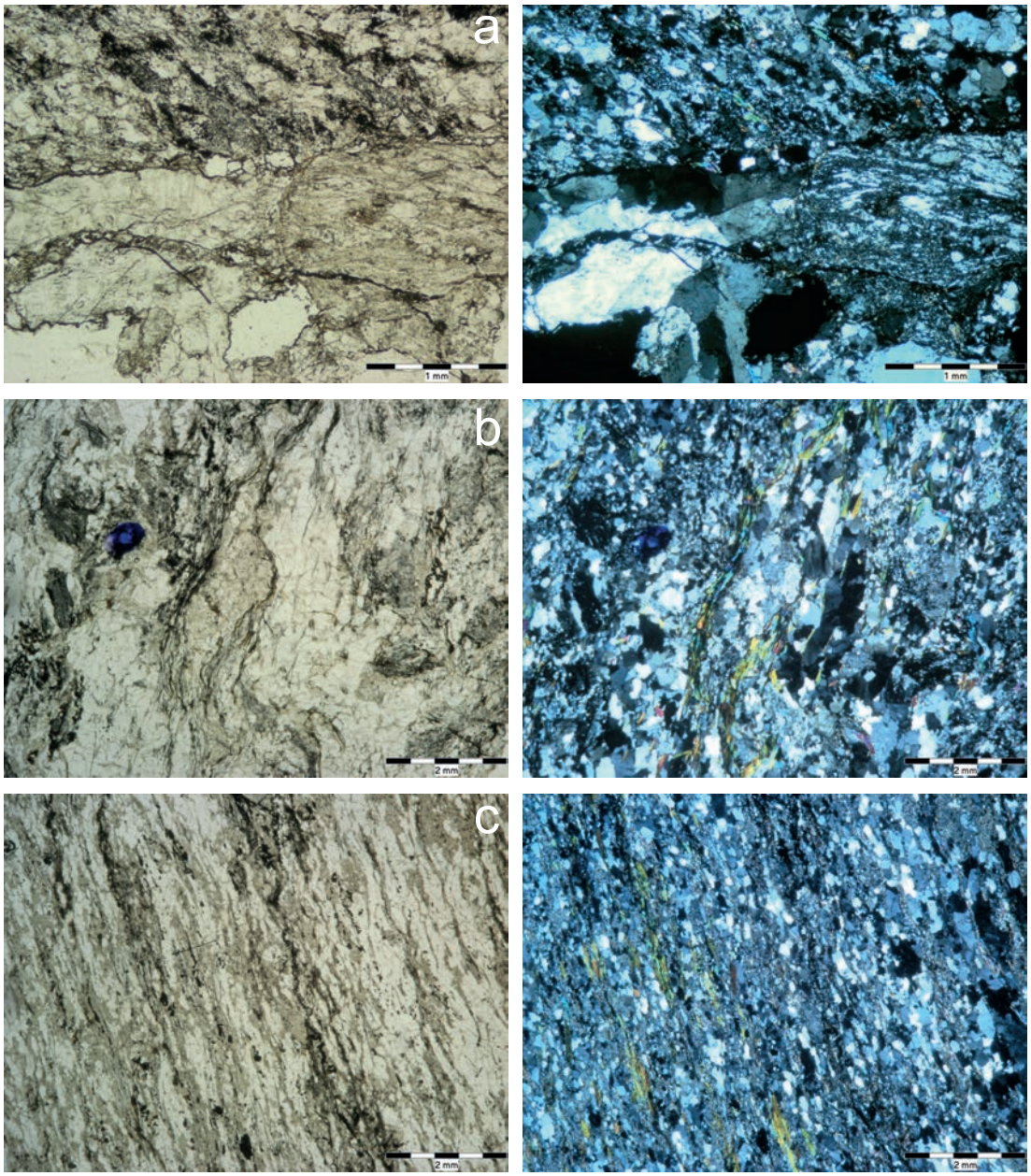

Obr. 6. Druhotne deformované leukokratné horniny: **a** – nepravidelne orientovaná diaftoretická deformácia sprevádzaná tlakovou rekryštalizáciou kremenných zŕn na jemné vláknité útvary (vpravo v strede) (vz. 210c); **b** – diaftoretická svetlá ortorula s reliktmi primárnej stavby; **c** – čiastočná rekryštalizácia muskovitu zo sericitu pozdĺž druhotnej bridličnatosti; pôvodná hrubozrnná štruktúra horniny je takmer zotretá (vz. 224a).

Fig. 6. Secondary deformed leucocrate rocks: **a** – irregularly oriented deformation accompanied with imposed recrystallization of quartz grains into fine fibre structure (on right side in the middle) (sample 210c); **b** – diapthorized light orthogneiss with relics of primary structure; **c** – partial recrystallization of muscovite from sericitic alterations along the secondary schistosity; the primary coarse-grained rock-structure is almost wiped off (s. 224a).

Druhotná deformácia a nízkostupňové metamorfné premeny

Granitoidné horniny, v menšej miere aj usmernené svetlé „ortoruly“, boli nezriedka postihnuté nízkotermálnymi premenami, ktoré sú zvyčajne sprevádzané aj krehkou, niekedy až krehko-duktilnou deformáciou (na rozdiel od živcov, kremeň má tendenciu duktilne rekryštalizovať na predĺžené zrná). V primárnej horninovej štruktúre sa vytvárali deformačné kremité prúžky („ribbony“), sprevádzané masívnou sericitizáciou živcovej hmoty a kataklastických zón. Premenám ľahko podlieha biotit, ktorý býva nahradený biotitom so zeleným pleochroizmom alebo vybieleným („baueritizovaným“) biotitom, nezriedka aj chloritom. Odmiešavaním rudnej zložky vznikajú zrnká hematitu, titanitu a leukoxénové fázy, občas ihličkový rutil. Ako druhotný akcesorický minerál sa objavuje epidot a zoisit.

K-živec odoláva týmto premenám spravidla lepšie, sericitizácia postupuje od okraja, zatiaľ čo v plagioklase býva sericitizácia celoplošná. Neobvyklú podobu získavajú lokálne alteračné produkty po K-živci, keď sa vyvíja ultrajemnozrnná svetlá hmota pripomínajúca jemnozrnnú felzitickú mikroštruktúru. Pri intenzívnych alochemických premenách živcov a ojedinelého granátu sa popri intenzívnej sericitizácii vyvíja aj veľmi jemnozrnný kremeň, lokálne aj chlorit.

Kataklastická deformácia postihuje zvyčajne celú horninu (obr. 6a, b). Vo viacerých prípadoch sa vyvíjajú aj úzke (asi do 1 mm) jemnozrnné mylonitové zóny, ktoré v prípade usmernených typov hornín prebiehajú často koso k dominujúcej vyššiestupňovej foliácii (obr. 6a). Z uvedeného nepriamo vyplýva, že *naložená deformácia má predalpínsky vek*. Nasvedčujú tomu aj rozmanité smery deformačných štruktúr obliakov, ktoré nemajú vzťah k sedimentárnej či alpínskej bridličnatosti mladopaleozoických hostiteľských sedimentov.

Z nižšiestupňových premien predstavuje krajný prípad hornina, ktorú možno petrograficky klasifikovať ako muskovitickú rulu. Otázka predmetamorfného pôvodu je zložitejšia, usudzujeme, že išlo o nejaký typ už opísanej leukokratnej granitickej horniny, neskôr prepracovanej do textúrnej podoby jemnozrnnej ruly. Daná rula (obr. 6c) má takéto minerálne zloženie: kremeň > sericitizovaný plagioklas > muskovit > opakové Fe minerály. Horninová štruktúra je vcelku homogénna – na základe poslednej deformačnej udalosti ju hodnotíme ako (lepido)-granoblastickú. Granoblastická zložka je jemnozrnná, s prevažujúcou zrnitosťou 0,2 – 0,3 mm, pričom sericitizovaný plagioklas dosahuje o niečo väčšiu veľkosť. Pre živce je charakteristická systematická sericitizácia, z ktorej sa v pokračujúcom metamorfnom procese vyvíjajú lupene muskovitu (obr. 6c).

Kremenno-živcová hmota javí prednostnú *semiduktilnú* orientáciu, jednotlivé zrná vytvárajú tzv. deformačné klasty. Novotvorený muskovit dosahuje maximálne 1 mm a kopíruje smer druhotnej metamorfnej bridličnatosti. Muskovit netvorí samostatné lepidoblastické pásiky, je takmer výlučne viazaný na sericitizovaný hostiteľský plagioklas. Keďže sericitizácia živcov v premenách kryštalických hornín je bežná, domnievame sa, že vo vyhranených strižných zónach došlo po úvodnej nízkotermálnej sericitizácii k metamorfnej rekryštalizácii muskovitu. Stupeň deformačného postihnutia a vývoj novotvoreného muskovitu naznačuje metamorfné podmienky stredného stupňa fácie zelených bridlíc a vyjadruje maximálne podmienky tejto naloženej tektonicko-deformačnej udalosti.

Sedimentárne a vulkanické horniny

Pieskovcové až mikrokonglomerátové obliaky odzrkadľujú litologický charakter zdrojovej oblasti a spolu s vulkanicko-sedimentárnymi horninami poukazujú na *intraformačnú príslušnosť*.

Klastické sedimentárne horniny možno s istotou identifikovať najmä pri hrubozrnnej polymiktnej povahe klastov, pretože pri viacerých jemnozrnných horninách bohatých na kremeň je v prípade naložených premien ťažké stanoviť, či ide primárne o sediment alebo o diaftorit kryštalinika. Nemetamorfované horniny obliakov zastu-

Obr. 7. Klastické sedimenty a kyslé vulkanity: **a** – polymiktný hrubozrnný pieskovec zložený z kremenných a živcových zŕn, litoklastov jemnozrnného silicitu (pri modrej bodke), kyslého vulkanitu (hnedý klast vpravo) a pod. (vzorka 94l); **b** – hydrotermálne alterovaný pieskovec(?) so žilkami ultrajemnozrnného kremeňa (vľavo) a hematitu (vpravo) (vz. 224b); **c** – kremitý arenit alebo premenená kremeňovo-živcová hornina z kryštalinika? (vz. 274, skrížené nikoly); **d** – úlomok svetlého drobnokryštalického felzitu je uzatváraný mierne devitrifikovaným vulkanickým sklom (vľavo) stýkajúcim sa s kyslým pyroklastikom (vpravo, vz. 94u, skrížené nikoly); **e** – usmernené vulkanické sklo (vľavo dole) a kyslý tuf (vpravo) sprevádza epiklastická zložka s hrubšou zrnitosťou (vľavo hore) (rovnobežné a skrížené nikoly).

Fig. 7. Clastic sediments and acid volcanites: **a** – coarse-grained polymict sandstone composed of quartz and feldspar grains, lithoclasts of fine-grained silicite (by the blue point), acid volcanite (brown on the right), etc. (sample 941); **b** – hydrothermally altered sandstone(?) with veinlets of ultra-fine quartz (left) and hematite silicite (on the right) (sample 224b); **c** – quartz arenite or transformed quartz-feldspar rock of crystalline basement? (s. 274, crossed nicols); **d** – small fragment od fine-crystalline felsite enclosed in weakly devitrified glass (on the left) on the contact with acidic pyroclastics (right, s. 94u, crossed nicols); **e** – oriented volcanic glass (left bottom corner) and acidic tuff (on the right) amalgamated with coarser-grained epiclastic matter (upper left corner) (planar and crossed nicols).

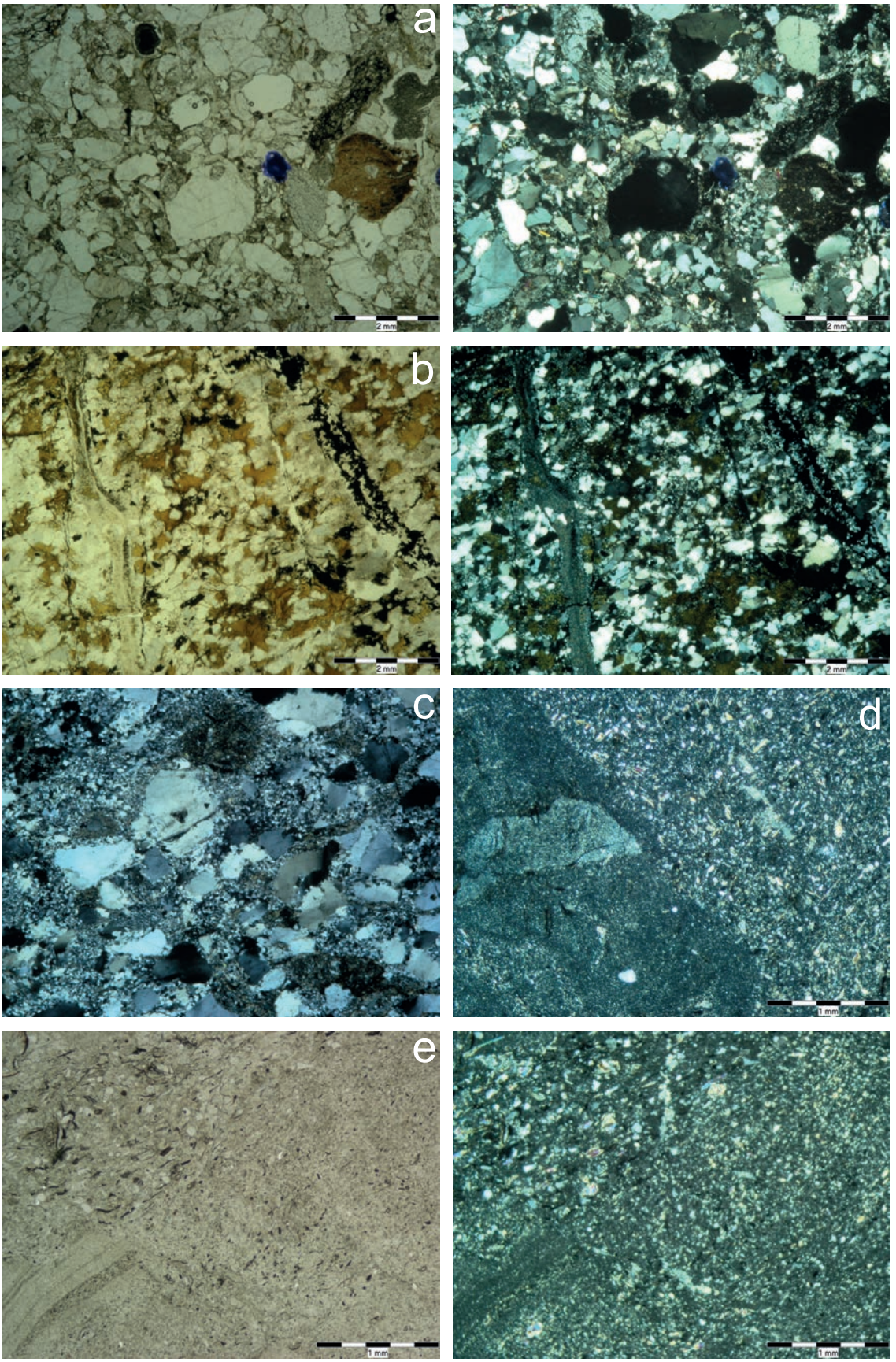
a
2 mm
2 mm
b
2 mm
2 mm
c
d
1 mm
e
1 mm
1 mm

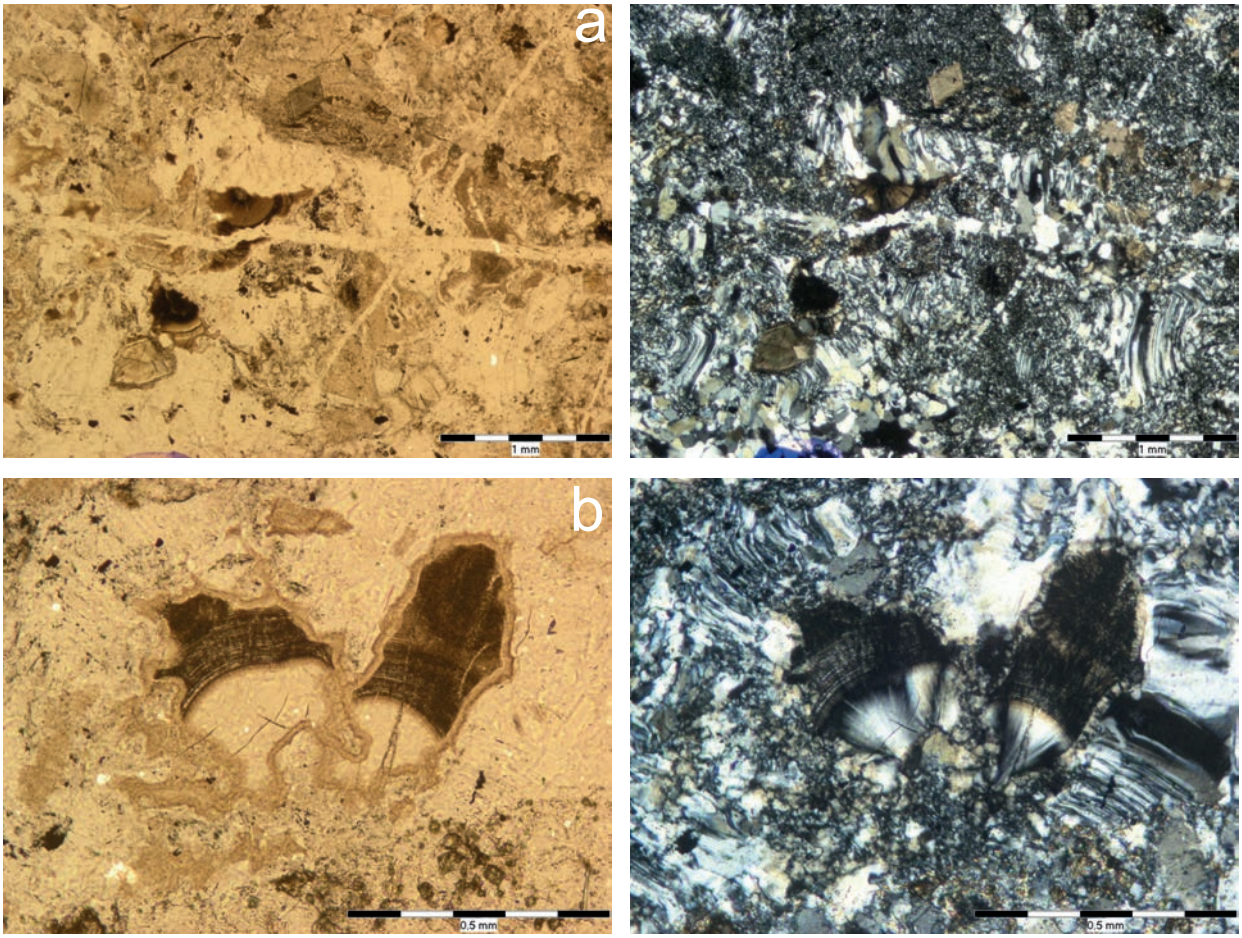

Obr. 8. Silicit s nízkotermálnou minerálnou paragenézou (rovnobežné a skrížené nikoly): **a** – jemnozrnná zakalená kremitá základná hmota (vrchná časť) so svetlými hniezdami chalcedónu a hnedých kryštálikov ankeritu (vz. 210a); **b** – v chalcedónovom útvare detail čírych lúčovitých vlákien chalcedónu (v strede snímky) dorastajúceho tmavým koncentrickým ankeritom.
Fig. 8. Low-thermal mineral paragenesis in silicite (planar and crossed nicols): **a** – beige fine-grained quartzite groundmass (upper part) with light chalcedony nest and fine brown ankerite crystals (s. 210a); **b** – detail of chalcedony nest: on light radial fibres of chalcedony (in the middle) grow up dark concentric ankerite.

pujú polymiktné hrubozrnné pieskovce, zložené z minerálnych a litických klastov v rôznom stupni opracovania. Okrem živcov, kremeňa a svetlej sľudy tieto pieskovce obsahujú litoklasty jemnozrnných kremencov, sericitických bridlíc, kyslých vulkanitov, ako aj fragmentov hornín rulovo-granitického pôvodu. Obrázok 7a ilustruje príklad horniny pozostávajúcej tiež z litoklastov sklovitej kyslej horniny podobnej vulkanitom, ktoré opisujeme ďalej. Pravdepodobne aj kremitý pieskovec s premenenými živcami nahradenými hnedými ílovými minerálmi (obr. 7b) predstavuje klastický sediment. V prípade určenia, či ide o kremitý arenit alebo blastomylonit kryštalinika (obr. 7c), zostáva pôvod neistý.

Jemnozrnné, zložito premiešané ***produkty kyslého vulkanizmu*** sú kvôli svojej rezistentnosti charakteristickou súčasťou obliakového materiálu. Niekoľko orientačných vzoriek bolo odobraných z peterklinských vrstiev, kde je prítomnosť vulkanických hornín príznačná. V horninovej kompozícii celkovo prevažuje jemnozrnný pyroklastický materiál zahŕňajúci aj sericit, ktorý sa pravdepodobne vytvoril ako diagenetický produkt premeny živcov. Obrázok 7d poukazuje na polyfázový vývoj kyslých vulkanických hornín – na zvlnenom kontakte sa stýka kyslý tuf (vpravo) s predpokladanou lapilou – vulkanickým sklom, uzatvárajúcim fragmenty jemnozrnnej felzitickej horniny (vľavo). Iná horninová doména obsahuje usmernenú sklovitú hmotu zmiešanú s veľmi jemnozrnným tufom (ignimbritom?) (obr. 7e, vľavo dole). Obsahuje aj klastickú prímes so zrnitosťou okolo 0,3 mm (vľavo hore na obr. 7e), kde lokálne pozorujeme aj väčší kremenný litoklast alebo poohýbaný klast muskovitu veľký až 2 mm. Takáto epiklastická litologická zložka býva usmernená a pozostáva z nerovnomerne opracovaného klastického kremeňa, živcov, drobných lišt muskovitu, Fe odmiešaných fáz, ako aj vulkanickej prímesi.

Pozoruhodný obliak z nižnobocianskeho súvrstvia predstavuje ***silicit*** *s chalcedónovými a karbonátovými útvarmi* (obr. 8). Vyše 95 % štruktúrne nehomogénnej horniny tvorí kremeň vystupujúci v rôznorodých podobách. V prevládajúcej jemnozrnnej kremitej hmote sa nachádzajú 3 až 5 mm veľké, morfologicky dobre vymedzené kremenné útvary predstavujúce rekryštalizovanú mikroštruktúru po chalcedóne (obr. 8a). (Nemožno celkom vylúčiť, že chalcedónové útvary sú pseudomorfózou po nejakom málo stabilnom mineráli – sadrovci?). Lamelované pásy kremeňa sú väčšinou rôzne pokrútené, v strede sa často nachádzajú veľmi jemnozrnné, hnedo zakalené agregáty chalcedónu, ktorý pripomína skôr rohovcovú štruktúru alebo rekryštalizovanú štruktúru po opáli(?). Tieto hnedasté chalcedónové agregáty sú zrejme staršie, ako to dokumentujú segmetované útržky, ktorých medzipriestory sú vyplnené čírymi, priečne usporiadanými vláknami kremeňa – taktiež najskôr rekryštalizovaným chalcedónom (obr. 8a). Inú mikroštruktúrnu formu chalcedónu reprezentujú radiálne vlákna (chalcedón II?; obr. 8b). Zhášajú rovnobežne, majú pozitívny (+) charakter minerálu a javia optickú zonalitu, najčastejšie v hnedastých a žltých odtieňoch.

Neoddeliteľnú súčasť horniny tvorí karbonatická zložka – ankerit (tab. 1) vystupujúci v podobe hnedých koncentrických či izometrických útvarov alebo vytvára drobné, nezriedka zonálne kryštály (obr. 8b). Na základe mikrosondovej identifikácie sa v hornine zistilo aj značné množstvo pyritových, barytových a xenotímových zrniek, ako aj jemná žilka galenitu. Táto mineralizácia spolu s vývojom chalcedónu svedčí o významnom pôsobení hydrotermálnych roztokov. Pravdepodobne aj základná hmota silicitu vznikla v dôsledku vyzrážania kremitých roztokov, zrejme viazaných na (post)vulkanickú aktivitu. Zachované zvyšky chalcedónu poukazujú na skutočnosť, že transformácia na vyššietermálnu modifikáciu kremeňa prebehla len čiastočne, čo dokumentuje veľmi nízke metamorfné podmienky. Toto z kandidatúry zdrojových hornín vylučuje hercýnsku metamorfno-magmatickú genetickú spojitosť a uprednostňuje predstavu o relikte z denudovaného vrchnokarbónskeho (karbónskeho?) vulkanického komplexu.

Málo zreteľnou ***puklinovou deformáciou*** boli postihnuté aj horniny sedimentárno-vulkanického pôvodu. Tenké a vcelku priame pukliny sú väčšinou vyhojené veľmi jemnozrnnou kremennou hmotou, miestami aj so zrudnením (obr. 7b, 8a). Táto deformácia má celkovo nižšiu intenzitu v porovnaní s opísanou penetratívnou kataklázou kryštalinika a je pravdepodobne aj mladšia. Domnievame sa, že ide o rané synsedimentárne pukliny preniknuté diagenetickými, prípadne hydrotermálnymi fluidami. Tieto horniny boli v priebehu vývoja vrchnopaleozoického bazénu redeponované a usadené v obliakovej forme.

Tektonogenetické aspekty a diskusia

Obliakový materiál, pozostávajúci predovšetkým z hornín bohatých na kremeň, svedčí o dynamickom režime vodných tokov, kde sa zachovávali odolnejšie typy hornín. Tieto horniny bývajú navyše v hojnej miere postihnuté deformáciou. Aj to môže prispievať k zriedkavému výskytu menej odolných sľudnatých metamorfovaných hornín. *Metamorfovaný plášť granitov* bol zrejme rýchlejšie dezintegrovaný a jeho piesčitý zvetraninový materiál sa uplatňoval v litologickom zložení vrchnopaleozoických klastických formácií.

V hroniku Malých Karpát sú *obliaky kyslých vulkanických hornín* rozšírené hojnejšie v permských usadeninách než vo vrchnokarbónskych. I keď táto situácia nemusí platiť generálne a existuje množstvo areálnych litologických odlišností (Vozárová a Vozár, 1988), otázka pôvodu kyslých vulkanitov nie je celkom ozrejmená. V nižnobocianskom súvrství sa občas vyskytujú drobné telesá syngenetického dacitového („kremité keratofýry“) až andezitového vulkanizmu (Vozárová, 1981; Kováčik, 2008), tie však svojou petrografickou povahou príliš nepripomínajú skúmané obliaky kyslých vulkanitov. Na druhej strane, v nižnobocianskom súvrství Malých Karpát sa vyskytujú polohy silicitov (Vozárová, 1981), ktoré mohli byť zdrojom opisovaného chalcedónového silicitu. V permských peterklinských vrstvách, na rozdiel od hojnejšieho výskytu kyslých vulkanitov, sme nezaznamenali obliaky takýchto silicitov. Vzhľadom na okolnosť, že obliaky kyslých vulkanitov predstavujú mechanicky odolný materiál a vyskytujú sa vo viacerých horizontoch, možno predpokladať ich diverzifikovaný zdroj. V prípade tohto obliakového materiálu v permskom súvrství nepovažujeme za vylúčené hľadať *primárny zdroj kyslého vulkanizmu* v susedných jednotkách, ako je napríklad horizont Harnobisu nachádzajúci sa v spodno- až stredno(?)permskom brusnianskom súvrství. Petrografický opis tohto vulkanogénneho horizontu (Vozárová, 1979) taktiež naznačuje viacero príbuzných znakov so skúmanými obliakmi. Pri predstave hlbšieho založenia hronického bazénu je možné uvažovať o istom prínose rezistentného materiálu aj z iných komunikujúcich vrchnopaleozoických vulkanicko-sedimentárnych bazénov.

Koreňové oblasti tzv. vrchného subtatranského príkrovu komentoval už Kettner (1927). Podľa neho leží južne od Hrona v pohorí Vepra alebo ešte ďalej. Tektonickou príslušnosťou a vekom melafýrových hornín na severných svahoch Nízkych Tatier a celkovo v Západných Karpatoch sa zaoberal Andrusov (1936). Jeho dovtedajšie znalosti ho viedli k poznaniu, že „poludnický príkrov“ nemožno zakoreniť v oblasti gemeríd. Roth (1938) rozoberal faciálne a tektonické otázky tejto oblasti. Poukazuje na faciálne odlišnosti vernárskeho a chočského pruhu a za pôvodnú sedimentačnú oblasť chočského príkrovu pokladá zónu

Kráľovej hole. Sedimentačná oblasť hronika sa v súčasnosti najčastejšie kladie do medzipriestoru veporika a gemerika (Biely a Fusán, 1967; Andrusov, 1968). Z iného pohľadu je koreňový systém hronika umiestnený do severnej oblasti gemerika (Maheľ, 1986).

V horninovom inventári skúmaných obliakov sa nepodarilo spoľahlivo preukázať horninové typy prislúchajúce ku gemeriku. Najskôr by sa mohli očakávať úlomky bázických a ďalších hornín severného pásma gemerika, prípadne porfyroidy, lydity a i. z gelnickej skupiny – teda podobné horniny, aké sa nachádzajú vo vrchnopaleozoických formáciách gemerika. Čierne kremité horniny sa síce objavujú v konglomerátoch (obr. 3), no takéto úlomky sa vyskytujú aj v iných jednotkách, napríklad v triasových siliciklastických horninách centrálnych Západných Karpát. V súvislosti s otázkou znosovej oblasti možno vysloviť predstavu, že vrchnopaleozoický hronický areál sa vyvíjal severne od ochtinského vulkanicko-sedimentačného priestoru a substrát hronickej panvy predstavuje tatroveporikum („slovenský blok“) – pohltená alebo tektonickým nadložím zakrytá časť kryštalinika, situovaná v dnešnom (alpínskom) ponímaní južne (juhovýchodne) od veporickej jednotky. Vrchnopaleozoický hronický bazén by sa z takéhoto pohľadu mohol umiestniť do blízkosti koreňovej oblasti *vernárskeho príkrovu* (definovaný Maheľom, 1986, v zmysle mezozoickej jednotky) s tým, že jeho predvrchnopaleozoický substrát najskôr nenáleží ku gemeriku ani k inej hypotetickej jednotke (napr. fundamentu ochtinského sedimentačného priestoru).

Na pôvodnú magmatickú alebo vysokoteplotnú, duktilne usmernenú horninovú štruktúru je často naložené *kataklastické až krehko-duktilné deformačné prepracovanie*, spojené s nízkostupňovými minerálnymi premenami (sericitizácia-muskovitizácia, chloritizácia). Deformačné podmienky, ale aj smerové usporiadanie foliačných plôch v obliakovom materiáli bolo rozmanité a nezávislé od vývoja bridličnatosti materských mladopaleozoických sedimentov hronika. To vylučuje úvahu o syngenetickom metamorfnom postihnutí spolu s hostiteľskými vrchnopaleozoickými sedimentmi. Všeobecne takéto premeny možno s väčšou istotou definovať len v obliakoch, pretože inde sa takáto deformácia stotožňuje s alpínskou metamorfózou, s ktorou má v podstate aj mnoho spoločných znakov. Interná deformácia obliakov svedčí v prospech neskorovariského deformačného prepracovania zdrojových hornín, ktoré sa odohrávalo v období približne po teplotnej konsolidácii variského kryštalinika a pred zapĺňaním vrchnopaleozoických panvových priestorov hronika alebo súbežne s ním.

Podľa všetkého ide o obdobu tzv. *variskej diaftorézy* v zmysle Kamenického (in Maheľ et al., 1967). Uvedomujeme si, že existujú domény kryštalinika (napr. Malá Magura, Považský Inovec alebo Malé Karpaty), kde druhotná deformácia kryštalinika nebýva taká výrazná a je ťažké ju prirovnávať k opísanej naloženej deformácii hornín obliakov. Vysvetlenie možno azda hľadať v tektonicky namáhaných zónach vrchnopaleozoickej (alebo len vrchnokarbónskej) tafrogenézy, kde došlo k pokročilej katakláze kryštalinika a vzdialené bloky kryštalinika nemuseli paušálne podliehať diaftoréze. Koncepcia o variskej diaftoréze bola v podstate definovaná zo štúdia vrchnokarbónskych obliakov v Považskom Inovci (Kamenický in Maheľ et al., 1967) a nie na základe sukcesie deformačno-metamorfných fáz priamo v kryštaliniku.

V netypickom silicite sa vytvárali hniezda vyplnené chalcedónom, ktorý občas sprevádza ankerit. Predpokladáme, že táto mineralizácia vznikala súbežne s chalcedónom z nízkotermálneho hydrotermálneho roztoku ako výsledok fluidnej aktivity vrchnokarbónskeho, viac-menej synsedimentárneho vulkanizmu. Tento proces bol sprevádzaný tektonickým nepokojom, ako nasvedčujú početné, zrejme extenzné mikroporuchy vyplnené novou generáciou jemného *chalcedónu*. Zachovaná nízkoteplotná paragenéza neumožňuje spájať túto horninu s prípadnými dozvukmi hercýnskeho granitoidného magmatizmu. Vývoj ankeritovej a asociujúcej sulfidicko(pyrit, barit, galenit)-fosfátovej (xenotím, monazit) *minerálnej paragenézy* možno v tomto prípade začleniť do *vrchnokarbónskeho metalogenetického obdobia*.

Záver

Zo skúmaného obliakového materiálu sa nepodarilo presvedčivo doložiť horniny gemerickej proveniencie, preto sa v otázke zdrojového materiálu malokarpatského mladšieho paleozoika hronika prikláňame k variským doménam južných častí kryštalinika vtedajšieho „tatroveporika“ (podložie blízke areálu neskôr štruktúrovaného „vernárika“?).

Druhotná bridličnatosť naložená na všesmerné alebo duktilne usmernené granitické horniny svedčí v prospech neskorovariskej deformácie („variskej diaftorézy“) – staršej alebo maximálne súvekej s vývinom vrchnopaleozoickej hronickej panvy. Je pravdepodobné, že táto, zväčša kataklastická deformácia sprevádzaná minerálnymi premenami v podmienkach nízkych častí fácie zelených bridlíc sa uplatňovala predovšetkým v zónach tektonogenézy vrchnopaleozoických paniev.

Metamorfovaný plášť granitov, ktorý sa v obliakovom materiáli takmer nenachádza, bol zrejme mechanicky menej rezistentný ako prevažujúce obliaky kremeňa a leukokratných granitov. Zriedkavé obliaky pieskovcov možno spoločne s hojnými obliakmi kyslých vulkanitov považovať za vrchnopaleozoické resedimentované hor-

niny. V prípade časti felzitických až sklovitých kyslých vulkanitov nevylučujeme ich redepozíciu zo susediacich vrchnopaleozoických areálov.

Pozoruhodný horninový typ predstavuje silicit, ktorý popri masívnej kremitej hmote pozostáva z chalcedónových útvarov, v menšej miere ankeritu, sulfidov a xenotímu. Nízkostupňová hydrotermálna genéza obliaka naznačuje metalogenetickú súvislosť danej mineralizácie s vrchnokarbónskym vulkanizmom.

Poďakovanie

Ďakujeme RNDr. Ľ. Hraškovi, PhD., RNDr. J. Madarásovi, PhD., a Ing. Z. Némethovi, PhD., za podnetné poznámky k manuskriptu, ktoré pomohli skvalitniť obsahovú aj formálnu stránku práce.

Literatúra/References

Andrusov, D., 1936: Subtatranské príkrovy v Západných Karpatoch. *Carpathica (Praha), 1, 3 – 50.*

Andrusov, D., 1968: Grundriss der Tektonik der Noerdlichen Karpaten. *Bratislava, Veda, Vyd. Slov. Akad. Vied, 188 s.*

Biely, A. & Fusán, O., 1967: Zum problem der Wurzelzonen der subtatrischen Decken. *Geol. Práce, Spr., 42, 51 – 64.*

Ďurovič, V., 1971: Sedimentárno-petrografický výskum vulkanogénno-sedimentárnej (melafýrovej) série centrálnych Západných Karpát. *Acta geol. geogr. Univ. Comen., Geol. (Bratislava), 23, 5 – 114.*

Kettner, R., 1927: Předběžná zpráva o dosavadních geologických výzkumech v Nízkých Tatrách. *Rozpr. Čes. Akad. Věd Umění, Tř. II (Praha), 4.*

Kováčik, M., 2012: Geologická stavba a metamorfóza vulkanicko-sedimentárneho pásma na sv. úpätí Kráľovej hole. *Miner. Slov., 44, 241 – 256.*

Kováčik, M. & Olšavský, M., 2012: Provenienčné štúdium obliakového materiálu mladšieho paleozoika hronika v Malých Karpatoch. *Miner. Slov., 44, 4, Geovestník, 17.*

Maheľ, M., 1986: Geologická stavba československých Karpát. Paleoalpínske jednotky 1. *Bratislava, Veda, 1 – 503.*

Maheľ, M., Kamenický, J., Fusán, O. & Matějka, A., 1967: Regionální geologie Československa, díl II, Západní Karpaty, sv. 1. *Praha, Academia, vyd. ČSAV, 496 s.*

Novotný, L., 1972: Sedimentológia a paleoprúdová analýza v perme chočskej jednotky medzi obcami Liptovská Teplička a Spišský Štiavnik. Rigorózna práca. *Manuskript. Bratislava, archív Št. Geol. Úst. D. Štúra, 86 s.*

Novotný, L. & Jančok, J., 1971: Sedimentologický výskum permských súvrství chočskej jednotky medzi Nižným Chmeliencom a Liptovskou Tepličkou. *Manuskript. Bratislava, archív Št. Geol. Úst. D. Štúra, 64 s.*

Olšavský, M., 2008: Faciálna analýza malužinského súvrstvia a jeho geologická stavba na SV svahoch Nízkych Tatier. Dizertačná práca. *Manuskript. Bratislava, archív Št. Geol. Úst. D. Štúra, 1 – 196.*

Polák, M., Kohút M., Elečko, M., Plašienka, D., Putiš, M., Bezák, V., Maglay, J., Olšavský, M., Havrila, M., Buček, S., Fordinál, K., Nagy, A., Hraško, Ľ. & Németh, Z., 2010: Geologická mapa regiónu Malých Karpát v mierke 1 : 50 000. Čiastk. záver. správa. Vysvetlivky ku geologickým mapám 1 : 25 000 listy: 35-313 Trstín, 34-424 Lakšárska Nová Ves, 34-442 Sološnica, 35-331 Smolenice, 34-444 Modra-Harmónia, 35-333 Častá, 34-443 Jablonové, 44-222 Pezinok, 44-241 Bratislava-Karlova Ves. *Manuskript. Bratislava, archív Št. Geol. Úst. D. Štúra, 384 s.*

Polák, M. (ed.), Plašienka D., Kohút M., Putiš M., Bezák V., Maglay J., Olšavský, M., Havrila, M., Buček, S., Elečko, M., Fordinál, K., Nagy, A., Hraško, Ľ., Németh, Z., Malík, P., Liščák, P., Madarás, J., Slavkay, M., Kubeš, P., Kucharič, Ľ., Boorová, D., Zlinská, A., †Siráňová, Z. & Žecová, K., 2012: Vysvetlivky ku geologickej mape regiónu Malé Karpaty 1 : 50 000. *Bratislava, Št. Geol, Úst. D. Štúra, 287 s.*

Roth, Z., 1938: Geologické poměry okolí Lučivné pod Vysokými Tatrami. *Rozpr. Čes. Akad. Věd Umění, Tř. II (Praha), 48, 13, 7 – 22.*

Tulis, J. & Novotný, L., 1998: Zhodnotenie geologických prác na U rudy v mladšom paleozoiku hronika v severnej časti Nízkych Tatier a Kozích chrbtov. *Manuskript. Bratislava, archív Št. Geol. Úst. D. Štúra, 144 s.*

Vďačný, M., 2013: Provenance of the Malužiná Formation sandstones (Western Carpathians, Slovakia): constraints from standard petrography, cathodoluminescence imaging, and mineral chemistry of feldspars. *Geol Quart. 57, 1, 61 – 72.*

Vďačný, M. & Bačík, P., 2015: Provenance of the Permian Malužiná Formation sandstones (Malé Karpaty Mountains, Western Carpathians): evidence of garnet and tourmaline mineral chemistry. *Geol. Carpath., 66, 2, 83 – 97.*

Vďačný, M., Vozárová, A. & Vozár, J., 2013: Geochemistry of the Permian sandstones from the Malužiná Formation in the Male Karpaty Mts (Hronic Unit, Western Carpathians, Slovakia): implications for source-area weathering, provenance and tectonic setting. *Geol. Carpath., 64, 1, 23 – 38.*

Vozárová, A., 1979: Litofaciálna charakteristika permu v severozápadnej časti veporika. *Západ. Karpaty, Sér. Mineral. Petrogr. Geochém. Metalogen. (Bratislava), 6, 61 – 116.*

Vozárová, A., 1981: Litológia a petrografia nižnobocianskeho súvrstvia. Západ. Karpaty, *Sér. Mineral. Petrogr. Geochém. Metalogen. (Bratislava), 8, 143 – 199.*

Vozárová, A. & Vozár, J., 1981: Litostratigrafická charakteristika mladšieho paleozoika hronika. *Miner. Slov. (Bratislava), 13, 5, 385 – 403.*

Vozárová, A. & Vozár, J., 1988: Late Paleozoic in the West Carpathians. *Bratislava, Geol. Úst. D. Štúra, 7 – 314.*

Vozárová, A., Konečný, P., Vďačný, M., Vozár, J. & Šarinová, K., 2014: Provenance of Permian Malužiná Formation sandstones (Hronicum, Western Carpathians): evidence from monazite geochronology. *Geol. Carpath., 65, 5, 329 – 338.*

Pebble-material of Hronic Upper Paleozoic sediments in the Malé Karpaty Mts. (Western Carpathians): petrogenetic and provenance aspects

During geologic mapping of the lower part of the Veterlín nappe (Olšavský in Polák, 2010), built of the Ipoltica Group sediments (Fig. 2), a collection of pebble material was taken (Fig. 3, 4). We have later petrographically studied about 40 thin-section samples of this material. The polymict material was taken mainly from the Petrklín Beds of Permian age and partially from the Nižná Boca Fm. of Late Carboniferous age.

The provenience studies of the source rocks of the Ipoltica Group (consisting of the Nižná Boca Fm. and Malužiná Fm., sensu Vozárová and Vozár, 1981) were addressed by further authors in the last century only marginally (Novotný and Jančok, 1971; Novotný, 1972; Vozárová, 1981; Vozárová and Vozár, 1988). Various petrographic varieties in pebbles have been identified, as well as their approximate percentages and interpretations of the source rocks providing clastic material were done. The more recent geochemical/geochronological studies, looking for the source area were focused on the Malužiná Fm. in the Malé Karpaty Mts. (Vďačný, 2013; Vďačný et al., 2013; Vozárová et al., 2014; Vďačný and Bačík, 2015).

Investigated pebble-material is rather resistant and generally well rounded, which indicates dynamic processing of the rock-fragments. An exposed environment during the water transport results in fewer opportunities for preservation of a softer mica- or clayey shists. Source rocks of the studied pebble material, which does not include the prevailing quartzitic pebbles, can be divided into following basic groups grounded on petrographic evaluation: basement rocks consisting mainly of leucocratic granitic rocks and acidic volcanic rocks. Sedimentary rocks of clastic origin or silicic rocks of not always clearly determined genesis are less common.

The secondary cleavage, overprinting the isotropic or ductile preferred orientation fabric in granitic rocks (Figs. 5 and 6) supports the concept of the Late Variscan deformation ("Variscan diapthoresis", sensu Kamenický in Maheľ et al., 1967) – which should be older or maximally coeval with evolution of the Upper Paleozoic Hronic basin. It is probable that this mostly cataclastic deformation, accompanied by mineral transformations under conditions of the lower part of the greenschist metamorphic facies, dominantly affected areas of the Upper Paleozoic (Upper Carboniferous?) basin tectonogenesis and it may not have expanded into the Tatro-Veporic crystalline, generally.

Rocks of the Gemeric provenance were not convincingly evidenced by means of petrographical pebble analysis. Therefore we are considering Variscan domains of a hidden/swallowed basement of "Tatro-Veporic" Unit, situated southerly (SE) of the present-day (Alpine) Veporic Unit basement to be the source material of the Upper Paleozoic Hronic Unit in the Malé Karpaty Mts. Paleotectonically, it is possible that the Upper Paleozoic Hronic Unit evolved northerly of the Ochtiná volcano-sedimentary area, probably in the vicinity of basement of the later structurated Mesozoic unit of Vernáricum (Vernár Nappe sensu Maheľ, 1986).

Metamorphosed mantle of the granitic rocks almost absents in the studied pebble material. We presume it was due to its smaller mechanical resistance than the dominant leucocratic granites have. Rare pebbles of sandstones and commonly present acidic volcanic pebbles (Fig. 7) may be considered as re-sediments of Upper Paleozoic age. It may be not ruled out, that a part of felsic and/or glassy acid volcanites could have been redeposited from juxtaposed Upper Paleozoic units into the Hronic basin.

A silicite, which besides the massive fine-grained quartzitic material, consists of chalcedony nests, as well as of a low percentage of ankerite, sulfides and xenotime, proves to be an interesting rock type present in the collected material (Fig. 8). The low temperature hydrothermal genesis of the pebble indicates a metallogenetic relationship of this mineralization with the Late Carboniferous volcanism.

Doručené / Received: 14. 12. 2017
Prijaté na publikovanie / Accepted: 19. 12. 2017

Mineralia Slovaca, 49 (2017), 141 – 156
Web ISSN 1338-3523, ISSN 0369-2086

Paleoecology of calcareous nannofossils from Paleogene formations of the Magura Unit in the Western Carpathians

KATARÍNA ŽECOVÁ

State Geological Institute of Dionýz Štúr, Mlynská dolina 1, SK-817 04 Bratislava, Slovakia;
katarina.zecova@geology.sk

Abstract: The main objective of this paper is to reveal how the calcareous nannofossils react to environmental changes at changed paleoecological conditions, which occurred during the Eocene/Oligocene transitional period. The calcareous nannofossils were identified and statistically evaluated in the time span from the Late Eocene to Early Oligocene.

The research results have demonstrated that the species *Coccolithus pelagicus* (Wallich) Schiller, *Coccolithus eopelagicus* (Bramlette et Riedel) Bramlette et Sullivan, *Reticulofenestra umbilica* (Levin) Martini et Ritzkowski and *Dictyococcites bisectus* (Hay, Mohler et Wade) Bukry et Percival enlarged their body dimensions as a response to changed paleoecological conditions. The reason for this effect was not just the cooling trend during the Late Eocene to Early Oligocene, but also eutrophication of the environment, supply of continental material, volcanic activity, as well as the presence of half-separated basin.

Based on evaluated biostratigraphic data, the relationships between the cold-water and warm-water species, as well as species present in the moderate tempered water, were statistically processed.

Key words: calcareous nannofossils, Late Eocene-Early Oligocene, biostratigraphy, paleoecology, Rača Unit, Zlín Formation, Krynica Unit, Malcov Formation, Magura nappe, Western Carpathians

Graphical abstract

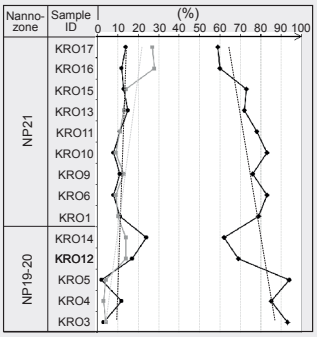

Percentage of individual taxons preferring different temperatures of the environment

- *warm-water species (WWS)*
- *temperate-water species (TWS)*
- *cold-water species (CWS)*

Highlights

- The Eocene and Oligocene were the periods of major changes in ocean water circulation and global climate.
- Enlarged body dimensions of several nannofossil species are a response to changed paleoecological conditions – cooling during the Late Eocene to Early Oligocene, and according to other authors, also to the eutrophication of environment, supply of continental material, volcanic activity and the change of nutritional conditions.

Introduction

The paper presents how the calcareous nannofossils react on changed paleoecological conditions during the Late Eocene and Early Oligocene. The study was focused on sedimentary rocks of the Tertiary Magura nappe – the Zlín Formation of the Rača Unit (the Krivá Oľka locality) and the Malcov Formation of the Krynica Unit (the Stuľany locality) in the region of the Nízke Beskydy Mts., located in the Flysch zone of the Outer Western Carpathians in the north-eastern Slovakia (Fig. 1). Recently this region underwent an extensive geological mapping and research, resulting in issuing of two new general geological maps at a scale 1 : 50 000 (Žec et al., 2011; Kováčik et al., 2012). During this research, as well as its further continuation in the project *Update of Geological Setting of Problematic Territories of the Slovak Republic*, the study of paleoecology of calcareous nannofossils from Paleogene formations of this region was done, being presented in this paper.

Brief review of the geological setting of the Nízke Beskydy region

In the Nízke Beskydy region, the Flysch zone is dominantly present in the Magura nappe, being a product of the Eocene and Early Miocene north-vergent thrusting (Fig. 1). From the southern side, the Magura nappe is bordered by the Klippen belt, and north-eastward it is thrust over the Dukla Unit (Fig. 1).

Based on lithofacial and lithostratigraphic differences, the Magura nappe is divided to three partial lithotectonic units (from the S/SW to N/ME): the Krynica, Bystrica

and Rača units (Fig. 1). Their lithotectonic characteristics, briefly reviewed in further text, were excerpted from the works of Žec et al. (1997, 2011) and Kováčik et al. (2012).

The Krynica Unit s.s. represents the southernmost located part of the Flysch zone, extending north-northeast of the Klippen Belt and consisting (from the footwall upwards) of the transitional formation (fine- to medium-rhythmic flysch sequences), Strihovce Fm., Inovce Fm., Menilite Fm. and Malcov Fm. All these formations are built of alternating flysch sediments - claystones to siltstones, sandstones, less abundant monomict and polymict conglomerates, as well as sporadic calcareous sediments and limestones. In the western part of the Nízke Beskydy region the Strihovce Fm. (E.-L. Eocene) is formed by several hundreds m thick complex of sandstones with interbeds of conglomerates and very small amount of claystones.

The Bystrica Unit, occurring in a narrow zone between the Krynica and Rača units, is represented from the south northward by the Beloveža Fm. (L. Paleocene–M. Eocene; variegated calcareous and non-calcareous, rarely silicified claystones, towards overlier more abundant sandstone facies occur) and the Zlín Fm. (M. to L. Eocene–calcareous claystones to marlstones with interbeds of glauconitic sandstones).

The Rača Unit, representing the northernmost lithotectonic unit of the Magura nappe, is divided by the Krivá Oľka tectonic line to inner and outer zones with lithofacial differences in the Zlín Fm. In the Outer Rača zone the glauconitic-sandstone lithofacies prevail and the sediments are more pelitic. The outer zone, located N/NE of the Krivá Oľka tectonic line, is built of Beloveža and Zlín fms.

The Inner Rača Unit, located south of the Krivá Oľka tectonic line, being more variegated than the Outer Rača zone, is characteristic with the Makovica sandstones in the lower part of the Zlín Fm.

Methodology

The sampled and studied Krivá Oľka and Stuľany profiles are situated in the Flysch zone of Magura nappe in the north-eastern Slovakia (Fig. 1). In the Krivá Oľka profile (49 07 47.44 N; 21 51 03.81 E; Figs. 2, 3 and 10) the grey-green to grey partly calcareous claystones of the Zlín Fm. of Rača Unit crop out. In the Stuľany profile (49 08 10.16 N; 21 23 40.37 E), the strongly calcareous claystones of brown-green colour crop out, as well as greenish grey to grey calcareous siltstones to claystones, dark grey calcareous claystones with fine disseminated mica and conchoidal disintegration, belonging to Malcov Fm. of the Krynica Unit.

Preparates for the research were pripared by classical decantation method (Haq and Lohman, 1976; Perch-Nielsen, 1985). Sample for the study of calcareous nannofossils was crushed and then poured into 200 ml of hydrogen peroxide (H_2O; 6-7 %) and allowed to stand for two days. Next it was stirred and boiled for 30 minutes with sodium bicarbonate $NaHCO_3$ (bicarbonate soda). After cooling, there was added the distilled water reaching a water column of 4.5 cm. The entire contents of the beaker was shortly stirred and allowed to sediment for 2-3 minutes. The water column was poured into a smaller beaker to a height of 4.5 cm, the coarse fraction was then removed. The sediment in the water column was stirred and left to stand for 45 minutes. After this time, the upper part was poured off and the coarsest fraction removed. We repeated this step until the brewed water became clean. After the last decantation, the beaker was filled with distilled water to the water column height of about 2 cm. We stirred it well. The suspension in the beaker was drawn into a pipette. The first 2-3 drops were removed by dripping and the residue was inserted on the microscope slide, Carefully torn into the square (the pipette must not touch the

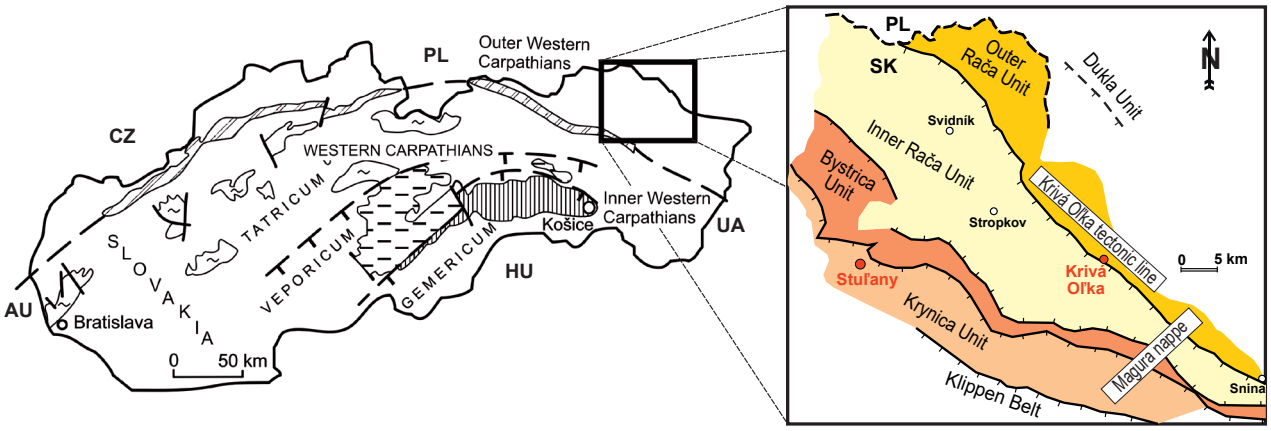

Fig. 1. The position of studied area in the tectonic scheme of the Western Carpathians (left) and location of sampling sites Stuľany and Krivá Oľka in the Krynica and Rača units of the Outer Western Carpatians.

glass) and allowed to dry. Then the Canadian balm was applied and the preparate overlapped with the cover glass. The preparations were studied applying the Axioscope 40 Carl Zeiss light microscope with magnification x1250 and documented with the Axiocam 105 color digital camera.

In paleochemical research, a quantitative analysis of nannofossil communities was performed, with recorded 500 specimens of each preparate. Data processing consisted of determining the number of individual species within the samples and their sorting, based on temperature conditions, changes in the size of the coccolith, nutrient content in the environment and autochtonity.

Subsequently, the shares of individual occurrences of observed species were deduced in terms of temperature conditions within individual samples. These shares were graphically displayed in the form of pie charts. These shares were then compared in the form of point correlation graphs to visualize the existence, resp. absence of relationship between species in different temperature conditions. Also, these shares were displayed in the form of vertical bar graphs to demonstrate a variation in the species abundance over time and its eventual trend, as well as to confirm hypotheses about relations at substitution of individual species at changed temperature conditions.

For the biostratigraphic classification of communities we used the Martini's zonation (1971).

Characteristics of the studied localities

The Krivá Oľka locality

Location, lithological characteristic and biostratigraphy

The quarry is situated south-east of the Krivá Oľka village. Outcropped beds belong to the Zlín Fm. of the Rača Unit of the Magura nappe (Fig. 2). Its perpendicular thickness is app. 32 m. The grey-green to grey variable calcareous claystones manifest significant prevalence over the sandstones. Sandstones are prevailingly fine-grained with well preserved gradation, horizontal, wavy and less moderately convolute lamination. The thickness of interbeds varies from 5 to 40 cm, rarely up to 150 cm. Coarser-grained sandstones are sporadically present at the base of thicker beds. The sandstone beds usually have the stable lateral thickness. The current traces or traces after towing objects in the stream indicate the paleocurrent direction from SSE to NNW.

Claystones are green, grey-green to grey, variable calcareous. They reach thickness of 0.5 to 10 m, sometimes even more. The significant predominance of claystone and character of lithofacies indicate their deposition from turbidity currents in the distal, northernmore part of the sedimentary system of the Magura basin, which was predominantly filled from the south and southeast.

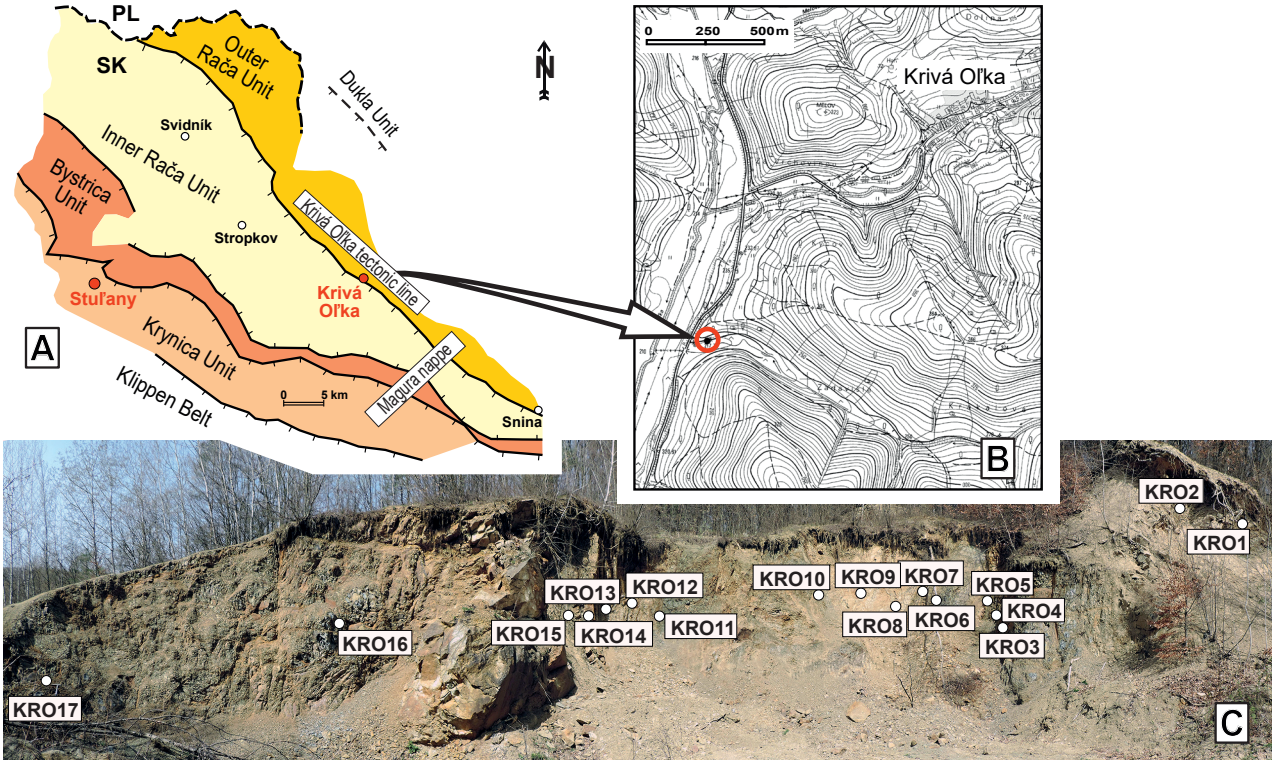

Fig. 2. Location of the quarry Krivá Oľka in the tectonic map of the Magura nappe (A), topographic map (B) and sampling sites on the quarry wall (C). The geological hammer positioned right of the sample KRO17 (left margin of the part C), long 40 cm, can serve as a scale for C.

The overthrust plane 260/65° with sinistral displacement (of ca 2 m) represents the dominating structural element in the central part of the quarry. The trend of the thrust plane corresponds with the bedding course north of the Krivá Oľka tectonic structure, which demonstrates its overthrust kinematics. Altogether 17 samples for the assessment of the calcareous nannofossils were taken from the quarry.

Paleoecological conditions

Based on the observation of calcareous nannofossils in the Krivá Oľka locality we can conclude that sedimentation of the Zlín Fm. took place during the Late Eocene with revealed zones NP 19/20 and NP 21. In the Table 1 the representation of each species is displayed.

In the vast majority of samples the poor and weakly diversified nannofossil communities have been found. The species of temperate marine environments predominated in them. The percentage of these species ranged from 59 % to 94 % (Fig. 3). The warm-water species in the communities were represented by 2-24 %, and the cold-water species by 3-28 %.

Obtained biostratigraphic data were evaluated and results were summarized in the graph (Fig. 4), expressing the interrelation of species that prefer different temperatures of the environment. From the graph, a distinctly negative relationship between the warm-water species (WWS) and those of the slightly temperate environment (TWS) is obvious in the lower part of the Late Eocene (NP19/20). This indicates the replacement of slightly temperate environment (TWS) species by the warm-water species (WWS), indicating a moderate warming of the environment.

In the higher part of the Late Eocene (NP21), the species of a moderately temperate environment (TWS) are replaced by the cold-water species (CWS), indicating the cooling of the environment (Fig. 4). The increase of the amount of cold-water species (CWS) is particularly noticeable in the nannofossil community present in samples KRO16 and KRO17.

The results are very similar to those of Oszczypko-Clowes et al. (2012), also indicating, on the basis of her research in the area of Leluchow in Poland, the negative relationship between warm-water species and the species of moderately tempered environment.

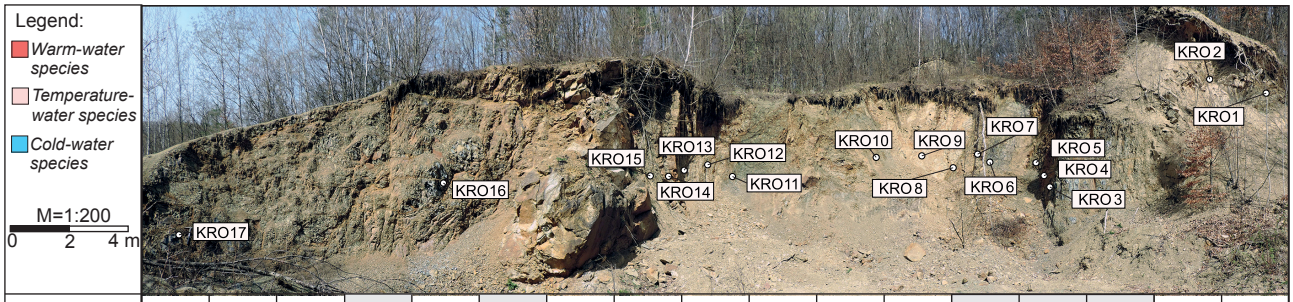

Sample ID	KRO17	KRO16	KRO15	KRO14	KRO13	KRO12	KRO11	KRO10	KRO9	KRO8	KRO7	KRO6	KRO5	KRO4	KRO3	KRO2	KRO1
Nanno-zone	Np21			NP19-20	Np21	NP19-20	Np21						NP19-20			Np21	
Proportion										N/A	N/A					N/A	
Percentage [%]	14 59 27	12 60 28	13 73 14	24 62 14	15 72 13	17 69 14	11 78 11	8 83 9	11 76 13	N/A	N/A	8 83 9	2 94 4	12 85 3	3 93 4	N/A	11 79 10

Fig. 3. Representation of individual species in relation on the temperature of the environment in the Krivá Oľka locality.

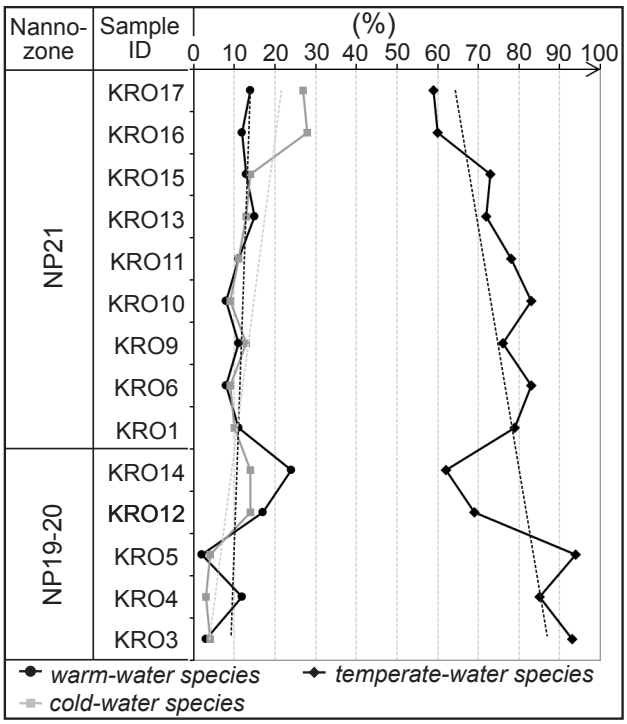

Fig. 4. Percentage of taxons of different temperatures of the environment.

Tab. 1
Representation of calcareous nannofossil species in the samples from the Krivá Oľka locality.

	KRO1	KRO3	KRO4	KRO5	KRO6	KRO9	KRO10	KRO11	KRO12	KRO13	KRO14	KRO15	KRO16	KRO17
Clausiococcus subdistichus													x	x
Coccolithus eopelagicus	x	x	x	x		x	x	x	x	x	x	x	x	x
Coccolithus pelagicus	x	x	x	x	x	x	x	x	x	x	x	x	x	x
Coccolithus formosus	x	x		x	x	x	x	x	x	x	x	x	x	x
Coronocyclus nitescens	x	x		x	x	x	x	x	x			x		
Corannulus germanicus	x					x								
Cribrocentrum reticulatum	x		x	x	x	x	x	x	x	x	x		x	x
Cribrocentrum coenurum		x		x	x									
Cruciplacolithus tenuis									x					
Cruciplacolithus sp.						x								
Cyclicargolithus floridanus	x	x	x	x	x	x	x	x	x	x	x	x	x	x
Chiasmolithus expansus											x			
Chiasmolithus grandis										x	x			
Chiasmolithus solitus														x
Chiasmolithus oamaruensis				x							x	x		x
Dictyococcites sp.				x		x	x							
Dictyococcites daviesii								x					x	x
Dictyococcites bisectus	x	x	x	x	x	x	x	x	x	x	x	x	x	x
Discoaster barbadiensis	x				x	x	x		x	x	x	x		x
Discoaster binodosus											x			
Discoaster deflandrei							x		x		x	x		
Discoaster lodoensis					x	x	x	x	x		x	x		
Discoaster mahmoudii							x							
Discoaster multiradiatus					x				x	x	x			
Discoaster nodifer							x							
Discoaster saipanensis	x	x			x	x	x	x	x	x	x	x		x
Discoaster septemradiatus												x		
Discoaster tanii					x	x				x	x			
Ellipsolithus macellus						x			x		x			x
Helicosphaera sp.												x		x
Helicosphaera compacta	x	x	x	x	x	x	x	x	x	x	x	x	x	x
Helicosphaera seminulum												x		
Helicosphaera wilcoxonii						x								
Isthmolithus recurvus	x	x	x	x	x	x	x	x	x	x	x	x	x	x
Nannotetrina sp.											x			
Lanternithus minutus	x		x	x		x				x	x	x	x	x
Neococcolithes dubius					x									
Pemma sp.								x	x	x				
Pontosphaera alta														x
Pontosphaera multipora						x					x			x
Pontosphaera exilis									x					
Prinsius martini											x			
Prinsius sp.		x	x	x	x	x	x	x	x	x		x	x	x
Reticulofenestra callida					x		x	x	x				x	x
Reticulofenestra dictyoda	x		x		x	x	x	x	x	x	x	x	x	x
Reticulofenestra hillae	x	x	x	x	x	x	x	x	x	x	x	x	x	x
Reticulofenestra umbilica	x	x	x	x	x	x	x	x	x	x	x	x	x	x
Reticulofenestra lockeri	x				x	x	x	x		x		x	x	x
Reticulofenestra oamaruensis	x				x		x	x						x
Reticulofenestra westerholdii		x		x										
Reticulofenestra sp.		x			x	x		x	x	x	x	x	x	x
Sphenolithus anarrhopus									x	x				
Sphenolithus moriformis	x	x	x	x	x	x	x	x	x	x	x	x	x	x
Sphenolithus pseudoradians						x								
Sphenolithus radians						x			x	x				
Sphenolithus spiniger											x			
Toweius eminens						x					x	x		
Toweius sp.										x	x			
Transversopontis obliquipons								x						
Tribrachiatus orthostylus						x								
Zygrhablithus bijugatus	x		x		x	x		x	x	x	x	x	x	x

A more detailed study of the relationship between the warm-water aand cold-water species has highlighted the fact that if the population of warm-water species (WWS) increases in number, the share of the cold-water species (CWS) also increases. This means that they are not mutually excluding each other, but the progress in the number of individual species will depend on the decline in the number of the moderately temperated environment (TWS), Fig. 5.

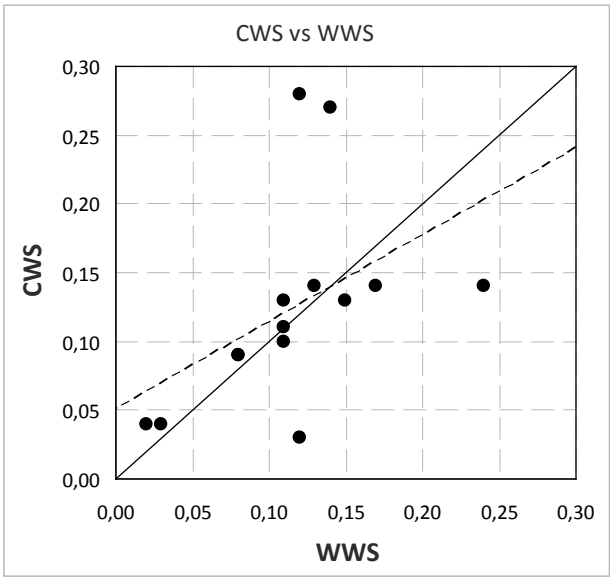

Fig. 5. Relation between the cold-watern and warm-water nannofossils populations in the Krivá Oľka locality.

If the environment has warmed up, then the number of species bound to moderate tempered environment (TWS) has lowered in the favour of warm-water species (WWS), Fig. 6.

Graph in Fig. 7, showing the relation of the moderate tempered environment species (TWS) to those of the cold-water species (CWS), documents that the cooling of the environment initiates the alternation of the species of moderate tempered environment (TWS) by the cold-water species (CWS).

Presented data show that the Paratethys cooling in the Late Eocene was also manifested by the nannofossil communities in the Krivá Oľka locality by a very small increase in the number of cold-water species (CWS).

The trend of the environment cooling during the Late Eocene and Early Oligocene was also manifested by the change in the size of the coccoliths. As a part of the research the coccolith sizes of the species *Coccolithus eopelagicus* (Bramlette et Riedel) Bramlette et Sullivan, *Dictyococcites bisectus* (Hay, Mohler et Wade) Bukry et Percival and *Reticulofenestra umbilica* (Levin) Martini et Ritzkowski were measured and the average values for individual samples were calculated (Fig. 8).

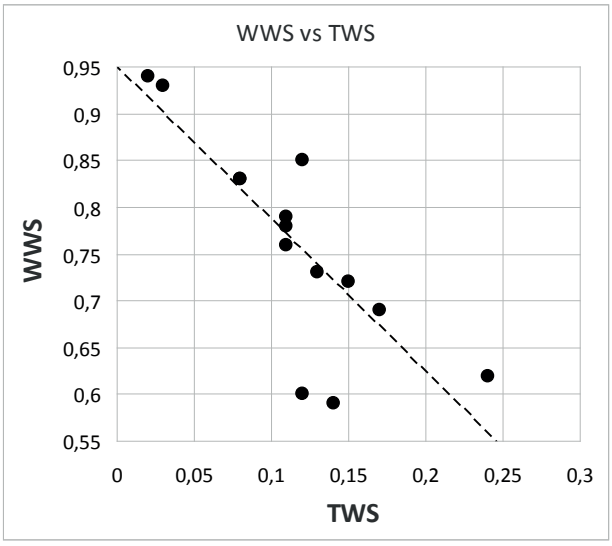

Fig. 6. Relation between the share of thermophilic species and those of moderate tempered environment in the Krivá Oľka locality.

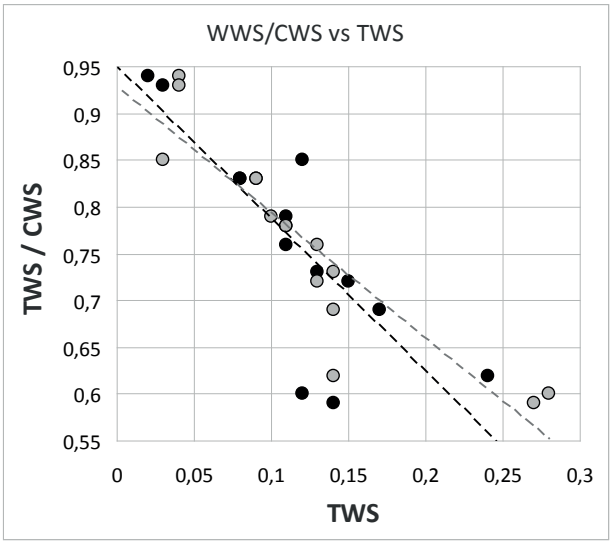

Fig. 7. Relation between the share of the cold-water (CWS) and moderate tempered environment species (TWS) in the Krivá Oľka locality.

The measured values manifest that the species *Dictyococcites bisectus* (Hay, Mohler et Wade) Bukry et Percival reached in NP 19/20 zone (Late Eocene) the dimensions from 8.7 µm to 9.5 µm. In the nannoplankton zone NP 21 (Late Eocene) it reached dimensions from 8.9 µm to 10.2 µm. This indicates that this species reached in the NP 21 zone a certain enlargement of the dimensions in comparison with the zone NP 19/20.

The *Coccolithus eopelagicus* (Bramlette et Riedel) Bramlette et Sullivan represents further observed species. It reached in the zone NP 19/20 dimensions from 11.2-13.9 µm and in zone NP 21 dimensions 11.4-14.2 µm.

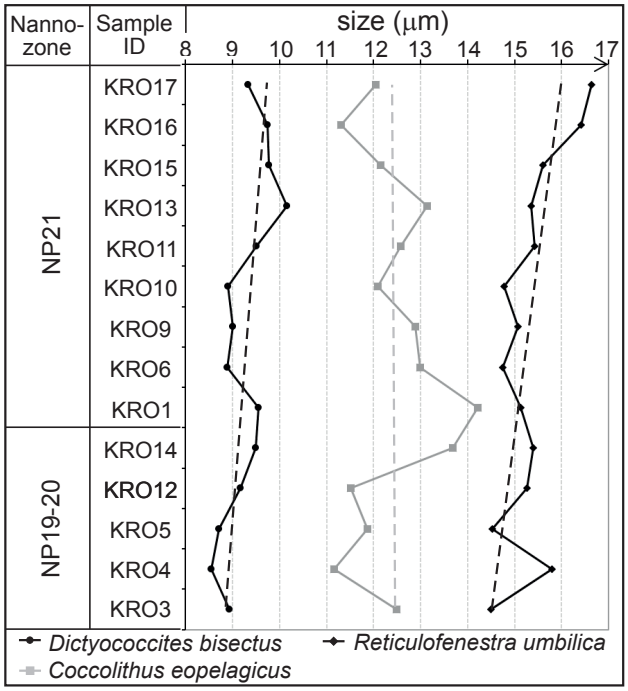

Fig. 8. Representation of species in individual samples in relation on their dimensions.

The individuals with the largest dimensions were reaveaded in the sample KRO1.

The last species with revealed change in the coccoliths size was a species of *Reticulofenestra umbilica* (Levin) Martini et Ritzkowski. This species, on the basis of the measured sizes, recorded the biggest changes. Its measured coccoliths sizes from the NP 19/20 zone samples ranged from 14.5 μm to 15.9 μm. In zone NP 21 the dimensions varied from 14.6 μm to 16.8 μm. In this zone a gradual increase in size of individuals of this species towards the hanging wall was observable (Fig. 8).

Evaluation of calcareous nannofossils concering to environmental conditions in the Krivá Oľka locality

Like the temperature, also the amount of nutrients in the marine environment is one of the most important factors affecting the distribution of calcareous nannoplankton in the Paleogene period (Aubry, 1992; Krhovský et al., 1992 and Villa et al., 2008). According to the work of Boresma et al. (1987) and Hallock et al. (1991), during the older Eocene the oligotrophic conditions prevailed in the euphotic zones of the oceans and the marginal seas. Subsequently, during the Middle and Late Eocene, the environment was gradually eutrophic due to cooling. In the course of the Late Eocene and Early Oligocene, conditions became more eutrophic, and the types of calcareous nannoplankton preferring the eutrophic environment are present.

However, some species may be adaptable to change in the nutritional values of the environment. As an example we can mention small forms of the species *Reticulofenestra*, capable of withstanding oligotrophic conditions, but only in a high nutrient environment. Similarly also *Zygrhablithus bijugatus* (Deflandre) Deflandre is a species adaptable to oligotrophic, as well as eutrophic conditions. Species preferring eutrophic conditions, being found in studied assemblages: *Chiasmolithus oamaruensis* (Deflandre) Hay, Mohler et Wade, *Chiasmolithus* sp., *Chiasmolithus expansus* (Bramlette et Sullivan) Gartner, *Chiasmolithus solitus* (Bramlette et Sullivan) Locker, *Coccolithus pelagicus* (Wallich) Schiller, *Cyclicargolithus floridanus* (Roth et Hay) Bukry, *Dictyococcites bisectus* (Hay, Mohler et Wade) Bukry et Percival, *Dictyococcites* sp., *Lanternithus minutus* Stradner, *Pontosphaera multipora* (Kamptner) Roth, *Reticulofenestra ornata* Müller, *Transversopontis pulcher* (Deflandre) Perch-Nielsen, *Transversopontis pulcheroides* (Sullivan) Romein and *Zygrhablithus bijugatus* (Deflandre) Deflandre, Villa et al., 2008.

The percentage of eutrophic species was evaluated in this work, since the eutrophic conditions at the Eocene/Oligocene boundary dominated, and species preferring these conditions should prevail in assemblages. Based on our assessments, we can conclude that the representation of eutrophic species does not correspond to the percentage of the cold-water species, which would characterize a significant cooling of the environment, as well as a change in its nutritional values.

Some change is observable in the samples KRO16 and KRO17, where the number of cold-water species, as well as, eutrophic species increases (Fig. 9). It is therefore probable that the cooling trend and changed nutritional conditions of the environment have been manifested in the Krivá Oľka locality during this period.

Occurrence of resedimented taxons in calcareous nannofossil assemblages in the Krivá Oľka locality

A typical phenomenon observable in nannofossil assemblages from Flysch zone sediments is a presence of both – autochthonous and resedimented species. This phenomenon is closely related to the dynamics of the environment during the sedimentation of flysch sequences in the deep-sea trogs.

During the quantitative analysis of species from individual samples, altogether 61 species were found, of which the percentage of autochthonous and resedimented species was calculated. Within the resedimented species, the percentage of Paleogene and Mesozoic resediments was also calculated and visualized (Fig. 9).

The most commonly represented autochthonous species: *Coccolithus pelagicus* (Wallich) Schiller, *Coc-*

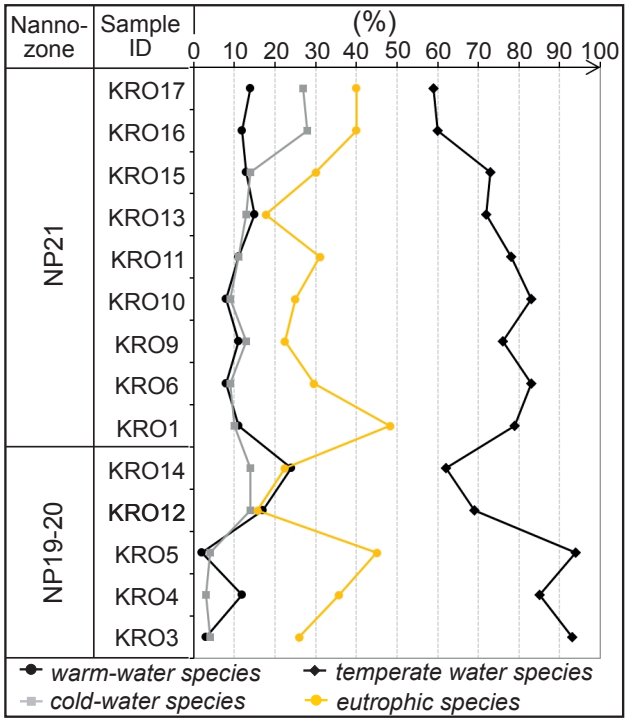

Fig. 9. Percentage of species bound to different temperatures of the environment and percentage of eutrophic species in the Kriva Ol'ka locality.

colithus eopelagicus (Bramlette et Riedel) Bramlette et Sullivan, *Cyclicargolithus floridanus* (Roth et Hay) Bukry, *Dictyococcites* sp., *Dictyococcites bisectus* (Hay, Mohler et Wade) Bukry et Percival, *Dictyococcites daviesii* Haq, *Discoaster deflandrei* Bramlette et Riedel, *Helicosphaera compacta* Bramlette et Wilcoxon, *Lanternithus minutus* Stradner, *Sphenolithus moriformis* (Brönnimann et Stradner) Bramlette et Wilcoxon, *Pontosphaera multipora* (Kamptner) Roth, *Reticulofenestra dictyoda* (Deflandre et Fert) Stradner, *Reticulofenestra umbilica* (Levin) Martini et Ritzkowski, *Sphenolithus radians* Deflandre, *Coronocyclus nitescens* (Kamptner) Bramlette et Wilcoxon and *Reticulofenestra lockeri* Müller.

The redeposited Paleogene species were *Cruciplacolithus tenuis* (Stradner) Hay et Mohler, *Chiasmolitus grandis* (Bramlette et Riedel) Radomski, *Discoaster multiradiatus* Bramlette et Riedel, *Discoaster barbadiensis* Tan, *Discoaster lodoensis* Bramlette et Riedel, *Discoaster saipanensis* Bramlette et Riedel, *Discoaster tanii* Bramlette et Riedel, *Ellipsolithus macellus* (Bramlette et Sullivan) Sullivan, *Neococcolithes dubius* (Deflandre) Black, *Prinsius martinii* (Perch-Nielsen) Haq, *Sphenolithus anarrhopus* Bukry et Bramlette and *Sphenolithus spiniger* Bukry. The percentage of redeposited Paleogene species ranged from 5 to 30 %.

A significant part of redeposited species was represented by Mesozoic ones, mainly by *Arkhangelskiella cymbiformis* Vekshina, *Biscutum* sp., *Broinsonia para constricta* Hattner, *Calculites* sp., *Cribrosphaerella ehrenbergii* (Arkhangelsky) Deflandre, *Eiffellithus eximius* (Stover) Perch-Nielsen, *Lucianorhabdus cauyexii* Deflandre, *Micula* sp., *Micula decussata* Vekshina, *Micranotlithus* sp., *Prediscosphaera cretacea* (Arkhangelsky) Gartner, *Retecapsa crenulata* (Bramlette et Martini) Grün, *Retecapsa surirella* (Deflandre et Fert) Grün, *Watznaueria barnesae* (Black) Perch-Nielsen, *Watznaueria* sp., *Watznaueria britannica* (Stradner) Reinhardt, *Watznaueria ovata* Bukry a *Zeugrhabdotus embergeri* (Noël) Perch-Nielsen. The percentage of redeposited Mesozoic species in assemblages ranged from 8 to 48 %.

The percentage of redeposited species indicates that this component represents a significant part of the nanofossil assemblages - in some samples it is more than 50 % of the assemblage (KRO1, KRO12, KRO13, KRO14 a KRO15), Fig. 10.

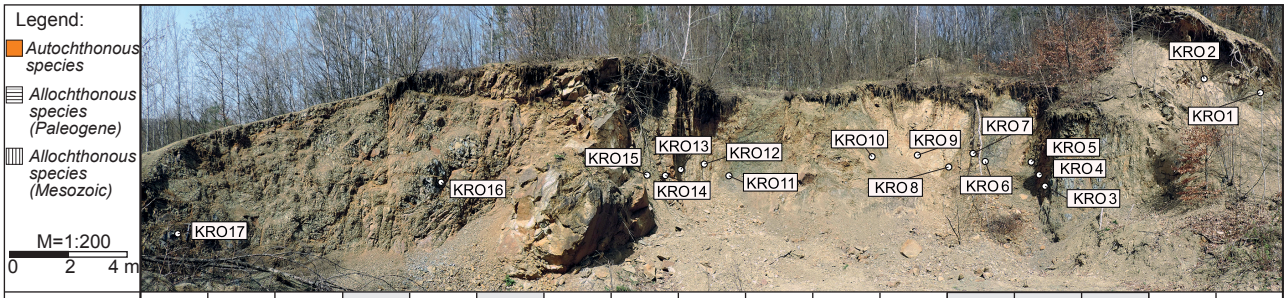

Sample ID	KRO17	KRO16	KRO15	KRO14	KRO13	KRO12	KRO11	KRO10	KRO9	KRO8	KRO7	KRO6	KRO5	KRO4	KRO3	KRO2	KRO1
Nanno-zone	NP21			NP19-20	NP21	NP19-20	NP21						NP19-20			NP21	
Proportion										N/A	N/A					N/A	
Percentage [%]	70 18 12	79 4 17	50 18 32	45 24 31	44 17 39	38 13 48	63 20 17	64 24 12	51 25 24	N/A	N/A	62 30 8	83 6 11	65 18 17	82 5 13	N/A	47 16 37

Fig. 10. Percentage of autochthonous and redeposited calcareous nannofossil species in the Krivá Ol'ka locality.

The Stuľany locality

From the locality, positioned ca 1.5 km to SW of the Stuľany village, built of Malcov Fm. of the Krynica Unit of the Magura nappe (Fig. 11), altogether 11 samples were taken for the evaluation of calcareous nannofossils.

The sedimentation of the Malcov Fm. in the locality Stuľany took part mainly in the zone NP 23, lower interbeds with samples STU 6 and STU 8 were enlisted to NP 21, Late Eocene, and samples STU 5 and STU 7 into the zone NP 22, Early Oligocene.

Table 2 presents the occurrence of individual species, found in nannofossils assemblages from the Stuľany locality.

In the sample STU 6 the species preferring the moderately tempered marine environment (76 %) have prevailed, the warm-water species represented only 3 % of the assemblage and cold-water species 21 %. Contrary to this, in the sample STU 8 the cold-water species dominated in the assemblage by 61 % representation, while the species of moderately tempered environment represented 35 % and the least abundant were warm-water species by 4 %.

In the samples STU 5 and STU 7 the least abundant were the warm-water species, in the sample STU 5 there prevailed cold-water species, forming 50 % and species of moderately tempered environment by 43 %. In the sample STU 7 these species formed the majoirty of the assemblage - 61 %, while the cold-water species 32 % and warm-water species only 7 % (Fig. 12).

In samples STU1-5 and STU 11 we have calculated the percentage of the species representation in relation on temperature. In samples STU 1 and STU 2 the species of the moderate tempered environment prevailed (58 % and 71 %). In assemblages the cold-water species (29 % and 22 %) were more abundant than the warm-water species (13 % and 7 %). In sasmples STU 3, STU 4, STU 5 and STU 11 the dominant were the cold-water species (53 %, 58 %, 50 % and 68 %). The second most numerous group represented the specie of moderately temperate environment (41 %, 37 %, 43 % and 28 %), and the smallest group represented the warm-water species (6 %, 5 %, 7 %, 4 %), Fig. 12.

Such composition of communities reflects changes in ecological conditions - cooling at the Eocene / Oligocene boundary. Similar results are reported in works by Mita (2001); Blaj (2009); as well as Persico and Villa (2004). In Slovakia, the research of changes in calcareous nannofossil assemblages at the Eocene / Oligocene boundary was done by Ozdínová (2013).

Graph (Fig. 13) shows the percentage representation of the species in relation on temperature. The relation between the shares of cold-water species (CWS) and the species of moderate tempered environment (TWS) is distinct in the graph. The share of these species over time shows inverse changes, indicating that the proportion of one nannofossil group is replaced by another, depending on the change in the temperature of the environment.

From a more detailed analysis of relationships between species bound to a different temperature of the environment, there is a significant, exclusive relationship between the CWS and TWS assemblages of species. This relationship points to the fact that the share of the cold-water species (CWS) increases at the expense of the species of moderately temperated environment (TWS). This means that the environment was cooled (Fig. 14).

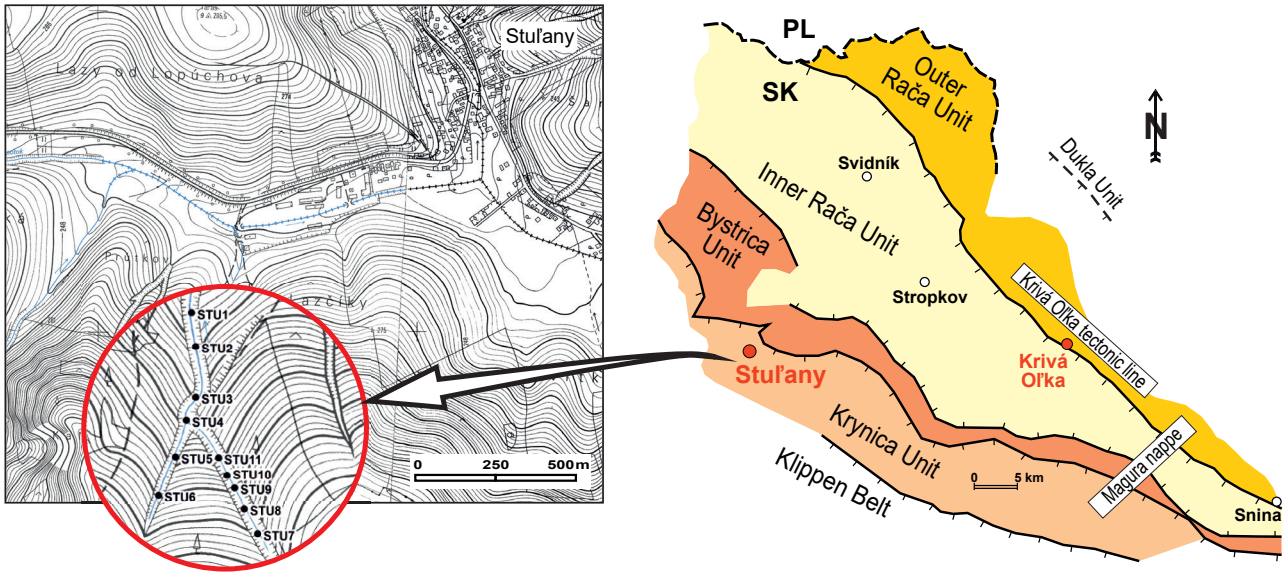

Fig. 11. Detail map of sampling sites in the branching tight valley localed ca 1.5 km to SW of the Stuľany village. The position of the map detail (red circle) on the basemap is in the centre of the circle.

Tab. 2
Calcareous nannofossils distribution in the Stuľany locality.

	STU1	STU2	STU3	STU4	STU5	STU6	STU7	STU8	STU11
Blackites spinosus			x	x	x			x	x
Clausiococcus subdistichus	x	x	x	x	x	x	x	x	x
Coccolithus eopelagicus	x	x	x	x	x	x	x	x	x
Coccolithus pelagicus	x	x	x	x	x	x	x	x	x
Coccolithus formosus		x	x		x		x		x
Coronocyclus nitescens	x	x	x	x	x			x	x
Cribrocentrum reticulatum	x	x	x	x	x			x	
Cribrocentrum coenurum				x					
Cruciplacolithus tenuis	x								x
Cyclicargolithus floridanus	x	x	x	x	x	x	x	x	x
Chiasmolithus eolatus					x				
Chiasmolithus oamaruensis	x					x			
Dictyococcites daviesii	x	x	x	x	x	x	x	x	x
Dictyococcites bisectus	x	x	x	x	x	x	x	x	x
Discoaster barbadiensis	x	x	x				x		x
Discoaster deflandrei	x								
Discoaster lodoensis	x	x							
Discoaster multiradiatus		x							
Discoaster saipanensis	x								
Discoaster tanii		x							
Helicosphaera alta	x								
Helicosphaera bramlettei	x		x	x	x		x		x
Helicosphaera compacta	x	x	x	x	x	x	x	x	x
Helicosphaera intermedia			x		x		x		
Helicosphaera lophota	x								
Helicosphaera papillata	x								
Helicosphaera euphratis	x								
Helicosphaera recta			x						
Helicosphaera reticulata			x						
Helicosphaera seminulum	x								
Isthmolithus recurvus	x	x	x		x		x	x	x
Lanternithus minutus	x	x	x	x	x	x	x	x	x
Neococcolithes dubius								x	
Orthozygus aureus					x	x	x	x	x
Pontosphaera alta				x					x
Pontosphaera enormis					x				
Pontosphaera multipora	x		x	x	x	x	x	x	x
Pontosphaera latelliptica	x						x	x	x
Pontosphaera rimosa	x								
Prinsius dimorphus		x							
Prinsius martini		x	x	x	x	x		x	x
Prinsius sp.							x		
Reticulofenestra callida	x	x	x	x	x	x	x	x	x
Reticulofenestra dictyoda	x	x	x	x	x	x	x		x
Reticulofenestra ornata	x	x	x	x	x		x		x
Reticulofenestra hillae	x	x	x	x	x	x	x		x
Reticulofenestra macmillanii									x
Reticulofenestra umbilica	x	x	x	x	x		x	x	x
Reticulofenestra lockeri	x	x	x	x	x	x	x	x	x
Reticulofenestra oamaruensis									x
Reticulofenestra sp.	x	x	x	x	x	x	x	x	x
Sphenolithus anarrhopus									
Sphenolithus moriformis	x	x	x	x	x	x	x	x	x
Sphenolithus radians			x						x
Transversopontis fibula	x	x	x	x					x
Toweius crassus				x					
Transversopontis pulcher			x					x	x
Transversopontis pulcheroides					x		x		
Zygrhablithus bijugatus	x	x	x	x	x	x	x	x	x

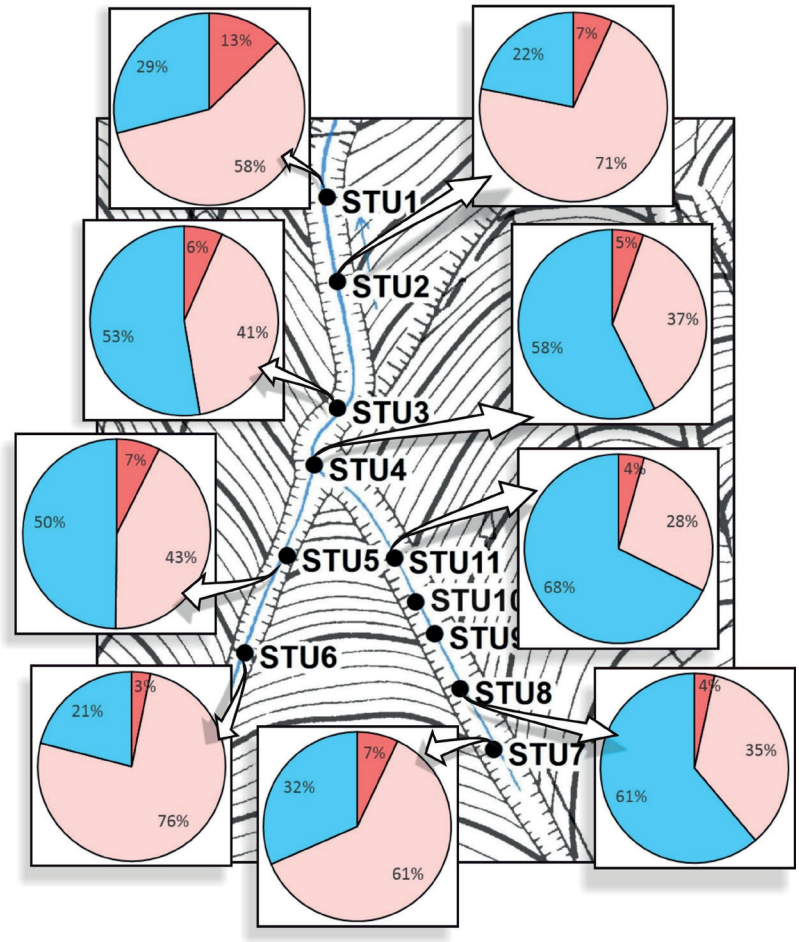

Fig. 12. Percentage representation of species in individual samples based on temperature, the Stuľany locality.

From the mutual comparison of the relationship between the warm-water species (WWS) and the moderately temperated species (TWS), there is a clear absence of a relationship between the share of the population of both groups of species (Fig. 15).

The non-existing relationship between shares of populations of cold-water species (CWS) and warm-water species (WWS) of calcareous nannofossils is shown in the graph (Fig. 16):

Similarly as in the Krivá Oľka locality, also in the Stuľany locality there were observed the changes of the coccolith dimensions in the case of species *Dictyococcites bisectus* (Hay, Mohler et Wade) Bukry et Percival and *Coccolithus eopelagicus* (Bramlette et Riedel) Bramlette et Sullivan.

The measured coccolith dimension of the species *Dictyococcites bisectus* in zone NP21 were 9.8 µm. In zone NP22 their ranged from 10.1 to 10.3 µm and in zone NP23 from 9.6 to 11 µm. The obtained values indicate that the largest increase in coccolith sizes of this species was in zone NP 23, namely in samples STU 3 and STU 1 (Fig. 17).

Similarly also a species of *Coccolithus eopelagicus* has registered a certain increase in coccolith size, namely in the nannoplankton zones NP22 and NP23 (Late Oligocene). In zone NP21 the coccoliths of this species reached dimensions from 11 to 11.2 µm, in zone NP22 it was 11.3 to 11.51 µm and in zone NP23 10.6 to 11.9 µm (Fig. 17).

Evaluation of calcareous nannofossils in terms of environmental conditions in the Stuľany locality

Eutrophic species from the Stuľany locality, similarly as those in the Krivá Oľka locality, did not manifest any distinct change in nutritional conditions. Some consistency is evident in the samples STU2 and STU3, where the increase of cold-water species is observabe, as well as the eutrophic species. It can indicate some cooling trend and certain change in nutrition conditions in the higher part of Early Oligocene in locality of Stuľany (Fig. 18).

The composition of autochthonous and resedimented species of calcareous nannofossils in the Stuľany locality

The presence of resedimented species in nannofossil assemblages was found also in samples from the Stuľany locality.

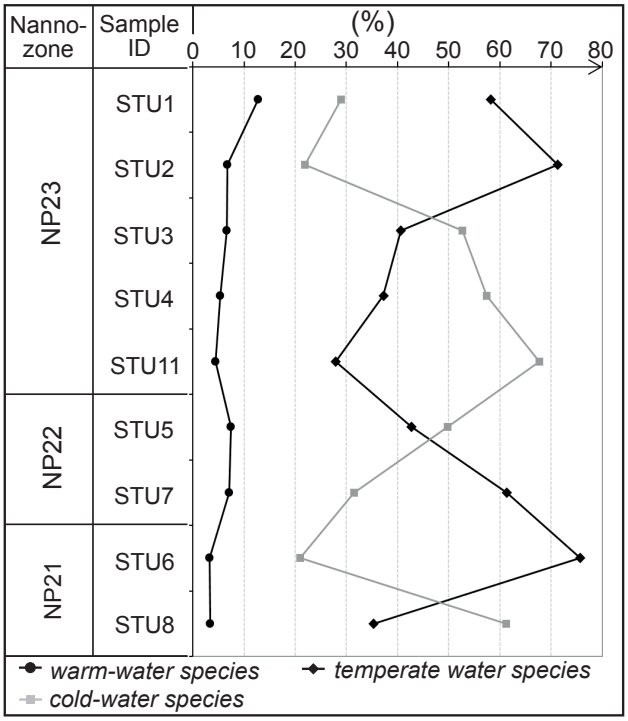

Fig. 13. Percentage representation of species according to temperature in the Stuľany locality.

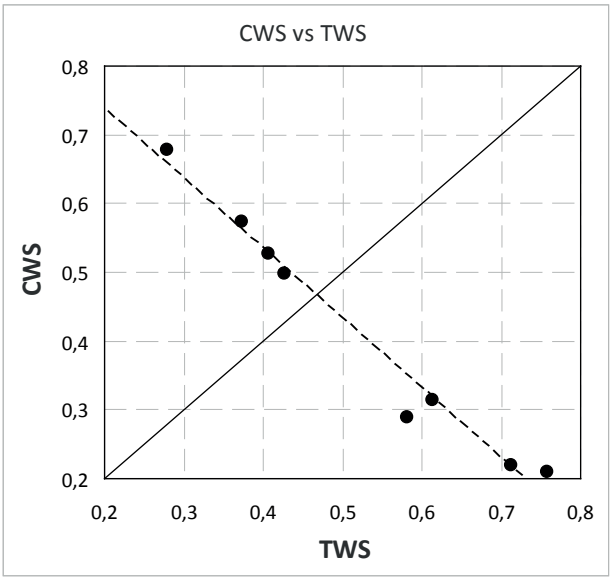

Fig. 14. The relation beween the share of cryophilic nannofossil population and that of moderately tempered environment in the Stuľany locality.

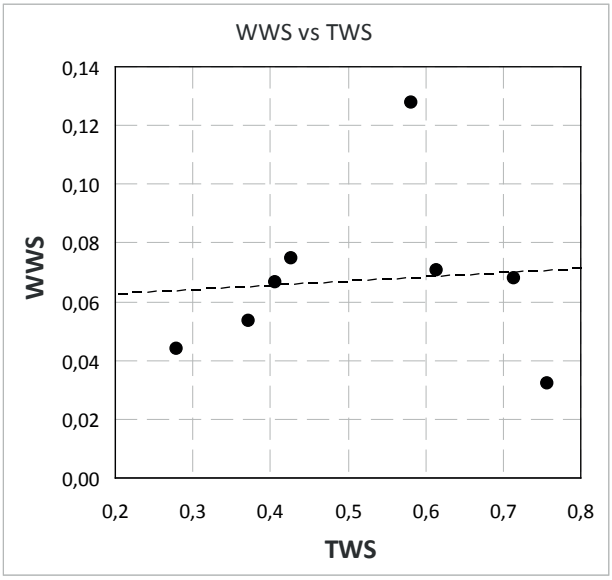

Fig. 15. The relation between the share of populations of the warm-water and moderately tempered environment species in the Stuľany locality.

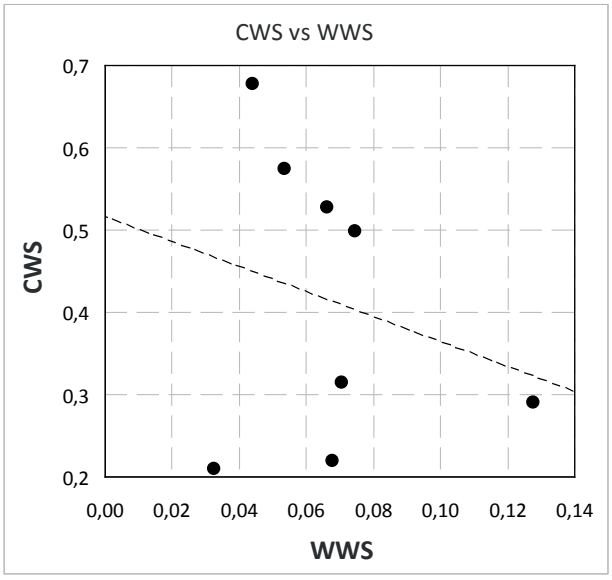

Fig. 16. The share of cold-water and warm-water nannofossil species in locality of Stuľany.

In revealed assemblages these species were present in amount of 38-62 %, from which the resedimented Mesozoic species represented 11-30 % and resedimented Paleogene species 23-33 % (Fig. 19). Relatively high percentage of resedimented species in nannofossil assemblages manifests the high activity of turbidite flows.

The most abundant resedimented species were *Cruciplacolithus tenuis* (Stradner) Hay et Mohler, *Discoaster barbadiensis* Tan, *Discoaster saipanensis* Bramlette et Riedel, *Discoaster lodoensis* Bramlette et Riedel, *Nanno-*

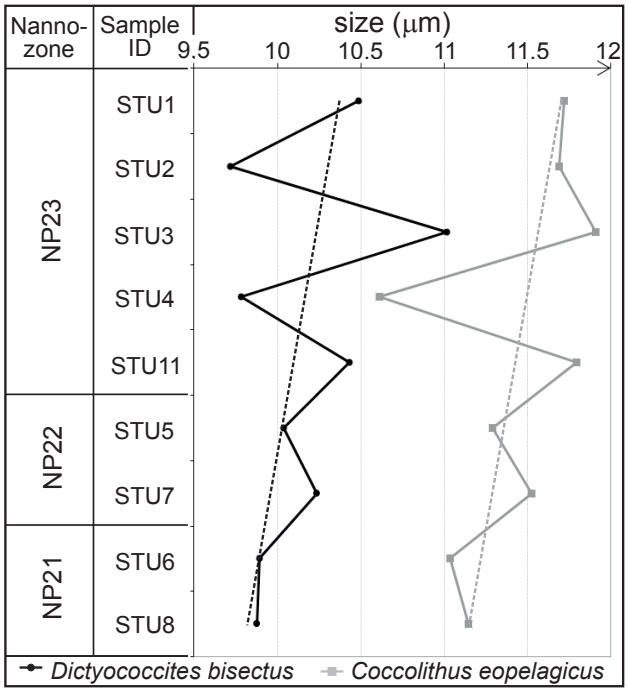

Fig. 17. The species average size values in locality of Stuľany.

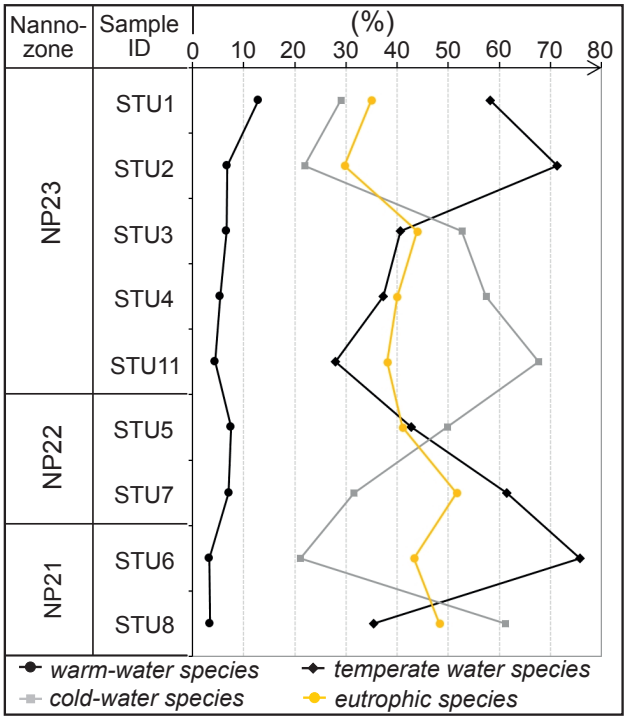

Fig. 18. Percentage of species bound to different temperatures of the environment and the percentage of eutrophic species in the Stuľany locality.

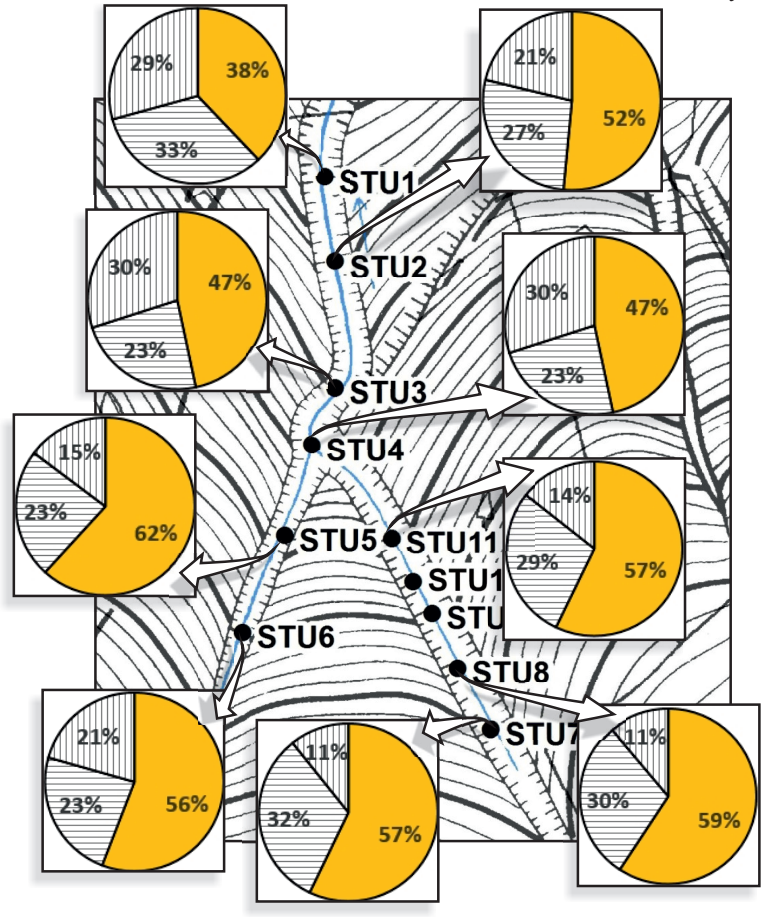

Fig. 19. Percentage representation of resedimented species in the Stuľany locality.

tetrina fulgens (Stradner) Achuthan et Stradner, *Helicosphaera seminulum* Bramlette et Sullivan, *Helicosphaera lophota* Bramlette et Sullivan, *Chiasmolithus expansus* (Bramlette et Sullivan) Gartner, *Ellipsolithus macellus* (Bramlette et Sullivan) Sullivan, *Helicosphaera papillata* (Bukry et Bramlette) Jafar et Martin and *Prinsius martini* (Perch-Nielsen) Haq.

The resedimented Mesozic species formed the smaller percentage in the nannofossil assemblages (11–30 %), being represented with *Arkhangelskiella cymbiformis* Vekshina, *Arkhangelskiella maastrichtiana* Burnett, *Biscutum* sp., *Braarudosphaera bigelowii* (Gran et Braarud) Def-landre, *Broinsonia parca constricta* Hattner, *Ceratolithina hamata hamata* Martini, *Cribrosphaerella ehrenbergii* (Arkhangelsky) Deflandre, *Eiffellithus eximius* (Stover) Perch-Nielsen, *Lucianorhabdus cauyexii* Deflandre, *Markalius inversus* (Deflandre) Bramlette et Martini, *Micula* sp., *Micula decussata* Vekshina, *Micula murus* (Martini) Bukry, *Micranotlithus* sp., *Microrhabdulus decoratus* Deflandre, *Prediscosphaera cretacea* (Arkhangelsky) Gartner, *Retecapsa crenulata* (Bramlette et Martini) Grün, *Retecapsa surirella* (Deflandre et Fert) Grün, *Watznaueria barnesae* (Black) Perch-Nielsen, *Watznaueria* sp., *Watznaueria britannica* (Stradner) Reinhardt, *Watznaueria ovata* Bukry and *Zeugrhabdotus embergeri* (Noël) Perch-Nielsen.

From autochthonous Paleogene species the most abundant were *Lanternithus minutus* Stradner, *Dictyococcites bisectus* (Hay, Mohler et Wade) Bukry et Percival, *Dictyococcites callidus* Perch-Nielsen, *Reticulofenestra umbilica* (Levin) Martini et Ritzkowski, *Reticulofenestra lockeri* Müller, *Clausiococcus subdistichus* (Roth et Hay) Prins, *Coccolithus formosus* (Kamptner) Wise, *Coccolithus eopelagicus* (Bramlette et Riedel) Bramlette et Sullivan, *Cyclicargolithus floridanus* (Roth et Hay) Bukry, *Helicosphaera compacta* Bramlette et Wilcoxon, *Helicosphaera recta* (Haq) Jafar et Martini, *Blackites spinosus* (Deflandre et Fert) Hay et Towe, *Isthmolithus recurvus* Deflandre, *Coronocyclus nitescens* (Kamptner) Bramlette et Wilcoxon, *Zygrhablithus bijugatus* (Deflandre) Deflandre, *Sphenolithus moriformis* (Brönnimann et Stradner) Bramlette et Wilcoxon, *Sphenolithus radians* Deflandre, *Transversopontis fibula* Gheta, *Dictyococcites daviesii* Perch-Nielsen, *Reticulofenestra* dictyoda (Deflandre) Stradner, *Helicosphaera euphratis* Haq, *Discoaster tanii* Bramlette et Riedel, *Pontosphaera latelliptica* (Báldi Béke et Báldi) Perch-Nielsen, *Pontosphaera multipora* (Kamptner) Roth, *Reticulofenestra hillae* Bukry et Percival, *Chiasmolithus oamaruensis* (Deflandre) Hay, Mohler et Wade, *Helicosphaera bramlettei* Müller, *Discoaster deflandrei* Bramlette et Riedel, *Transversopontis obliquipons* (Deflandre) Hay, Mohler et Wade and *Coccolithus pelagicus* (Wallich) Schiller. Percentage of autochthonous species in nannofossil assemblages varied in the range of 38-62 %.

The research of resedimented species in Poland was partly done by M. Oszczypko-Clowes (Oszcypko-Clowes & Żydek., 2012), studying the nannofossil assemblages of the Malcov Formation of the Krynica Unit of Magura nappe in the area south of Leluchow. The author (l.c.) based on study of the nannofossil assemblages revealed than the percentage of resedimented species of the Malcov Formation represents ca 31.35 %. In comparison with our research, the data found by Oszczypková have demonstrated a smaller amount of resedimented species in the areas she was studying. It manifests a smaller activity of turbuditic currents in the Early Oligocene in the Leluchow area (Oszczypko-Clowes et al., 2012).

Conclusion

The found assemblages of calcareous nannofossils in localities Krivá Oľka and Stuľany were distinctly depleted. Low diversity of species was typical for the majority of assemblages. This phenomenon is typical for the Late Eocene and Early Oligocene period. The significant part of the assemblages was formed also by the species of moderately tempered environment.

Based on research of the calcareous nannofossil assemblages in the Krivá Oľka locality we can conclude that the Zlín Formation sedimentation took part during Late Eocene in the zones NP 19/20 and NP 21.

The found data manifest the fact that no more significant increase of the cold-water species was in the Late Eocene in the Krivá Oľka locality, the strongest cooling was reflected in the samples KRO16 and KRO17 (NP21). In these samples the biggest share of cold-water species was registered.

The environment cooling trend during the Late Eocene and Early Oligocene was manifested also by the change of the coccolith dimensions, being registered in the case of the species *Coccolithus eopelagicus*, *Dictyococcites bisectus* and *Reticulofenestra umbilica*.

Similarly as in the Zlín Formation of the Rača Unit in the Krivá Oľka locality, also in the Malcov Fm. of the Krynica Unit in Stuľany locality the species bound to moderately tempered environment (TWS) formed the significant part of the assemblage. The results of the nannofossil assemblages study indicate the distinct relation between the population shares of cold-water species (CWS) and those of moderate tempered environment (TWS). The share of the populations of these species in time shows the inverse changes, which indicates the replacement of the share of one group by another in relation to the change of the environment temperature.

The climatic changes were reflected in changed species dimensions also in Stuľany locality. We have investigated the species *Dictyococcites bisectus* and *Coccolithus eope-*

lagicus. The species *Dictyococcites bisectus* reaches the dimensions in the zone NP23 (Early Oligocene). However, the signs of increasing the coccolith size in this species are already observable in the samples included into the zones NP 21 and NP 22.

An important factor in the environment that affects the distribution of calcareous nannoplankton is represented also by the amount of nutrients in the marine environment. In the Kriva Oľka locality, only a small change in nutritional conditions was recorded, namely in the samples KRO16 and KRO17. The sedimentation of the Zlín Fm. here probably took place in the cold-water environment with its gradual eutrophication.

Similarly, in the Stuľany locality was not found a significant change in the nutritional conditions of the environment. Some change is observable in the samples STU2 and STU1. The species *Reticulofenestra ornata* Müller and *Transversopontis fibula* Gheta were found in the assemblages, being typical for the moderately brackish cold-water environment. The species *Reticulofenestra ornata* represents an endemite species of the Paratethys. Based on the obtained data we assume that the sedimentation of the Malcov Fm. in the Stuľany locality probably took place in the slightly brackish and cold-water environment.

The representation of large numbers of resedimented species reflects the high activity of turbidic currents during sedimentation in the case of the Zlín Fm. in locality of Krivá Oľka, as well as of the Malcov Fm. in locality of Stuľany.

Acknowledgement:

Author expresses thanks to K. Fordinál and S. Antolíková for reading the manuscript and suggesting several improvements which increased its quality. Further there is appreciated the assistance by L. Vizi, Ľ. Gazdačko, Z. Németh, L. Martinský and S. Židekova, contributing to high quality visualization of data in figures. The paper belongs among the research outcomes of the project *Update of Geological Setting of Problematic Territories of the Slovak Republic*, financed by the Ministry of Environment of the Slovak Republic.

References

Aubry, M. P., 1992: Late Paleocene calcareous nannoplankton evolution: A tale of climatic deterioration. In: Prothero, D. R. & Berggren, W. A. (Eds.): Eocene-Oligocene climatic and biotic evolution. *Princeton Univ. Press,* 272 – 309.

Blaj, T., 2009: Late Eocene through Oligocene calcareous nannofossils from the paleoequatorial Pacific Ocean – taxonomy, preservation, history, biochrobology and evolu-tion. *Stockholm University.*

Boresma, A., Premoli-Silva, I. & Shackleton, N. J., 1987: Atlantic Eoceneplanktonic foraminiferal pleohydrographic indicators and stable isotope paleoceanography. *Paleoceanography, 2, 287 – 331.*

Hallock, P., Premoli-Silva, I. & Boresma, A., 1991: Similarities between planktonic and large foraminiferal evolutionary trends through Paleogene paleoceanographic changes. *Palaeogeogr. Palaeoclimatol. Palaeoecol., 83, 49 – 64.*

Haq, B. U. & Lohmann, G. P., 1976: Early Cenozoic calcareous nannoplankton biogeography of the Atlantic Ocean. *Mar. Micropaleont., 1, 119 – 197.*

Kováčik, M., Bóna, J., Gazdačko, Ľ., Kobulský, J., Maglay, J., Žecová, K., Derco, J., Zlinská, A., Siráňová, Z., Boorová, D., Bónová, K., Buček, S., Kucharič, Ľ., Kubeš, P., Bačová, N., Petro, Ľ. & Vaněková, H., 2012: Vysvetlivky ku geologickej mape Nízkych Beskýd-západná časť 1 : 50 000. *Bratislava, Št. Geol. Úst. D. Štúra, 5 – 180.*

Krhovský, J., Adamová, M., Hladíková, J. & Maslowská, H., 1992: Paleoenvironmental changes across Eocene/Oligocene boundary in the Ždánice and Pouzdřany Units (Western Carpathians, Czechoslovakia): the long-term trend and orbitally forced changes in calcerous nannofossil assemblages. In: Hamršmíd, B. & Young, J. R. (Eds.): Nannoplankton research. Vol. II. *Proc. 4th INA Conference, Prague, 1991. Knih. Zem. Plyn Nafta, 14b, 105 – 155.*

Martini, E., 1971: Standard Tertiary and Quaternary calcareous Nannoplankton zonation. *Proc. of the ll. Planktonic Conference, Roma.*

Mita, I., 2001: Data Report: Early to late Eocene calaceroue nannofossil assemblages of Sites 1051 and 1052, Blake Nose, northwestern Atlantic Ocean. *In: Kroon, D. & Norris, R. D. A. (Eds.): Proceedings of the Ocean Deep Sea Drilling Program, Scientific Results, College Station, TX (Ocean Drilling Program), 171B, 1 – 28.*

Oszczypko-Cloves, M. & Żydek, B., 2012: Reworked nannofossils from the Lower Miocene deposits inthe Magura Nappe (Outer Western Carpathians, Poland). *Geol. Carpath., 63, 5, 407 – 421.*

Ozdínová, S., 2013: Paleoecological evaluation of calcareous nannofossils from the Eocene and Oligocene sediments of the Subtatric Group of the Western Carpathians. *Miner. Slov., 45, 1 – 10.*

Perch-Nielsen, K., 1985: Cenozoik calcareous nannofossils. *In: Bolli, H., Saunders, J. B. & Perch-Nielsen, K.: Plankton stratigraphy. Cambridge, Cambridge Univ. Press, 427 – 554.*

Soták, J., 2010: Paleoenvironmetnal changes across the Eocene-Oligocene boundary: insights from the Central-Carpatian Paleogene Basin. *Geol. Carpath., 61, 5, 393 – 418.*

Villa, G., Fioroni, C., Pea, L., Bohaty, S. & Persico, D., 2008: Middle Eocene – late Oligocene climatic variability: Calcareous nannofossil response at Kerguelen Plateau Site 748. *Mar. Micropaleont. 69, 173 – 192.*

Persico, D. & Villa, G., 2004: Eocene-Oligocene calcareous nannofossils from Maud Rise and Kerguelen Plateau (Antarctica): paleoecological and paleoceanographic implications. *Mar. Micropaleont. 52, 153 – 179.*

Žec, B. (ed.), Kaličiak, M., Konečný, V., Lexa, J., Jacko, S., ml., Baňacký, V., Karoli, S., Potfaj, M., Rakús, M., Petro, Ľ., Spišák, Z., Bodnár, J., Jetel, J., Boorová, D. & Zlinská, A., 1997: Vysvetlivky ku geologickej mape Vihorlatských a Humenských vrchov, M 1 : 50 000. *Bratislava, GS SR, Výd. D. Štúra, 254 s.*

Žec, B., Gazdačko, Ľ., Kováčik, M., Kobulský, J., Bóna, J., Potfaj, M., Pristaš, J., Žecová, K., Derco, J., Kucharič, Ľ., Marcin, D., Petro, Ľ., Zlinská, A., Siráňová, Z., Vaněková, H., Buček, S. & Konečný, P., 2011: Vysvetlivky ku geologickej mape Nízke Beskydy-stredná časť, M 1 : 50 000. *Bratislava, Št. Geol. Úst. D. Štúra*, *188 s.*

Paleoekológia vápnitých nanofosílií z paleogénnych súvrství magurskej jednotky Západných Karpát

Témou článku sú vápnité nanofosílie a ich reakcia na zmenu paleoekologických podmienok v období mladšieho eocénu a staršieho oligocénu. Predmetom výskumu boli vápnité nanofosílie sedimentárnych hornín patriacich do dvoch litotektonických jednotiek magurského príkrovu Vonkajších Západných Karpát. Na lokalite Krivá Oľka (vzorky KRO1 – 17; geografické koordináty vo WGS84: 49 07 47,44 S; 21 51 03,81 V; obr. 1, 2, 3 a 10) sme skúmali vápnité nanofosílie zo sivozelených až sivých, premenlivo vápnitých ílovcov zlínskeho súvrstvia račianskej jednotky magurského príkrovu. V profile Stuľany (vzorky STU 1 – 11; koordináty 49 08 10,16 S; 21 23 40,37 V; obr. 1, 11, 12, 19) boli predmetom skúmania silno vápnité ílovce hnedozelenej farby, zelenkavo sivé až sivé vápnité siltovce až ílovce a tmavosivé vápnité ílovce s jemne dispergovanou sľudou a lastúrnatým rozpadom, ktoré patria k malcovskému súvrstviu krynickej jednotky magurského príkrovu. Skúmaná oblasť je súčasťou regiónu Nízke Beskydy na severovýchodnom Slovensku a vystupuje severovýchodne od bradlového pásma.

Preparáty na výskum boli pripravené klasickou dekantačnou metódou (Haq a Lohman, 1976; Perch-Nielsen, 1985). V rámci paleoekologického výskumu sa robila kvantitatívna analýza spoločenstiev nanofosílií. Z každého preparátu bolo zaznamenaných 500 jedincov. Spracovanie údajov spočívalo v určení početnosti jednotlivých druhov v rámci odobraných vzoriek a ich triedení podľa teplotných podmienok, zmien veľkosti kokolitov, obsahu živín v prostredí a autochtonity. Študovali sme ich polarizačným mikroskopom Axioskop 40 Carl Zeiss pri zväčšení 1 250x a dokumentovali digitálnym fotoaparátom Axiocam 105 color. Na biostratigrafické zaradenie spoločenstiev bola použitá Martiniho zonácia (1971).

Na základe analýz spoločenstiev nanofosílií sa zistilo, že sedimentácia zlínskeho súvrstvia na lokalite Krivá Oľka (obr. 2 a 3) prebiehala počas mladšieho eocénu (NP 19/20 a NP21). Získané údaje poukazujú na fakt, že v tomto období na lokalite Krivá Oľka nedošlo k výraznému nárastu chladnomilných druhov, napriek tomu určitý nárast počtu chladnomilných druhov sa zistil vo vzorkách KRO16 a KRO17. Zmenené paleoekologické podmienky sa prejavili aj zmenou veľkosti plakolitov, ktoré boli zaznamenané v prípade druhov *Coccolithus eopelagicus*, *Dictyococcites bisectus* a *Reticulofenestra umbilica*. Významným faktorom prostredia, ktorý ovplyvňuje distribúciu vápnitého nanoplanktónu, je aj množstvo živín v morskom prostredí. Na lokalite Krivá Oľka sme zaznamenali len malú zmenu nutričných podmienok, a to vo vzorkách KRO16 a KRO17. Kvantitatívnou analýzou spoločenstiev vápnitých nanofosílií sa zisťovalo percentuálne zastúpenie preplavených a autochtónnych druhov. Zastúpenie veľkého počtu preplavených druhov odráža vysokú aktivitu turbiditných prúdov počas sedimentácie zlínskeho súvrstvia na lokalite Krivá Oľka. Z urobených analýz vyplýva, že sedimentácia zlínskeho súvrstvia na lokalite Krivá Oľka prebiehala pravdepodobne v chladnom prostredí s jeho postupnou eutrofizáciou (obr. 3 – 10).

Podobným spôsobom sa robila kvantitatívna analýza spoločenstiev nanofosílií aj na lokalite Stuľany (obr. 11, 12 a 19), kde je zastúpené malcovské súvrstvie krynickej jednotky magurského príkrovu. Spoločenstvá nanofosílií preukázali, že sedimentácia na lokalite Stuľany prebiehala počas staršieho oligocénu (NP21 – NP23). Zistené spoločenstvá boli chudobnejšie a málo diverzifikované. Dominantnou zložkou spoločenstiev boli druhy viazané na mierne temperované prostredie (TWS). Aj na lokalite Stuľany sa robila analýza veľkosti plakolitov. Z výsledkov vyplýva, že podobne ako na lokalite Krivá Oľka, aj tu vápnité nanofosílie reagovali na zmenené paleoekologické podmienky zmenenými rozmermi. Zmenené paleoekologické podmienky sa prejavili v malej miere určitým nárastom počtu eutrofických druhov, a to vo vzorkách STU1 a STU2. Výrazná dynamika prostredia sa prejavila zastúpením veľkého počtu preplavených druhov, podobne ako na lokalite Krivá Oľka. Vzhľadom na zistené údaje môžeme konštatovať, že sedimentácia malcovského súvrstvia na lokalite Stuľany pravdepodobne prebiehala v mierne brakickom a chladnom prostredí (obr. 13 – 19).

Doručené / Received: 12. 12. 2017
Prijaté na publikovanie / Accepted: 19. 12. 2017

Mineralia Slovaca, 49 (2017), 157 – 168
Web ISSN 1338-3523, ISSN 0369-2086

Caves in magnesite – a rare phenomenon of karstification: The case study from Slovakia

ĽUDOVÍT GAÁL[1], ZOLTÁN NÉMETH[2], PAVEL BELLA[1,3], and PETER KODĚRA[4]

[1]State Nature Conservancy of the Slovak Republic, Slovak Caves Administration,
Hodžova 11, SK-031 01 Liptovský Mikuláš, Slovakia; ludovit.gaal@ssj.sk, pavel.bella@ssj.sk
[2]State Geological Institute of Dionýz Štúr,
Mlynská dolina 1, SK-817 04 Bratislava, Slovakia; zoltan.nemeth@geology.sk
[3]Catholic University, Pedagogical Faculty, Department of Geography,
Hrabovská cesta 1, SK-031 04 Ružomberok, Slovakia; Pavel.Bella@ku.sk
[4]Comenius University, Faculty of Natural Sciences, Department of Geology of Mineral Deposits,
Ilkovičova 6, SK-842 15 Bratislava; kodera@fns.uniba.sk

Abstract: The existence of underground karst cavities in magnesite deposits in Slovakia was indicated already at the end of the 1950s. Their speleological survey started only from 1983, when the caves were investigated in magnesite deposits Podrečany, Burda, Lubeník and Bankov in the Carboniferous rock belt 120 km long between Lučenec and Košice towns, located along the boundary zone between the Gemeric and Veporic tectonic units of the Western Carpathians in the Slovenské rudohorie (Slovak Ore) Mountains. Until now, altogether 16 caves in magnesite deposits were speleologically investigated and mapped in Slovakia. Except of one, all of them are accessible only from the mine workings. Generally their lengths are between 10 and 20 m but the longest cave reaches up to 73 m. These caves occur in Carboniferous magnesite-dolomite lenses surrounded by graphite-sericite schists or phyllites of the Gemeric Unit. As our research has manifested, the caves in magnesite originated due to the post-Upper Cretaceous shearing of the Alpine deformation phase AD_3. Shearing during this deformation phase caused the origin of the penetrative NE-SW trending regional shear faults in the western segment of the magnesite bearing Carboniferous belt, encompassing the caves in the Podrečany, Burda, Lubeník and Dúbrava Massif magnesite bodies. In the eastern segment of the belt with the Bankov deposit the NW-SE trending faults of the AD_3 phase were dominant. In particular cases, the faults of the AD_3 phase may represent the reactivated discontinuities of earlier Alpine phases AD_1 and AD_2. The azimuth and dip parameters of the caves manifest that besides the main AD_3 discontinuities, parallel with the shear faults, the extensional AD3 antithetic shears in-between individual shear faults have the supreme importance at the origin of the cave open spaces. Faults cutting the whole magnesite bodies allowed penetration of hydrothermal fluids throughout them. The fissures were widened by a hydrothermal karst process, accelerated by oxidation of Fe in the oxidation zone (FeO as an isomorphic admixture in the magnesite is represented app. by 3 %). Hydrothermal process related to the cave formation was caused by low-salinity fluids probably with progressively higher proportion of meteoric water and with the temperature less than 150 °C. In Neogene, after the first uplift of the magnesite bodies, the water level decreased in relation to the incision of adjacent valleys and the aragonite crystals and palygorskite started to crystallize in the vadose conditions.

Key words: magnesite, dolomite, karst, cave, faults, shear zones, synthetic and antithetic shears, hydrothermal speleogenesis, hypogene cave, Lower Carboniferous, Gemeric Unit, Western Carpathians

Graphical abstract

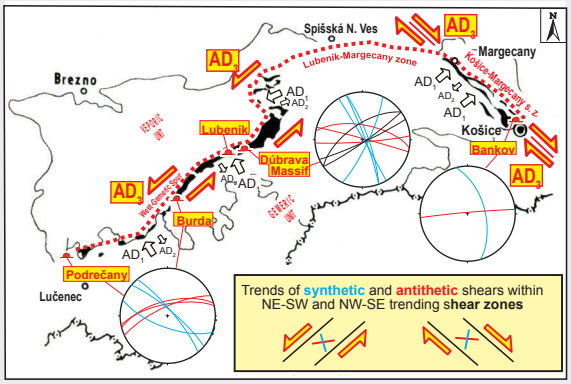

Highlights

- Geological control, morphology and hydrothermal origin of magnesite caves were deciphered.
- The post-Upper Cretaceous tectonic shearing of the AD_3 deformation phase contributed to the origin of opened fissures in magnesite bodies and contributed to their penetration by hydrothermal fluids.
- Primary fissures were enlarged by the weathering of magnesite due to the oxidation of Fe in the host rock.
- The growth of aragonite crystals and palygorskite in the vadose conditions after the incision of adjacent valleys was due to the Neogene and Quaternary uplift.

Introduction

Caves in magnesite represent a specific lithological group of underground karst phenomena. In the world they occur far less often than the caves in limestones. The reason for this scarcity is the rare occurrence of magnesite bodies and the low ability of magnesite to dissolve. The dissolution rate of magnesite is about four orders of magnitude lower than that of calcite (Chou et al., 1989).

Some smaller underground cavities in magnesite were mentioned from magnesite deposits in California and Nevada, USA (Hess, 1908; Gale, 1912) and in Ceara and Brumado Bahia, Brazil (Bodenlos, 1950, 1954). The existence of underground karst cavities in magnesite deposits in Slovakia was indicated by Guľa (1959), Klír (1962, 1968) and Cabala (1976), but their speleological survey began in the Dúbrava Massif near the Jelšava town in 1983 (Gaál and Ženiš, 1984). Thereafter, further caves were investigated in another magnesite deposits including Podrečany near Lučenec, Burda near Hnúšťa, Lubeník near Jelšava and Bankov in Košice (Ženiš and Gaál, 1986a, b). Some small caves in magnesite were surveyed also in Tasmania, that originated by dissolution of magnesite owing the water inriched in CO_2 or H_2SO_4 (Houshold, 1998; Houshold et al., 1999).

Altogether 16 caves in magnesite deposit have been speleologically investigated and mapped in Slovakia until now. Except of one, all of them are accessible only from the mine workings. Generally, their lengths are between 10 – 20 m, but the longest caves reach up to 73 m (BU-2) or 51 m (DM-3). Several papers and reports, dealing with mining, geology or hydrogeology of magnesite deposits, contain mentions about further underground spaces in magnesite of various sizes, though they have been not speleologically surveyed yet (Guľa, 1959; Klír, 1962, 1968; Cabala, 1976, 1985; Mitter and Pavlarčík, 1996; Cicmanová, 2002; Bajtoš, 2004). A part of magnesite caves was destroyed by mining or flooded by water.

The origin of magnesite caves in Slovakia was explained by oxidation of Fe in the magnesite along tectonic faults, and the formation of Fe-oxyhydroxides with clay minerals (ochre), that were out washed from underground cavities (Trdlička, 1959; Gaál and Ženiš, 1984; Ženiš and Gaál, 1986a,b). Magnesite deposits present karst-fissure aquifers with a similar hydrography as limestone karst areas (Klír, 1962, 1968, a.o.). Preliminary evidences on the possible hydrothermal origin of some magnesite caves resulted from the stable isotope and fluid inclusions analyses of cave mineral fills (Bella et al., 2013).

Surface landforms and normal (non-hydrothermal) caves originated by dissolution or chemical decomposition of magnesite are considered as parakarst (Kiernan, 1988). Within a parakarst, caves in magnesite with an admixture of iron, that originated mainly by magnesite decomposition due to the oxidation Fe^{2+} to Fe^{3+} along faults guiding the flow of groundwater, can be classified as bradykarst (Bella, 1994, 2011).

This study presents a new knowledge on the role of tectonic processes for the origin of appropriate discontinuities, processes widening the caves and estimated age of the origin of caves in magnesite bodies in the southern part of Slovakia.

Magnesite karst in Slovakia – location and geological setting

Magnesite lenses in Slovakia occur in the Slovenské rudohorie (Slovak Ore) Mountains in ca 120 km long arcuate belt between Lučenec and Košice towns (Fig. 1). From the geological point of view, they belong to two principal Western Carpathians units: the Veporic and Gemeric ones. The lenses are located in the close vicinity of the Lubeník-Margecany thrust plane separating both units.

In the **Veporic Unit,** the magnesite lenses are present in the Lower Paleozoic chlorite-sericite and garnet-mica-schists with talc (Slavkay et al., 2004). Bezák (1999) and Németh et al. (2004) showed that their host lithology corresponds to the Lower Carboniferous Ochtiná Formation, which hosts magnesite bodies in the Gemeric Unit south of the Lubeník-Margecany thrust plane. Altogether three well-known magnesite deposits are located in the Veporic Unit including Hnúšťa (Mútnik mine), Sinec (Samo mine) and Kokava, but no karst phenomena have been revealed here yet.

In the **Gemeric Unit**, magnesite bodies occur in two horizons. The magnesite lenses in the Lower Paleozoic horizon occur in black schists, chlorite-sericite schists with porphyroids and talc of the volcanic-sedimentary Gelnica Group (Grecula et al., 1995). Here, the magnesite bodies are mostly replaced to talk, which is exploited near the Gemerská Poloma village, but no karst phenomena is known from here. These magnesite bodies do not reach the surface, with the uppermost parts ca 200 m beneath the surface. Their setting is known from extensive borehole survey and a new adit constructed for talc extraction.

Until now, the karst and caves in magnesite lenses are known only from the Lower Carboniferous horizon of the Ochtiná Formation (Tournaisian-Viséan until Serpukhovian), containing dolomite and magnesite lenses hosted by graphite-sericite schists. The carbonate lenses represent original coral reefs, later replaced by calcite to dolomite and magnesite (Abonyi and Abonyiová, 1981; Ilavský et al., 1991; a.o.). The origin of Mg fluids was interpreted by several recent stable isotope and fluid inclusions studies. Radvanec and Prochaska (2001), Németh et al. (2004) and Radvanec et al. (2010) have demonstrated that the Mg-bearing fluids came from the Upper Permian to Lowermost Triassic shallow evaporite basins in which

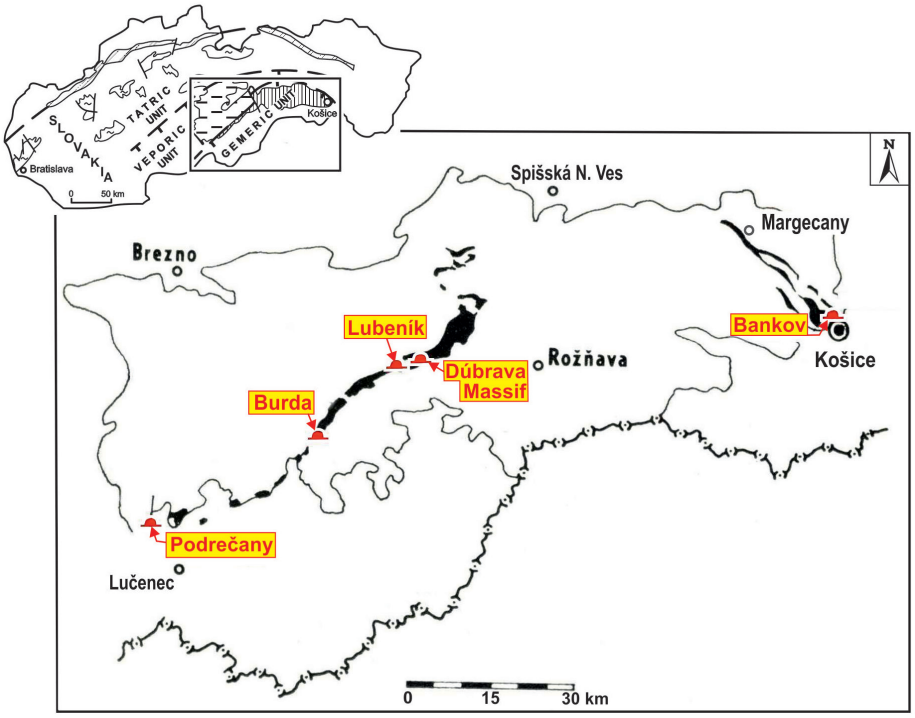

Fig. 1. Position of studied caves within the magnesite bodies belt (black planes) in the south-eastern Slovakia.

heavier Mg-bitter brines concentrated at its bottom. During the Upper Permian, the extensional tectonic regime in Gemeric Unit allowed the penetration of Mg-rich brines depthward along faults, where they reached the Lower Carboniferous limestone lenses. At the temperature 370–400 °C the exchange reaction between the Mg-rich fluids and the reef limestone resulted in the crystallization of a coarse-grained magnesite (Radvanec and Prochaska, 2001; Németh et al., 2004; Radvanec et al., 2010). So, the Mg-metasomatism is linked with the infiltration of bitter brines to limestones along faults during the onset of Permo-Triassic (Paleo-Alpine) rifting on continental crust. An important prerequisite for the replacement was the elevated temperature (370–400 °C).

Hurai et al. (2011) also suggest the presence of evaporated seawater component in the magnesite-forming fluid and opened hydrothermal system, based on fluid inclusion and stable isotope data, including high Br/Cl ratio of the paleofluids. This interpretation (l.c.) states that the Mg-metasomatism could have occurred during the remobilisation of the buried Permian evaporitic brines in the early stage of Alpine orogeny in Late Jurassic to Early Cretaceous (l.c.). However, this interpretation is not supported by the compressional field producing the "cold" north-vergent imbrication and thrusting within the Gemeric Unit during that time.

According to Németh et al. (2004) and Sasvári & Kondela (2007), the host lithology and magnesite bodies have underwent 3 principal Alpine (post-Permian) deformation overprints. The oldest, Lower Cretaceous $\mathbf{AD_1}$ north-vergent imbrication of Paleozoic sequences of the Gemeric Unit and thrusting of this unit as a basement nappe over the Veporic Unit caused "sandwiching" of schist and magnesite bodies of the Ochtiná Formation between both tectonic units. The second – post-collision (post-AD_1) deformation phase $\mathbf{AD_2}$ was in progress in the Upper Cretaceous (84–88 Ma; Maluski et al., 1993; Dallmeyer et al., 1996), when due to previous Alpine $\mathbf{AD_1}$ collision and crust thickening the Alpine thermal metamorphism and the post-collision unroofing have occurred. This process caused steatitization of already existing magnesite bodies and the origin of talc along discontinuities due to the SiO_2 ingress. The main planar structures being produced by the $\mathbf{AD_2}$ phase are moderately south-(south-east, south-west)-dipping normal faults.

During following third deformation phase $\mathbf{AD_3}$ a conjugate system of transpressional shear zones originated: the sinistral NE-SW trending system is dominant in the western part of the contact zone between Gemeric and Veporic units (Lubeník-Margecany zone), while the dextral NW-SE trending system dominates in the eastern part of the contact zone (Košice-Margecany shear zone). Taking into account the whole Western Carpathians, both shear systems were developed simultaneously, though having unequal representation in various parts of this orogenic belt (Grecula et al., 1990). The NE-SW trending system is the most significant in the western part of the Western Carpathians, causing even the NE-SW course of the mountain

ranges there. The NW-SE trending system is prominent in the eastern part of the Western Carpathians. Mutual offsets along both shear systems caused the origin of arcuate bend of the Western Carpathians (l.c.).

Methods

The main aim of the presented research was to obtain an integrated image about position of magnesite caves in the tectonic plan of the Gemeric Unit, as well as to reveal their genesis and age. For mapping of the caves and documenting of all tectonic discontinuities (the direction of dip and the size of dip) in underground spaces a geological compass was preferably used. During our research we have utilized also earlier data of Gaál and Ženiš (1984) and Ženiš and Gaál (1986a). Obtained data were correlated with the tectonic plan of the Gemeric Unit (Németh et al., 2004; Sasvári & Kondela, 2007; Radvanec et al., 2010).

In intention to reveal the genesis of the caves, the samples of dolomite crystals from the DM-7 Cave in the Dúbrava deposit have been used for fluid inclusion study. Fluid inclusions hosted in these dolomite crystals were studied using doubly polished wafers (~200 μm thick) using a high resolution optical microscope. The observed inclusions were assigned a primary or secondary origin according to the criteria by Roedder (1984). The thermometric behaviour of fluid inclusions was studied on a Linkam THMSG-600 heating-freezing stage. The equipment was calibrated with natural fluid inclusions with pure CO_2 (-56.6 °C), pure water (0 °C) and inorganic standards ($K_2Cr_2O_7$, 398 °C). The precision and accuracy of the microthermometric measurements, based on standard calibration procedures, is estimated as ±0.1 °C for the freezing runs and ±2 °C for the heating runs. Salinity estimates are based on the last melting temperatures of ice in the system NaCl-H_2O (Bodnar, 1993).

Caves in magnesite

The karst phenomena of magnesite bodies are evident on the surface only very rarely. Sporadically, there occur some badly developed karren, but no sinkholes are known. In the Dúbrava deposit only one small cave named Pod Dúbravou in dolomite is accessible from the surface. Underground spaces in magnesite are known only in the deep parts of magnesite bodies, being discovered by the mining works.

Until now the following magnesite bodies were speleologically surveyed (from W to E):

Podrečany

Five lenses of magnesite and dolomite with the dip of 30–50° to SE are covered by Pliocene gravel and sand. The upper part of carbonate and surrounding schists occur in the strongly weathered zone, about 40–60 m thick (Abonyi and Abonyiová, 1981). In the mine 110 m under the surface a cavity of 13 x 9 m was surveyed in magnesite which was particularly filled with a yellow ochre clay (Fig. 2). The cavity was formed inside a tectonic fault trending 200/70° (direction of dip and size of dip) (Ženiš and Gaál, 1986a).

Burda

One magnesite-dolomite lens in phyllite is trending NE-SW with the dip 25–55° to SE. Its directional length is 1.5 km and thickness 150–200 m (Varga, 1992). Three caves were surveyed in this magnesite deposit. The biggest is BU-2 with the length of 73 m in the 5th horizon of the mine. Three parallel corridors of this cave originated along the tectonic faults 345/65° and 335/75°, which are crossed by faults of about 40/80° (Fig. 3). The walls of the cave are covered by weathered magnesite and ochre sporadically with the crusts of palygorskite. Near this cave an another similar cave was found with the length of 45 m. In other horizon a cavity of 13.5 x 8.5 m occurs with the height of 5–6 m (Ženiš and Gaál, 1986a).

Lubeník

The magnesite-dolomite lens with the total length of 880 m and max. thickness of 200 m is trending NE-SW with dip of 55–60° to SE. Only one the LK-1 Cave was found in the 7th horizon of the mine. This cave in magnesite has an irregular spheroidal shape with the length of 9.7 m. Its filling represents only ochre (Fe-oxyhydroxide) in the bottom of the cave (Gaál and Ženiš, 1986).

Dúbrava Massif

This is the largest magnesite-dolomite body in Slovakia with the directional length of more than 4 km and with the thickness of 600–1000 m (Fig 4). It is trending E-W with a dip of 45–85° to S (Tréger and Baláž, 2001). The carbonate body is surrounded by impermeable dark schists, therefore it behaves as an autochthonous collector, primarily drained by the spring Teplá voda with a deep circulation, which is indicated by its relatively high temperature 14.5 °C (Halečka, 1983). In the first stage of the speleological survey in 1983 and 1984 altogether 7 caves were mapped in the mining level 350 and 400 m a.s.l. (Gaál and Ženiš, 1984). Later, in 2012 a new research was made with sampling and surveying of two other caves (Bella et al., 2013). The shape of underground spaces of caves follows mainly tectonic faults but sporadically there also occur geode-like cavities (DM-2, DM-7 and Ostrohovitá Cave). The basic data of the surveyed caves are presented in Table 1.

As clearly demonstrated by the parameters of associated faults (their trend and dip), the geological structure controlling the origin of caves is the product of a translation

Tab. 1.
The basic data of surveyed caves in the Dúbrava magnesite deposit.

Cave	Host rock	Length (m)	Associated faults	Minerals
DM-1	magnesite	25	15/88°	palygorskite
DM-2	magnesite	2		
DM-3	magnesite, dolomite, ochre	51	10/65°, 325/65°	dolomite, calcite, aragonite, palygorskite
Pod Dúbravou	dolomite (in surface)	4	135/88°	
DM-5	dolomite	10.3	115/80°	
DM-6	magnesite, ochre	10.4	5/88°	dolomite
DM-7	magnesite	10		calcite, dolomite, palygorskite
Ostrohovitá	magnesite	7.6	250/80°	calcite, dolomite
Kryštálová	magnesite	28.2	60/88°, 70/85°, 145/85°, 176/86°, 155/85°	calcite, dolomite

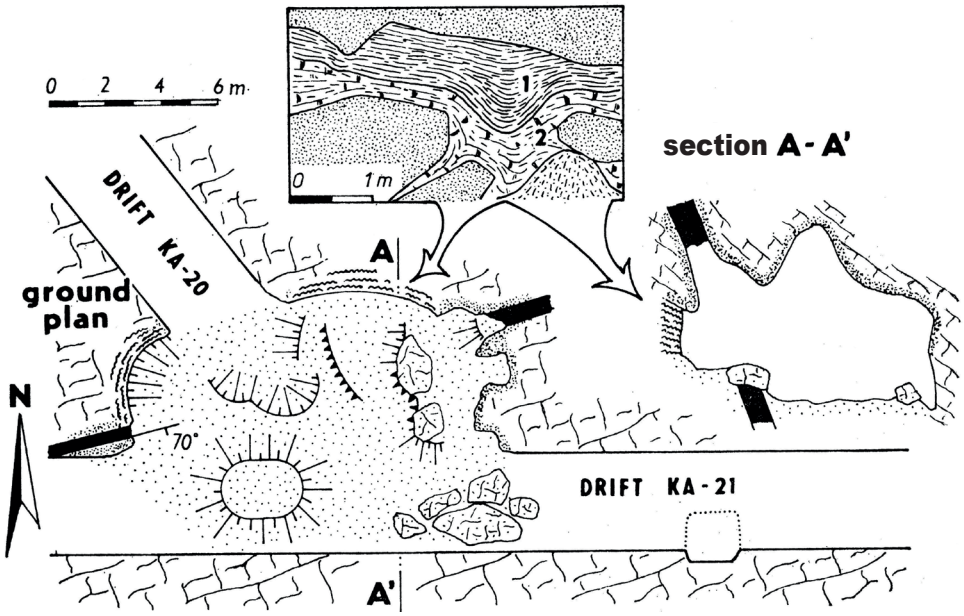

Fig. 2. Cavity in magnesite particularly filled with ochre in the Podrečany magnesite mine. 1 – thin laminated yellow ochre, 2 – bedded yellow ochre (Ženiš and Gaál, 1986a).

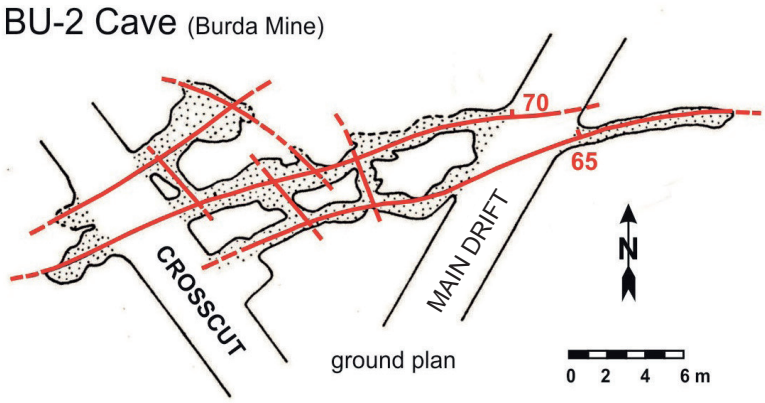

Fig. 3. Map of the BU-2 Cave in the Burda magnesite mine. Mapped by Ľ. Gaál, L. Benedek, J. Svoreň, P. Ženiš, 1985.

Fig. 4. View of the Dúbrava Massif magnesite deposit near Jelšava town. (Photo: Ľ. Gaál.)

along the fan-like shear system trending NE-SW (DM-3 – 325/65°, Fig. 5; Pod Dúbravou – 135/88°; Kryštálová – 145/85°, 155/85°, Figs. 6 and 7) but also along related antithetic faults (DM-1 – 15/88°; DM-3 – 10/65°; DM-6 – 5/88°; Ostrohovitá – 250/80°; Kryštálová – 60/88°, 70/85°). In minor cases related synthetic shears are also present (DM-5 – 115/80°).

A sample with idiomorphic dolomite crystals from the DM-7 Cave was studied by fluid inclusion microthermometry (Fig. 8). Rare fluid inclusions showed here various degree of fill which could be related to partial or total dehermetization, necking down or heterogeneous trapping of liquid and vapour during boiling of the fluid. Only assemblages of primary inclusions that showed roughly constant degree of fill were analysed by microthermometry. During heating homogenization to liquid occurred in a broad range of temperatures from 117 to 277 °C, and some of inclusions showed signs of dehermetization (growing of vapour bubble) on heating. During freezing runs fluid inclusion produced ice melting temperatures in two intervals: -0.3 to 0.0 °C and -4.5 to -2.8 °C, corresponding to salinities 0.0–0.5 and 4.6–7.2 wt % NaCl eq. The higher salinity inclusions showed eutectic temperatures in the range -25.0 to -23.7 °C, indicating the predominance of NaCl

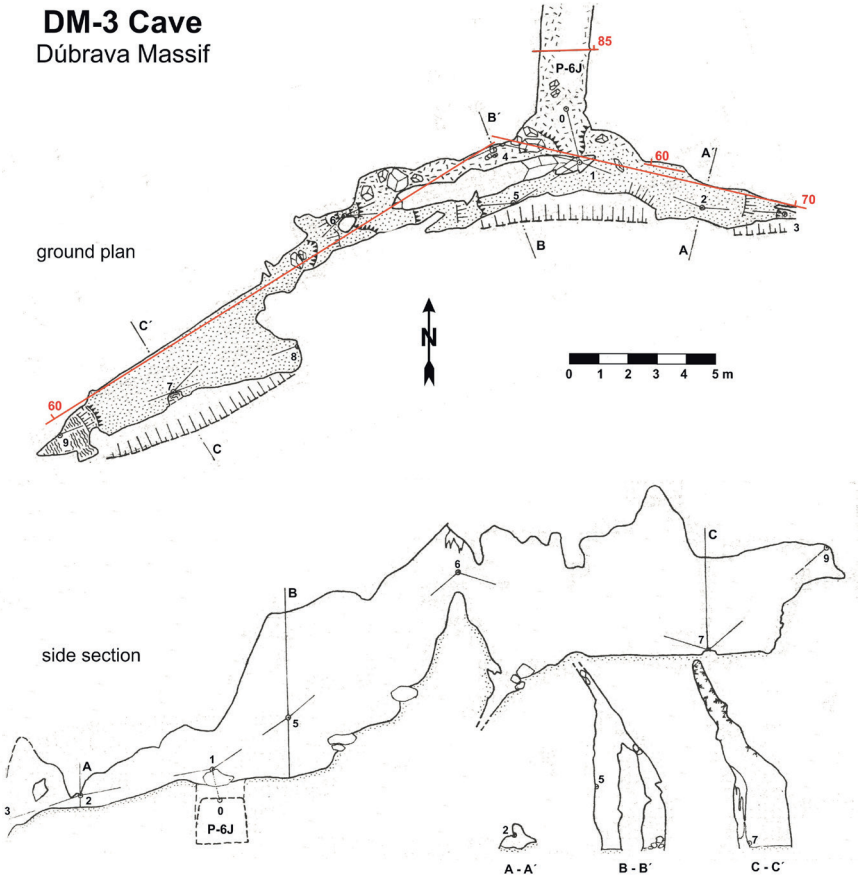

Fig. 5. Map of the DM-3 Cave in the Dúbrava Massif magnesite deposit. Mapped by Ľ. Gaál and P. Ženiš (1984).

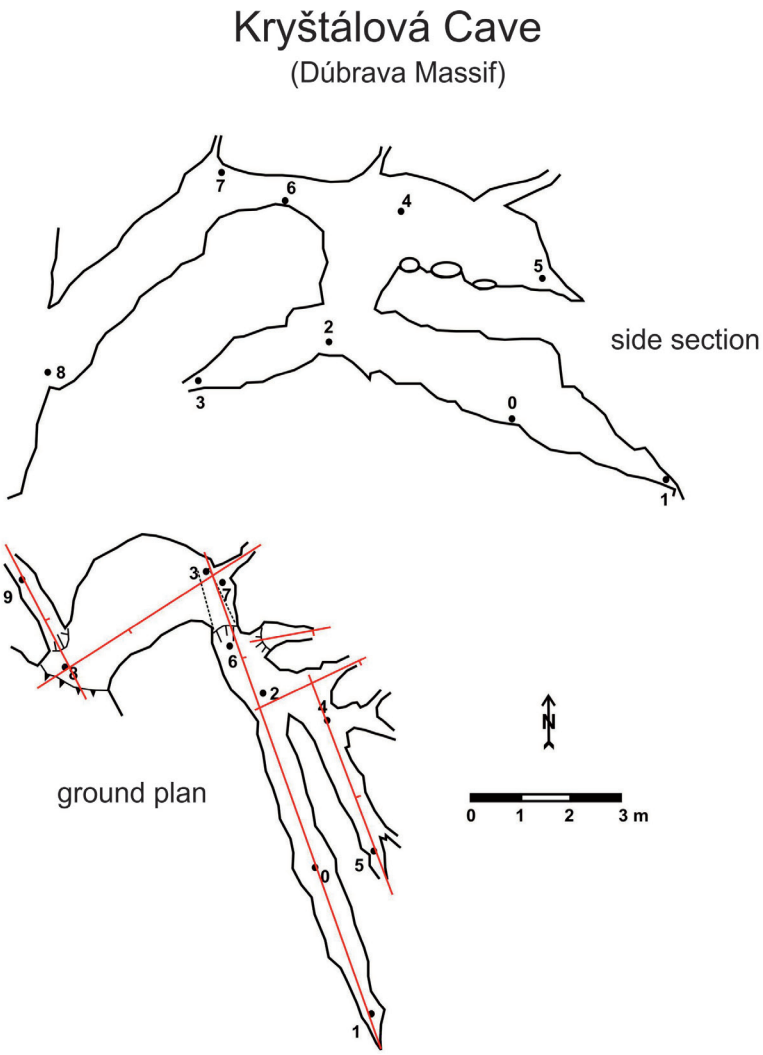

Fig. 6. Map of the Kryštálová Cave in the Dúbrava Massif magnesite deposit. Mapped by: Ľ. Gaál, L. Vlček, 2012.

over KCl in the fluid. The high variability of homogenization temperatures affects inclusions from both salinity intervals, thus the temperatures above 150 °C probably result from post-entrapment modification of inclusions or heterogeneous trapping of boiling fluids. Because the low salinity inclusions are located usually in outer parts of zonal carbonate crystals, it is likely that the crystals have grown from fluids with progressively higher proportion of meteoric water.

Bankov

The Bankov deposit in Košice situated in the eastern side of the magnesite-bearing Carboniferous zone (Fig. 1) consists of two irregular lenses oriented to NW-SE with a dip of 40–70° to SW. Its directional length is 1.6–1.8 km, max. thickness is 280 m (Grecula et al., 1995). Two caves were surveyed at 6th mining level of this deposit. The first of them is Bankov-1, which originated in crossing of two tectonic faults with dominant W-E direction. Its total length is 43.7 m. The second cave with a small lake is Bankov-2 with the length of 14 m originated along two parallel tectonic faults 75/60° (Ženiš and Gaál, 1986a).

Fig. 7. Irregular morphology of the Kryštálová Cave. (Photo: Ľ. Gaál.)

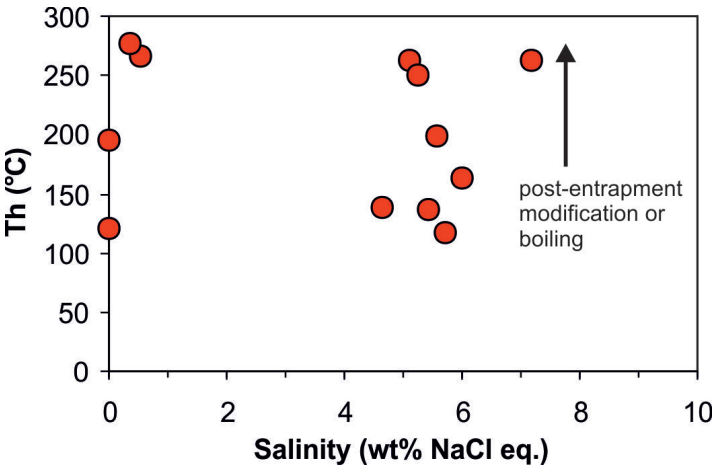

Fig. 8. Diagram showing the results of fluid inclusion microthermometry on a sample of carbonate from the DM-7 Cave in the Dúbrava massif. This salinity vs. homogenization temperature (Th) diagram shows high variability of Th values probably due to post-entrapment modification of inclusions or heterogeneous trapping of liquid and vapour, but in both cases, the temperatures above ~150 °C are higher than the real trapping temperatures.

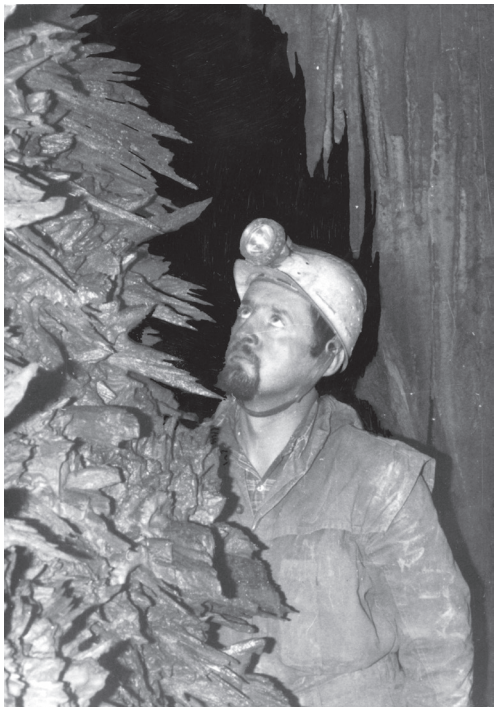

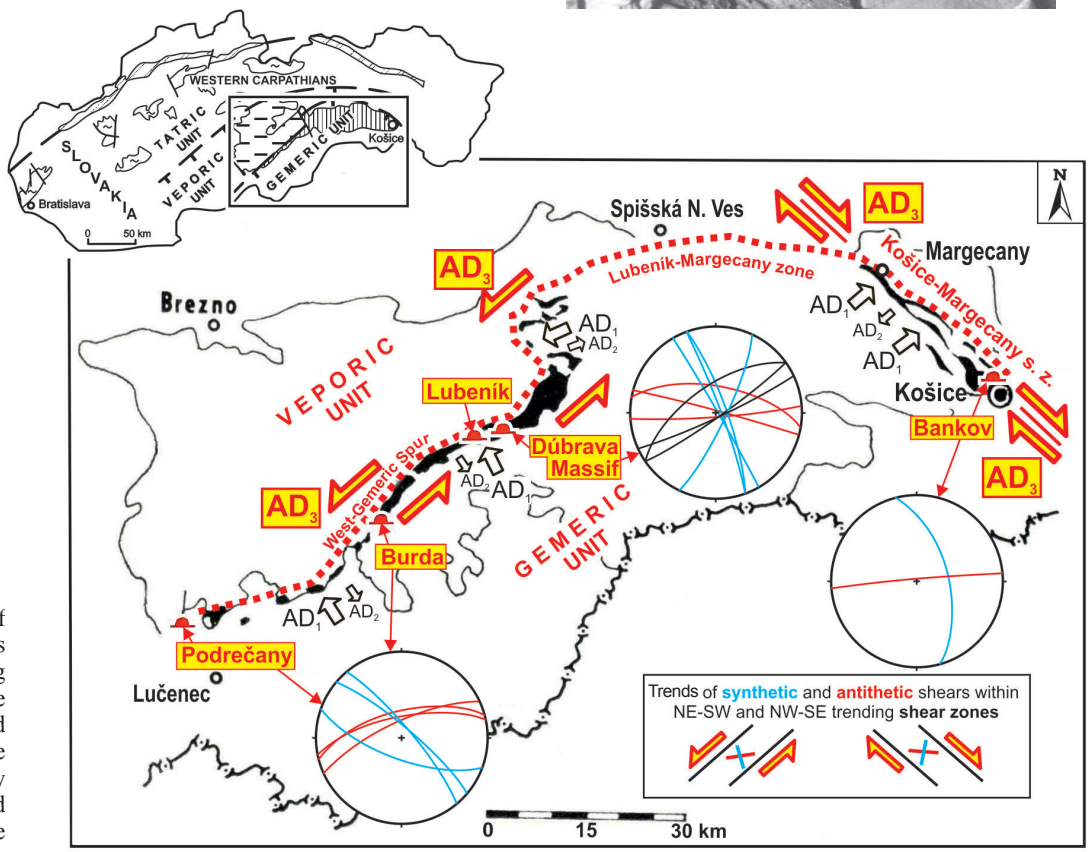

Fig. 10. Position of magnesite deposits bearing caves along the contact zone of the Veporic and Gemeric units (the Lubeník-Margecany zone) with indicated kinematics of Alpine deformation phases AD1 (Lower Cretaceous thrusting), AD2 (Upper Cretaceous unroofing) and AD3 (Tertiary-Recent subhorizontal shearing). Open spaces in magnesite deposits indicate that their genesis is related preferably to AD3 antithetic and synthetic shears accompanying the main NE-SW and NW-SE trending shear zones. Tectonograms manifest projection of open spaces into the lower hemisphere. Left tectonogram – data from the Podrečany and Burda deposits, middle tectonogram – open spaces in the Dúbrava Massif magnesite deposits. In both cases the open spaces are related to NE-SW trending AD3 shear zone in the West-Gemeric Spur. Right tectonogram – open space in the Bankov deposit, which genesis is related to the Košice-Margecany shear zone.

Discussion

The relation of open fissures to regional tectonic plan

On the basis of measurements of tectonic faults in the surveyed caves we can assert that their predominant directions are WSW-ENE and NW-SE, in all cases having steep or nearly vertical dip. The most representative caves with these directions are BU-2 in the Burda deposit and Kryštálová in the Dúbrava Massif. These parameters correspond to the fault system originated during **the deformation phase AD_3** in the Slovenské rudohorie (Slovak Ore) Mountains, as being ascertained by Németh et al. (2004), as well as Sasvári and Kondela (2007). The brittle faulting allowed the origin of open fissures and their penetration by hydrothermal fluids. Typical examples of open fissure caves are DM-1, DM-3 (with aragonite, Fig. 9), DM-5, DM-6 and Kryštálová Cave in the Dúbrava Massif and also Bankov-1 or Bankov-2 in the Bankov deposit.

Antithetic shears of direction **WNW-ESE** represent the most important structures between individual NE-SW trending shear faults. The sinistral **NE-SW** trending **AD_3** shear zones are dominant in the western part of the Lubeník-Margecany zone and the Ochtiná Lower Carboniferous belt. Synthetic shears of the direction close to **N-S** are of minor importance (Fig. 10). Described directions are the most frequent trends of fractures and caves in magnesite bodies located in the western segment of the Lubeník-Margecany zone in the so-called West-Gemeric Spur (Podrečany, Burda, Lubeník, Dúbrava Massif deposits), though the most prominent for opening of the cave spaces are **WNW-ESE** trending antithetic shears.

In the eastern part of the contact zone of the Gemeric and Veporic units and parallel magnesite-bearing belt, the dominant role had the dextral **NW-SE** trending Košice-Margecany shear zone (firstly defined by Grecula et al., 1990). This zone hosts the magnesite body Bankov (Fig. 10). The fractures (including the dominant cleavage) are parallel to this zone, but open spaces are related to antithetic shears trending **ENE-WSW**, while less important for the origin of the caves are synthetic shears of **NNW-SSE** direction.

Processes contributing to the formation of magnesite caves and their age

At the beginning of the karstification the prevalent part of open spaces in magnesite was probably filled with hydrothermal fluids, what is indicated by irregularly spherical shapes of several caves, such as DM-7, Ostrohovitá and Kryštálová. These caves correspond to the main strike-slip faults and related antithetic and synthetic shears of the **AD_3** phase; which is **post-AD_2** i. e. **post-Upper Cretaceous** in age. On the cave walls the carbonate crystals precipitated from the hydrothermal fluids. The carbonates were identified by Raman spectroscopy as dolomite and calcite (realized by R. Milovský – see Bella et al., 2013). It is not clear what was the temperature of the source fluids, but based on the limited fluid inclusion data it was probably less than 150 °C. Interestingly, this is significantly lower temperature compared to hydrothermal solutions that have formed metasomatic magnesite deposits of the Gemeric Unit (180–310°C; Hurai et al., 2011), which host the caves. The fluid inclusion data and morphology indicate, that these caves can be classified as hydrothermal or hypogene caves (Bella et al., 2013; Bella and Gaál, 2014a,b, 2017; Bella, 2016).

Calcite on the walls of open spaces is younger in the contact with dolomite there is a thin film of goethite with hematite, representing a supergene alteration product. In the Kryštálová Cave (Fig. 7) the carbonate crystals grow upon dark-brown substratum, consisting of oxides of Mn (hollandite) and Fe (goethite, magnetite and hematite), as identified by Raman spectroscopy (Bella et al., 2013). It indicates that the hydrothermal crystals started to grow after weathering of magnesite on cave walls, i.e. after widening of fissure-like cavities (Bella et al., 2013).

The primary fissures have been enlarged by weathering of magnesite mainly due to the presence of Fe. Approximately 3 % of FeO, as an isomorphic admixture, was revealed in magnesite (Abonyi and Abonyiová, 1981). FeO is not stable in the oxidation zone and so it was removed from magnesite and re-precipitated as amorphous FeO(OH) and goethite. The process of oxidation of Fe was probably accelerated by the impact of earlier hydrothermal fluids. The role of Fe in widening of underground spaces is also supported by the fact that in the magnesite bodies without increased Fe content no cave is known (in magnesite deposits Kokava, Sinec, Hnúšťa and Gemerská Poloma).

Since the occurrence of secondary sulfate minerals is relatively common in magnesite deposits, water enriched with sulfate ions (most of sulfate minerals are easily soluble in water) is more aggressive and is one of the main factors of secondary changes (formation of Fe-oxyhydroxides) in magnesite deposits (Vančová and Turan, 1979). The sulfate minerals probably originate here by the decomposition of pyrite in the oxidation zone (ibid.).

The yellow-brown Fe-oxyhydroxides (ochre) deposits occur in majority of surveyed caves. The ochre enabled growing of aragonite crystals in the DM-3 Cave, which required adjusted climatic conditions in this cave (Fig. 9). The aragonite and palygorskite have probably appeared in the caves after decreasing of water level in the carbonate massif. This situation started in **Neogene** when the belt, bearing the magnesite bodies, was uplifted and later cut by fluvial erosion, mainly during **Quaternary** (Lukniš, 1964).

Conclusions

Data obtained by the structural geological and mineralogical research of the caves hosted by magnesite bodies in Slovakia suggest that:

The origin of caves in magnesite in the Gemeric Unit was markedly influenced by the Alpine post-Upper Cretaceous (Tertiary–Recent) $\mathbf{AD_3}$ tectonic deformation, when in transpression regime the NE-SW and NW-SE trending conjugate fault systems were formed. The NE-SW trending system manifests sinistral subhorizontal shearing. This system is dominantly developed in the western part of the Gemeric Unit and so-called West-Gemeric Spur, where it represents a continuation of the ENE-WSW trending Transgemeric shear zone (Grecula et al., 1990; Fig. 10). In the eastern part of the Gemeric Unit, the NW-SE trending dextral shear system – so-called Košice-Margecany shear zone (l.c.) dominates. The regional shearing in both systems was accompanied by the origin of numerous faults and cleavage parallel to shear systems in rheologically weaker lithology. The weakened zones had a predisposition for the penetration of fluids. Principal importance in opening of the fissures in magnesite also had antithetic shears in-between individual faults in shear systems. Combination of principal faults of individual shear systems and related antithetic shears were the principal factors for the origin of caves, especially in the competent (rigid, rheologically hard) lithology, represented by magnesite. However, the faults of the $\mathbf{AD_3}$ phase might in some cases represent the reactivated earlier discontinuities originated in the $\mathbf{AD_1}$ and $\mathbf{AD_2}$ phases, which can especially be the case of the $\mathbf{AD_3}$ NE-SW trending shear zone in the West-Gemeric Spur and the NW-SE trending Košice-Margecany shear zone.

The tectonic shearing allowed the origin of opened fissures and their penetration by hydrothermal fluids.

Hydrothermal process related to the cave formation was caused by low-salinity fluids probably with progressively higher proportion of meteoric water and with the temperature less than 150 °C, as indicated by fluid inclusions in the newly formed dolomite crystals in the DM-7 Cave in the Dúbrava magnesite deposit. The fissures were widened by karstification process and oxidation of Fe has accelerated the hydrothermal impact.

After the Neogene and Quaternary uplift of the West-Gemeric Spur (the zone hosting magnesite deposits Podrečany, Burda, Lubeník and Dúbrava Massif) and the incision of adjacent valleys, the decrease of water level has allowed the growth of aragonite crystals and palygorskite in the vadose conditions.

Considering magnesite deposits as karst-fissure aquifers and their hydrographical zones, probably also vadose and epiphreatic/phreatic non-hydrothermal caves could have originated in the southern part of Slovakia. Vadose fissure caves were formed by meteoric waters seeping along steep faults (Gaál and Ženiš, 1984, 1986; Ženiš and Gaál, 1986a, b; Mitter and Pavlarčík, 1996). Subhorizontal epiphreatic dissolution caves were formed by normal or mixing waters along the water table in relation to phases of stabilized local erosion base on the surface. Mostly irregular phreatic cavities with oval hollows or steep chimneys originated in the deeper phreatic parts of karst-fissure aquifers. Caves of hydrothermal origin could be remodelled or enlarged during the younger developmental stages (in the epiphreatic and vadose zone) after lowering of the local erosion base by the incision of surrounding valleys (Bella and Gaál, 2014a).

Acknowledgements

The authors are grateful to the director of the Slovak Magnesite Works, Mr. Jaroslav Švejkovský for agreement to entry the Dúbrava magnesite mine. The study is the result of projects of the Scientific Grant Agency of the Ministry of Education, Science, Research and Sport of the Slovak Republic and the Slovak Academy of Sciences (VEGA) No. 1/0030/12, 1/0430/15 and 1/0560/15.

References

Abonyi, A. & Abonyiová, M., 1981: Magnezitové ložiská Slovenska. *Miner. Slov., Monogr., 125 p.*

Bajtoš, P., 2004: Groundwater chemical composition changes in the Dúbravský Massif hydrogeological structure, induced by magnesite exploitation. *Acta Petrol. Sinica, 20, 4, 887 – 898.*

Bella, P., 1994: Genetické typy jaskynných priestorov Západných Karpát. *Slov. Kras, 32, 3 – 22.*

Bella, P., 2011: Genetické typy jaskýň. *Ružomberok, VERBUM, 220 p.*

Bella, P., 2016: Jaskyne na Slovensku – genetické typy a morfológia. *Ružomberok, VERBUM, 124 p.*

Bella, P., Gaál, Ľ., Milovská, S., Milovský, R. & Koděra, P., 2013: Jaskyne v magnezitoch – ďalší príklad hydrotermálnej speleogenézy na Slovensku. *Aragonit, 18, 1, 42 – 44.*

Bella, P. & Gaál, Ľ., 2014a: Jaskyne v magnezitoch: morfogenetické odlišnosti a základná typológia. *Aragonit, 19, 1 – 2, 3 – 10.*

Bella, P. & Gaál, Ľ., 2014b: Vznik a morfológia hydrotermálnych jaskýň v Západných Karpatoch a ich predpolí. *Geomorphol. Slov. Bohem., 14, 2, 15 – 30.*

Bella, P. & Gaál, Ľ., 2017: Hypogene caves in Slovakia. *In: Klimchouk, A., Palmer, A., De Waele, J., Aurel, A. & Audra, P. (Eds.): Hypogene Karst Regions and Caves of the World. Cave and Karst Systems of the World. Cham, Springer, 299 – 311.*

Bezák, V. (ed.), Hraško, Ľ., Kováčik, M., Madarás, J., Siman, P., Pristaš, J., Dublan, L., Konečný, V., Plašienka, D., Vozárová, A., Kubeš, P., Švasta, J., Slavkay, M. & Liščák, P., 1999: Vysvetlivky ku geologickej mape Slovenského rudohoria-západná časť 1 : 50 000. (Explanations to the geological map of the Slovak Ore Mountains-western part 1 : 50 000.) *Bratislava, GS SR, Vyd. D. Štúra, 1 – 176.*

Bodenlos, A. J., 1950: Magnesite deposits of central Ceara, Brazil. *Geol. Surv. Bull., 962-C, 121 – 153.*

Bodenlos, A. J., 1954: Magnesite deposits in the Serra das Éguas, Brumado Bahia, Brazil. *Geol. Surv. Bull., 975-C, 87 – 170.*

Bodnar, R. J., 1993: Revised equation and table for determining the freezing point depression of H_2O-NaCl solutions. *Geochim. Cosmochim. Acta, 57, 683 – 684.*

Cabala, D., 1976: Riešenie hydrogeologických pomerov magnezitových ložísk na príklade ložiska Burda. *Miner. Slov., 8, 4, 369 – 377.*

Cabala, D., 1985: The water problem in relation to mining at magnesite deposits in Slovakia. Proceedings, 2nd *International Mine Water Association Congress, 2, Granada, 919 – 930.*

Cicmanová, S., 2002: Geoenvironmental assessment of magnesite deposit Jelšava – Dúbrava Massif. *Boletim Paranaense Geoci., 50, 87 – 95.*

Dallmeyer, R. D., Neubauer, F., Handler, R., Fritz, H., Müller, W., Pana, D. & Putiš, M., 1996: Tectonothermal evolution of the internal Alps and Carpathians: Evidence from $^{40}Ar/^{39}Ar$ mineral and whole-rock data. *Eclogae geol. Helv., 89, 1, 203 – 227.*

Chou, L., Garrels, R. M. & Wollast, R., 1989: Comparative study of the kinetics and mechanisms of dissolution of carbonate minerals. *Chem. Geol., 78, 3 – 4, 269 – 82.*

Gaál, Ľ. & Ženiš, P., 1984: Jaskyne v magnezitoch Dúbravského masívu. *Spravodaj SSS, 15, 4, 3 – 11.*

Gaál, Ľ. & Ženiš, P., 1986: Kras Revúckej vrchoviny. *Slov. Kras, 24, 27 – 60.*

Gale, H. S., 1912: Late developments of magnesite deposits in California and Nevada. U. S. *Geol. Surv. Bull., 540, 483 – 520.*

Grecula, P., Návesňák, D., Bartalský, B., Gazdačko, Ľ., Németh, Z., Ištván, J. & Vrbatovič, P., 1990: Shear zones and arc structure of Gemericum, the Western Carpathians. *Miner. Slov., 22, 2, 97 – 110.*

Grecula, P., Abonyi, A., Abonyiová, M., Antaš, J., Bartalský, B., Bartalský, J., Dianiška, I., Drnzík, E., Ďuďa, R., Gargulák, M., Gazdačko, Ľ., Hudáček, J., Kobulský, J., Lőrincz, L., Macko, J., Návesňák, D., Németh, Z., Novotný, L., Radvanec, M., Rojkovič, L., Rozložník, O., Varček, C. & Zlocha, J., 1995: Ložiská nerastných surovín Slovenského rudohoria. Zv. 1. (Mineral deposit of the Slovak Ore Mountains, vol. 1.) *Miner. Slov., Monogr., Bratislava, 1 – 834.*

Guľa, J., 1959: Geologické pomery magnezitového ložiska Lubeník a jeho okolia. *Geol. Práce, Zpr., 16, 79 – 99.*

Halečka, J., 1983: Záverečná správa Dúbravský masív – PP, hydrogeologické zhodnotenie ložiska magnezitu. *Manuscript. Bratislava, archive ŠGÚDŠ,128 p.*

Hess, F. L., 1908: The magnesite deposits of California. U. S. *Geol. Surv. Bull., 355, 67 p.*

Houshold, I., 1998: Magnesite karst in Tasmania. *Australasian Cave & Karst Management Assoc. J., 33, 43 – 50.*

Houshold, I., Claver, C. & Sharples, C., 1999: Magnesite karst in Northwest Tasmania: geology, geomorphology and hydrology. Report to Division of Investment. *Tasmania, Trade and Development Department of State Development, 148 p.*

Hurai, V., Huraiová, M., Koděra, P., Prochaska, W., Vozárová, A. & Dianiška, I., 2011: Fluid inclusion and stable C-O isotope constraints on the origin of metasomatic magnesite deposits of the Western Carpathians, Slovakia. *Russ. Geol. Geophys., 52, 11, 1 474 – 1 490.*

Ilavský, J., Turan, J. & Turanová, L., 1991: Magnesite deposits and occurrences in the West Carpathians of Czecho-Slovakia. *Ore Geol. Rev., 6, 6, 537 – 561.*

Kiernan, K., 1988: Caves and karst areas of Tasmania. J. *Sydney Speleol. Soc., 32, 6, 112.*

Klír, S., 1962: Hydrogeologie slovenských magnesitových ložisek v karbonu gemerid. *Geol. Práce, Zpr., 24, 97 – 122.*

Klír, S., 1968: Subsurface waters of the magnesite karst in Czechoslovakia. *Steir. Beitr. Hydrogeol., 20, 5 – 22.*

Lukniš, M., 1964: Pozostatky starších povrchov zarovnávania reliéfu v Československých Karpatoch. *Geogr. Čas., 16, 3, 289 – 298.*

Maluski, H., Rajlich, P. & Matte, P., 1993: ^{40}Ar-^{39}Ar dating of the Ihned Carpathians Variscan basement and Alpine mylonitic overprint. *Tectonophysics, 223, 313 – 337.*

Mitter, P. & Pavlarčík, S., 1996: Niektoré poznatky o krasovatení magnezitov v okolí Jelšavy. In: Lalkovič, M. (Ed.): Kras a jaskyne – výskum, využívanie a ochrana. *Proceedings, Liptovský Mikuláš, 39 – 44.*

Németh, Z., Prochaska, W., Radvanec, M., Kováčik, M., Madarás, J., Koděra, P. & Hraško, Ľ., 2004: Magnesite and talc origin in the sequence of geodynamic events in Veporicum, Inner Western Carpathians, Slovakia. *Acta Petrol. Sinica, 30, 837 – 854.*

Radvanec, M. & Prochaska, W., 2001: Successive replacement of Upper Carboniferous calcite to dolomite and magnesite in Dúbrava magnesite deposit (Western Carpathians, Slovakia). *In: Radvanec, M., Gondim, A. C. & Németh, Z. (Eds.): IGCP 443 Newsletter No. 1. Miner. Slov., 33, 6, 517 – 525.*

Radvanec, M., Bajtoš, P., Németh, Z., Koděra, P., Prochaska, W., Roda, Š., Tréger, M., Baláž, P., Grecula, P., Cicmanová, S., Kráľ, J. & Žák, K., 2010: Magnesite and talc in Slovakia – genetic and geoenvironmental model. *Bratislava, Št. Geol. Úst. D. Štúra, 189 p.*

Roedder, E., 1984: Fluid inclusions. *Rev. Mineral., Mineral. Soc. America, 12, 644 p.*

Sasvári, T. & Kondela, J., 2007: Demonstration of alpine structural phenomena at the structure of magnesite deposit Jelšava – Dúbrava Massif. *Metalurgija, 46, 2, 117 – 122.*

Slavkay, M. (Ed.), 2004: Ložiská nerastných surovín Slovenského rudohoria, vol. 2. *Miner. Slov., Monogr., Bratislava, 282 p.*

Tréger, M. & Baláž, P., 2001: Economic assessment of magnesite and talc deposits in the Slovak Republic. *Miner. Slov., 33. 6, 527 – 534.*

Turan, J. & Vančová, L., 1979: Bridlice magnezitových ložísk v karbóne Spišsko-gemerského rudohoria. *Miner. Slov., 11, 3, 205 – 218.*

Vančová, L. & Turan, J., 1979: Výskyty síranov na magnezitových ložiskách v karbóne Spišsko-gemerského rudohoria. *Miner. Slov., 11, 3, 219 – 227.*

Varga, I. (Ed.), 1992: Záverečná správa úlohy Prognózne zdroje nerastných surovín SR – magnezit. *Manuscript. Bratislava, archive ŠGÚDŠ, 177 p.*

Ženiš, P. & Gaál, Ľ., 1986a: Nové jaskyne v magnezitoch Slovenského rudohoria. *Spravodaj SSS, 17, 1 – 2, 41 – 47.*

Ženiš, P. & Gaál, Ľ., 1986b: Magnesite karst in the Slovenské rudohorie Mts. (Czechoslovakia). *Communications, 9th International Congress of Speleology, 2, Barcelona, 36 – 39.*

Jaskyne v magnezitoch – vzácny fenomén krasovatenia: príkladová štúdia zo Slovenska

O existencii podzemných dutín na niektorých magnezitových ložiskách Slovenska sa zmienili viacerí autori (napr. Guľa, 1959; Klír, 1962, 1968; Cabala, 1976), prvý speleologický prieskum jaskýň v magnezitoch však vykonali až v roku 1983 v Dúbravskom masíve (Gaál a Ženiš, 1984). Následne boli preskúmané jaskyne aj v ďalších magnezitových ložiskách 120 km dlhej zóny karbónskych hornín pozdĺž severného okraja gemerika, a to v Podrečanoch, Burde, Lubeníku a na Bankove pri Košiciach (Ženiš a Gaál, 1986a, b; obr. 1). Doteraz je v slovenských magnezitoch preskúmaných 16 jaskýň s dĺžkou najčastejšie medzi 10 a 20 m, najdlhšie však dosahujú 73 m (BU-2 na Burde) a 51 m (DM-3 v Dúbravskom masíve). Z genetického hľadiska pri vzniku jaskýň v magnezitoch obsahujúcich Fe hrá podstatnú úlohu oxidácia Fe pozdĺž tektonických zlomov usmerňujúcich cirkuláciu atmosférickej vody a následný oxidačný rozklad železitých magnezitov na oker (hydroxidy Fe). Oker vyplavuje cirkulujúca voda, čím vznikajú voľné podzemné priestory (Trdlička, 1959; Gaál a Ženiš, 1984; Ženiš a Gaál, 1986a, b; Mitter a Pavlarčík, 1996). Novšie výskumy vykonané pomocou stabilných izotopov a fluidných inklúzií v minerálnej výplni jaskýň Dúbravského masívu dokázali ich hydrotermálny pôvod (Bella et al., 2013). Počas pôsobenia hydrotermálnych procesov oxidácia Fe prebiehala intenzívnejšie, ale prebieha aj v súčasnosti pôsobením presakujúcich atmosférických vôd vo vadóznych podmienkach či pri miešaní vôd v epifreatických, resp. freatických podmienkach. Koncepciu vytvárania jaskýň oxidáciou Fe v magnezitoch podporuje aj úplná absencia voľných podzemných priestorov na ložiskách bezželezitých magnezitov vo veporiku (napr. Hnúšťa-Mútnik, Sinec, Kokava) či v Gemerskej Polome v zóne centrálneho gemerika. Na základe merania úložných pomerov zlomov vo všetkých preskúmaných jaskyniach v magnezitoch sa zistilo, že podzemné priestory sa vytvorili ako dôsledok predispozícií vzniknutých povrchnokriedovými tektonickými strihmi alpínskeho deformačného štádia AD_3 pozdĺž lubenícko-margecianskej a košicko-margecianskej strižnej zóny (obr. 10). Toto deformačné štádium spôsobilo vznik strižných systémov smeru SV – JZ v západnej časti karbónskeho magnezitového pásma. Zistili sa v jaskyniach na lokalitách Podrečany, Burda, Lubeník a Dúbravský masív. Naproti tomu, vo východnej časti pásma a v jaskyni na lokalite Bankov dominuje smer tektonických diskontinuít SZ – JV. V niektorých prípadoch zlomy deformačného štádia AD_3 môžu reprezentovať reaktivované diskontinuity starších alpínskych deformačných štádií AD_1 alebo AD_2. Smery a sklony zlomov v preskúmaných jaskyniach dokazujú, že v rámci hlavných diskontinuít deformačného štádia AD_3 smerov SV – JZ a SZ – JV hrali hlavnú úlohu v genéze podzemných priestorov aj ich asociované AD_3 syntetické a antitetické strihy. Extenzné zlomy umožnili ľahkú cirkuláciu hydrotermálnych roztokov. Na základe vykonaných analýz fluidných inklúzií v dolomitových kryštáloch z jaskyne DM-7 v Dúbravskom masíve (obr. 8) išlo o nízko salinické roztoky s teplotou menej ako 150 °C. V neogéne, po prvých intenzívnych klenbovitých výstupoch územia Slovenského rudohoria a vyhĺbení dolín, výrazne poklesla hladina podzemnej vody a časť podzemných priestorov sa dostala do vadóznej zóny. Vo voľných priestoroch sa tým vytvorili vhodné podmienky na vznik aragonitu a palygorskitu, aké sa zistili v jaskyni DM-3 v Dúbravskom masíve (obr. 9). Preskúmané jaskyne v slovenských magnezitových ložiskách majú značný význam, pretože podobných jaskýň je vo svete známych len veľmi málo. Opísané sú z Tasmánie (Houshold, 1998; Houshold et al., 1999), z oblasti Ceara a Brumado Bahia v Brazílii (Bodenlos, 1950, 1954) alebo z Kalifornie a Nevady v USA (Hess, 1908; Gale, 1912). Sú to však menšie dutiny, ktoré podľa údajov známych v súčasnosti nedosahujú rozmery slovenských jaskýň v magnezitových telesách. Povrchové i podzemné formy reliéfu, ktoré vznikajú rozpúšťaním alebo chemickým rozkladom magnezitu, považuje Kiernan (1988) za parakras. V rámci parakrasu možno jaskyne v magnezitoch obsahujúcich Fe, ktoré vznikajú najmä rozkladom magnezitov v dôsledku oxidácie Fe, klasifikovať ako bradykras (Bella, 1994, 2011).

Doručené / Received: 13. 12. 2017
Prijaté na publikovanie / Accepted: 19. 12. 2017

Mineralia Slovaca, 49 (2017), 169 – 176
Web ISSN 1338-3523, ISSN 0369-2086

Cryptomelane, $K(Mn^{4+}_7Mn^{3+})O_{16}$, from the Dúbravica-Zolnica Fe deposit (North Veporic Unit, Slovak Republic)

ĽUBOŠ POLÁK[1*], JOZEF VLASÁČ[1], LUBOŠ VRTIŠKA[2] and TOMÁŠ MIKUŠ[3]

[1]Matej Bel University, Faculty of Natural Sciences, Department of Geography and Geology, Tajovského 40, 974 01, Banská Bystrica, Slovak Republic; *silur.devon7@gmail.com
[2]Department of Mineralogy and Petrology, National Museum, Cirkusová 1740, 193 00 Prague 9 - Horní Počernice, Czech Republic
[3]Earth Science Institute of the Slovak Academy of Sciences, Ďumbierska 1, 974 11, Banská Bystrica, Slovak Republic

Abstract: Cryptomelane, $K(Mn^{4+}_7Mn^{3+})O_{16}$, representing a member of the coronadite group and hollandite supergroup, is described from the abandoned Fe deposit Dúbravica-Zolnica (near the town of Banská Bystrica, Central Slovakia). Cryptomelane occurs in association with two generations of goethite and *limonite*. Cryptomelane is located on the cracks and in cavities of Lower Triassic quartzites, arkoses and sandstones of the Lúžna Formation (North Veporic Unit). It forms net of irregular veins of the steel grey to blue grey colour and botryoidal aggregates of steel grey colour. The thickness of veins is up to 3 mm. Botryoidal aggregates occur on the area of up to 2 x 3 mm. The lustre is in both cases earthy to dull, or metallic. Cryptomelane was confirmed by Raman spectroscopy and EPMA-WDS analyses. Its empirical formula is (in the mean of 8 point analyses): $(K_{0.64}Na_{0.06}Ba_{0.02}Sr_{0.01}Ca_{0.01}Zn_{0.01}Co_{0.01})_{\Sigma 0.76}[(Mn^{4+}_{6.97}U^{6+}_{0.02}P_{0.01})_{\Sigma 7.00}(Mn^{3+}_{0.83}Fe^{3+}_{0.12})_{\Sigma 0.95}]O_{16.00}$. Cryptomelane has a tunnel structure, in the case of this study these tunnels are occupied by water molecules. It is a weathering product of primary manganese mineral phases (probably rhodonite, pyrolusite or braunite). Formation of cryptomelane indicates slight change in pH and Eh. It precipitates at higher pH values, than associated Fe oxihydroxide minerals. The coexistence of iron and manganese oxidic minerals well corresponds to iron residual deposit.

Key words: cryptomelane, manganese minerals, Fe deposit, Dúbravica-Zolnica, North Veporic Unit, Western Carpathians

Graphical abstract

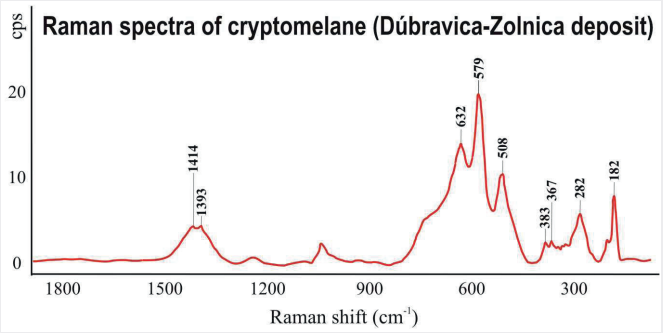

Highlights

- A new occurrence of cryptomelane in the territory of Slovakia – in the deposit Dúbravica-Zolnica – was confirmend by electron microanalyses and Raman spectroscopy
- Found cryptomelane extends the knowledge about the mineral forms of Mn in weathered Fe-oxihydroxide deposits
- Paper presents one of a few published Raman spectra of cryptomelane

Introduction

In the nature, the occurrences of manganese are very common and the Mn minerals are commonly in association with Fe minerals. The same is valid also in the case of the less known historical deposit of iron ores Dúbravica-Zolnica (district of Banská Bystrica, Slovakia). So far in Slovakia, the cryptomelane was identified in several geotectonic units. Specifically in the Neogene volcanic rocks of the Štiavnica Stratovolcano on the Banská Štiavnica deposit (Terézia vein), in Pieniny Klippen Belt on the Šarišské Jastrabie site, in North Veporic Unit in the Ľubietová-Podlipa deposit and in South Gemeric Unit in the Čučma deposit and the Malá Hekerová site (Jeleň et al., 2006; Luptáková et al., 2012; Rojkovič, 2001; Rojkovič et al., 2003). Cryptomelane belongs to the hollandite supergroup, respectively coronadite group. The ideal chemical formula is $K(Mn^{4+}_7Mn^{3+})O_{16}$. It is extended mainly in the oxidation zone of Mn deposits, most often fills intergranular spaces or replaces primary minerals, containing manganese (Biagioni et al., 2013). The subject of the contribution is the mineralogical characteristic of the cryptomelane, identified in the investigated deposit of Dúbravica-Zolnica.

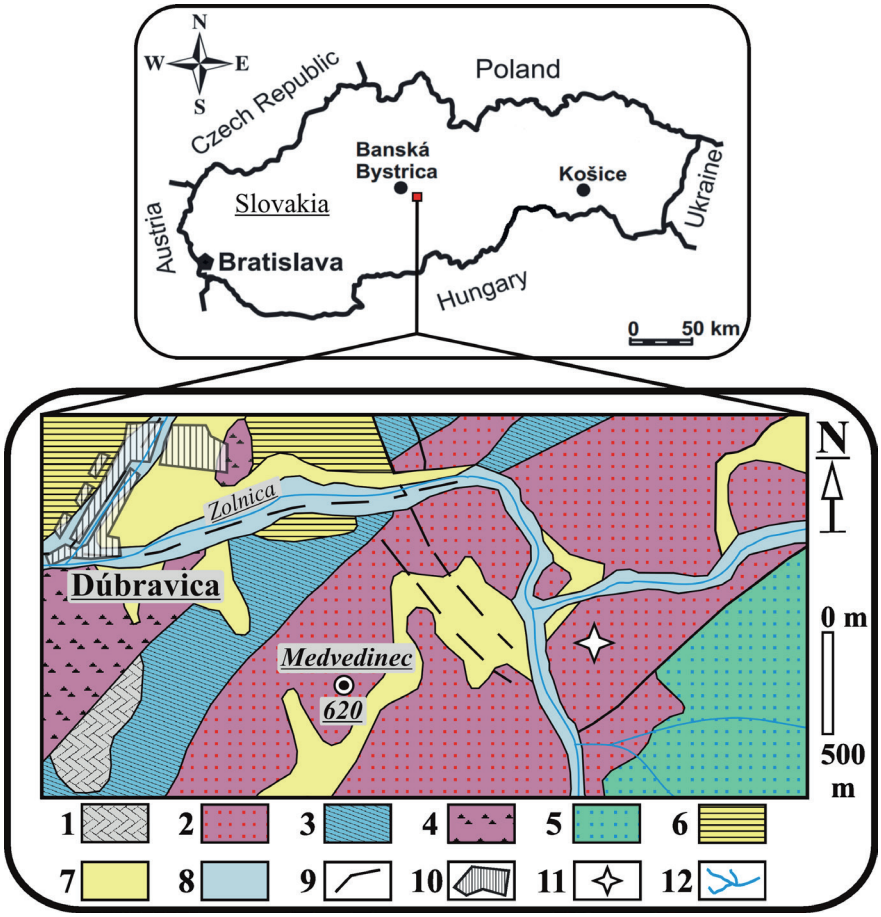

Fig. 1. Geological map of the occurrences of cryptomelane in the Dúbravica-Zolnica area (Dublan et al, 1997a, b). 1 - undivided Upper Permian colorful sandstones, conglomerates, shales, 2 - Lower Triassic quartzites, quartz to arkoses sandstones, 3 - Werfenian beds, 4 - Triassic dolomitic breccias and rauchwackes, 1-4 – Veporic Unit; 5 - lapilli-pumice tuffite, epiclastic vulcanic breccias, Lower-Middle Sarmatian; 6 - kaolinic tuffite, sandstones, claystones, Miocene; 7 - undivided deluvial sediments, Pleistocene; 8 - fluvial flood plain loams, Holocene; 9 - faults; 10 - built-up area; 11 - studied occurrence; 12 - stream.

Geological setting

The Dúbravica-Zolnica deposit is located in the Poľana Mountains, on the eastern side of the Zolnica creek, ca 2.5 km ESE from Dúbravica village (Fig. 1) and ca 1 km ENE from the Medvedinec hill (620 m a.s.l.). GPS coordinates of the cryptomelane occurrence are as follows: 48.67324° N and 19.30667° E.

Iron ores are developed on the cracks in light grey quartzite (Lower Triassic) of the Lúžna Formation of North Veporic Unit (Fejdiová, 1980). Deposit was open with a large number of prospect and mining galleries (towards the south), and also open cuts. The mining works are located on ca 300 x 300 m large area. Mined directional length was about 200 m and mined inclined length was 65 m (Petro et al., 2001).

Based on the distribution of open cut, there can be assumed that ores (*limonite* ores) are created by richer nest accumulation. During the earlier study of fragments of partially weathered dump pile material goethite and *limonite* were identified, which probably originated from hematite by weathering by meteoritic waters (Slavkay et al., 2004). The last analyses of ores were probably performed at the time of the deposit mining in 1872, when there is a mention, that the Fe_2O_3 content in the mined ores attains 46.31 wt. % and P_2O_5 2.94 wt. % (Bergfest, 1951).

Analytical methods

The optical properties of minerals were studied with the Nikon ECLIPSE LV 100 POL polarizing microscope in combination with the Nikon DS-Fi2 digital camera (Department of Geography and Geology, Faculty of Natural Sciences, Matej Bel University in Banská Bystrica, Slovak Republic), used for photography in transmitted and reflected light.

Chemical composition of cryptomelane was determined by the Jeol-JXA-8530F electron microprobe in WDS mode (Earth Science Institute of Slovak Academy of Sciences, Banská Bystrica, Slovak Republic). WDS microanalyses was determined under these conditions: acclerating voltage 15kV, probe current 20nA, beam diameter 5-10 µm, ZAF correction. Used elements, lines and detection limits (in ppm) are as follows: K(Kα, 21-66) - orthoclase, Ca (Kα, 25-27) - diopside, U (Mß, 57-65) - UO_2, Pb (Mß, 66-98) - crocoite, S (Kα, 31-36) - barite, P (Kα, 45-58)

- apatite, Na (Kα, 48-56) - albite, Si (Kα, 54-59) - albite, Al (Kα, 34-37) - corundum, As (Lα, 90-101) - $GaAs_2$, Mg (Kα, 32-38) - olivine, Zn (Kα, 231-267) - willemite, Cu (Kα, 98-112) - cuprite, Ni (Kα, 85-98) - pentlandite, Co (Kα, 48-55) - Co, Fe (Kα, 114-155) - olivine, Mn (Kα, 111-138) - rhodonite, V (Kα, 141-340) - $ScVO_4$, Ti (Kα, 131-197) - rutile, Ba (Lα 71-72) - barite, Sr (Lα 70-74) - celestine. Contents of the above elements, which are not included in Table 1, were quantitatively analyzed, but the detected contents were below the detection limits. Photo-documentation were made also in backscattered electron mode (BSE), applying the same device.

Cryptomelane was also identified by the Raman spectroscopy study by DXR dispersed spectrometer (Thermo Scientific) connections with confocal microscope Olympus (Department of Mineralogy and Petrology, National Museum, Prague). The analyses were held at following measurement conditions: lens zoom 50x, used laser 532 nm, measuring range 50-1880 cm^{-1}, exposure time 1 s, total exposure 1000, set laser power 4 mW, 50 µm slit of the aperture used, beam size 1.6 µm.

Results

Cryptomelane forms a net of irregular veins from steel grey to blue grey colour on crack walls in quartzites, less arkoses and sandstones. The thickness of veins is max. 3 mm, in average it is 1 mm in size (Fig. 2). Cryptomelane rarely creates botryoidal steel grey aggregates in the cavities of rocks (Fig. 3), of which the largest area size is 2 x 3 mm. The lustre is in both cases earthy to dull or metallic. The texture of ores is brecciated (Fig. 4) and coloform. Cryptomelane is in association with goethite of 1st generation (I), goethite of 2nd generation (II) and *limonite*, or occurs separately. Goethite II often replaces cryptomelane (Fig. 5) and goethite I is replaced by cryptomelane. In studied materials (thin sections) there were identified also quartz grains with the grain-size up to 1.5 mm, manifesting distinct undulose extinction. They are angular to subangular. Less often there are present feldspar, rarely micas, their size is up to 0.3 mm. Matrix is mostly of quartz or sericite type.

Study of chemical composition of cryptomelane (Table 1) has revealed the admixtures of Co and Zn (up to 0.013-0.022 apfu) in the cryptomelane structure. In the cationic position A there is characteristic the predominance of potassium (0.734 apfu) over sodium (0.082 apfu), barium (0.024 apfu) and stroncium (0.016 apfu). There was also found the presence of Ca (0.015 apfu). Interesting there is also the increased contents of Fe (0.215 apfu), U (0.021 apfu) and P (0.021 apfu) in position M1/2. Chemical composition of cryptomelane (average of 8 point analyses) can be expressed by the following

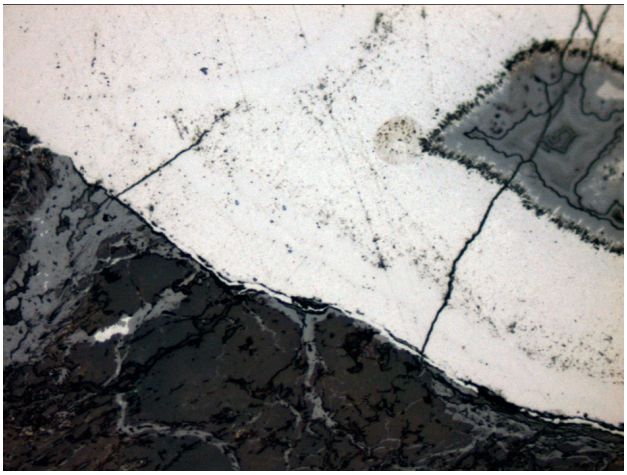

Fig. 2. Vein of cryptomelane (light) in association with Fe oxyhydroxides (grey). Length of bottom side is 50 µm. Photo: L. Vrtiška.

Fig. 3. Steel grey botryoidal aggregates of cryptomelane in the cavity in the limonitized quartzite. Length of bottom side is 6 mm. Photo: J. Vlasáč.

Fig. 4. Brecciated texture of iron ores. Length of bottom side is 12 cm. Photo: Ľ. Polák.

Tab. 1
Chemical composition of the cryptomelane from the Dúbravica-Zolnica deposit.

	1	2	3	4	5	6	7	8
P_2O_5	0.12	0.14	0.11	0.21	0.11	0.11	0.10	0.05
Al_2O_3	0.03	0.03	0.03	0.07	0.04	0.02	0.00	0.00
V_2O_3	0.00	0.06	0.09	0.00	0.00	0.00	0.00	0.01
Fe_2O_3	1.46	1.70	2.42	2.27	0.77	0.53	0.48	0.74
UO_3	0.53	0.59	0.62	0.69	0.46	0.83	0.60	0.59
SiO_2	0.00	0.04	0.00	0.00	0.00	0.00	0.02	0.00
TiO_2	0.00	0.00	0.02	0.00	0.00	0.00	0.00	0.03
MnO_2	93.72	92.85	93.31	92.15	95.21	94.23	93.34	95.08
CaO	0.12	0.11	0.11	0.08	0.09	0.09	0.11	0.10
CoO	0.14	0.10	0.10	0.13	0.12	0.10	0.10	0.10
BaO	0.41	0.44	0.51	0.41	0.31	0.18	0.22	0.15
SrO	0.19	0.21	0.19	0.22	0.20	0.23	0.21	0.14
ZnO	0.16	0.08	0.10	0.07	0.26	0.14	0.17	0.17
PbO	0.03	0.02	0.00	0.02	0.00	0.00	0.04	0.00
Na_2O	0.22	0.30	0.22	0.20	0.23	0.30	0.35	0.36
K_2O	3.80	3.97	4.36	4.83	3.48	4.26	4.28	4.71
H_2O	1.26	1.26	1.25	1.25	1.26	1.25	1.25	1.25
∑	102.19	101.90	103.54	102.60	102.80	102.28	101.29	103.47
Na^+	0.052	0.069	0.050	0.046	0.051	0.068	0.082	0.082
K^+	0.574	0.603	0.655	0.734	0.524	0.645	0.654	0.705
Ca^{2+}	0.015	0.014	0.014	0.010	0.012	0.012	0.014	0.012
Co^{2+}	0.013	0.010	0.009	0.013	0.012	0.010	0.010	0.009
Ba^{2+}	0.019	0.021	0.024	0.019	0.014	0.008	0.010	0.007
Sr^{2+}	0.013	0.015	0.013	0.015	0.014	0.016	0.015	0.010
Zn^{2+}	0.014	0.007	0.009	0.007	0.022	0.012	0.015	0.015
Pb^{2+}	0.001	0.001	0.000	0.001	0.000	0.000	0.001	0.000
∑A	0.701	0.840	0.774	0.845	0.649	0.771	0.801	0.840
cation charge A	0.777	0.807	0.842	0.908	0.721	0.830	0.867	0.891
Si^{4+}	0.000	0.005	0.000	0.000	0.000	0.000	0.003	0.000
Ti^{4+}	0.000	0.000	0.002	0.000	0.000	0.000	0.000	0.002
Mn^{4+}	6.975	6.966	6.972	6.962	6.979	6.968	6.972	6.978
P^{5+}	0.012	0.014	0.011	0.021	0.010	0.011	0.010	0.005
U^{6+}	0.013	0.015	0.015	0.017	0.011	0.021	0.015	0.015
∑M1	7.000	7.000	7.000	7.000	7.000	7.000	7.000	7.000
cation charge M1	28.000	28.000	28.000	28.000	28.000	28.000	28.000	28.000
Al^{3+}	0.004	0.004	0.005	0.010	0.006	0.003	0.001	0.000
V^{3+}	0.000	0.005	0.009	0.000	0.000	0.000	0.000	0.000
Mn^{3+}	0.712	0.684	0.627	0.617	0.769	0.756	0.753	0.731
Fe^{3+}	0.130	0.153	0.215	0.203	0.068	0.048	0.044	0.065
∑M2	0.846	0.846	0.856	0.830	0.843	0.807	0.798	0.796
cation charge M2	2.538	2.540	2.566	2.490	2.529	2.419	2.393	2.389
∑cation charge A, M1, M2	31.315	31.347	31.408	31.398	31.250	31.249	31.260	31.280
difference compared to neutral value	-0.685	-0.653	-0.592	-0.602	-0.750	-0.751	-0.740	-0.720

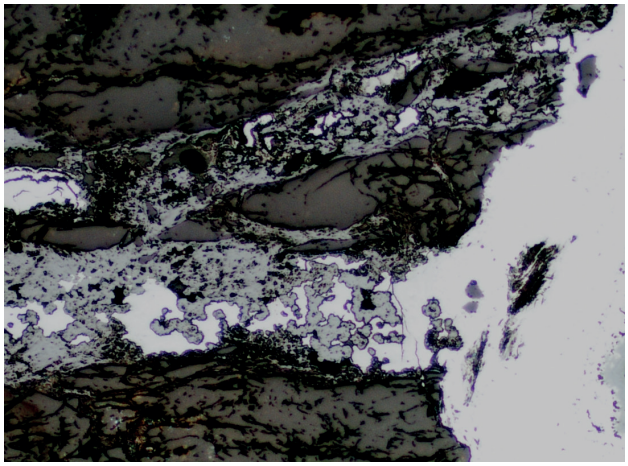

Fig. 5. Goethite II (2nd generation; light grey) replaces cryptomelane veins (white). Reflected light, parallel polaroids. Length of bottom side is 250 µm. Photo: Ľ. Polák.

empirical formula: $(K_{0.64}Na_{0.06}Ba_{0.02}Sr_{0.01}Ca_{0.01}Zn_{0.01}Co_{0.01})_{\Sigma 0.76}[(Mn^{4+}_{6.97}U^{6+}_{0.02}P_{0.01})_{\Sigma 7.00}(Mn^{3+}_{0.83}Fe^{3+}_{0.12})_{\Sigma 0.95}]O_{16.00}$.

Obtained Raman spectrum (Fig. 6) correlates very well with published cryptomelane spectra (Gao et al., 2008; Baranchikov et al., 2015).

Interpretation of the Raman spectrum of cryptomelane is as follows: The Raman spectrum shows low frequency bands at ~ 182 cm^{-1} (translation motion of MnO_6 octahedra), 282, 367 and 383 cm^{-1} (bending vibrations of Mn - O bonds). Strong high frequency bands at ~ 508, 579 and 632 cm^{-1} correspond to symmetrical vibrations of oxygen atoms relative to manganese atoms along the octahedra chains and Mn-O stretching vibrations in the direction perpendicular to the double chains of MnO_6 octahedra. At the same time sharp bands at 579 and 632 cm^{-1} indicate a well-developed tetragonal structure of cryptomelane with an interstitial space consisting of tunnels (2 x 2). Bands at 1393 a 1414 cm^{-1} can be assigned to OH^- bond. Other bands in Raman spectrum which were not assigned with any bonds are the result of very minor admixtures contributing to the overall chemical composition of cryptomelane.

Discussion

In the area of the North Veporic Unit, the mineralogical research has been devoted mainly to Cu minerals (e.g. the Ľubietová deposit) and less to manganese oxides and hydroxides. Rarely, the manganese minerals were identified in the Ľubietová-Podlipa deposit (Luptáková et al., 2012) and recently revealed Poniky-Holý Vrch deposit, without detailed characteristics (Polák and Vlasáč, 2017).

In the case of cryptomelane and its occurrences in the Slovak Republic it is important to mention that the occurrences of this mineral have not been always clearly identified, which relates the cases of cryptomelane from

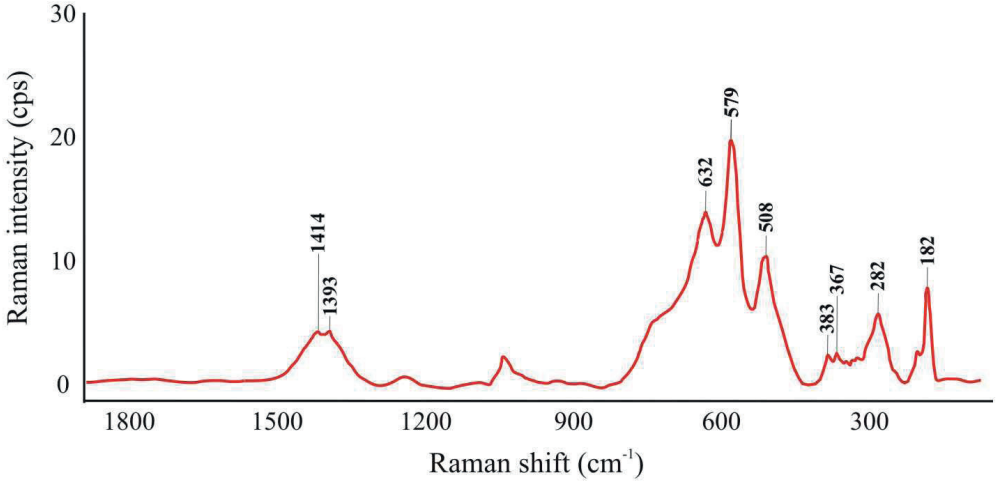

Fig. 6. Raman spectrum of cryptomelane from the Dúbravica-Zolnica deposit.

the Čučma deposit and the Malá Hekerová site in South Gemeric Unit (Rojkovič, 2001), as well as the cave Skalistý Potok in the Silicic Unit (Bónová et al., 2008). In the first two cases, the potassium content in cryptomelane is very low, occurring in its cationic position A. In the third case, cryptomelane was determined only by X-ray powder diffraction analyses and major cryptomelane reflexes overlap with vernardite reflexes. Cryptomelane from the Dúbravica-Zolnica deposit has a similar composition as the cryptomelane, which has been uniquely identified by other authors (e.g. Jirásek et al., 2015; Maleňáková et al., 2016).

Only slightly increased amount of chemical analyses of cryptomelane is probably caused by its hydratation, resp. by the presence of zeolite water in its crystal structure (Pasero, 2005). Hollandite supergroup, respectively coronadite group to which cryptomelane belongs, has five valid end members (Biagoni et al., 2013). The difference is mainly in position A, where the tunnel cation can be occupied by potassium, lead, barium, sodium and strontium (Pasero, 2005). The first mention about the increased content of manganese on the Dúbravica-Zolnica deposit occurs in work by Kerpely (1872, ex Bergfest, 1951). The Mn_3O_4 content was 5.99 wt. %. Content of Fe_2O_3 was 46.31 wt. % and P_2O_5 2.94 %. Despite the increased phosphorus content in the deposit, no phosphorus bearing minerals were identified yet, having this element present in its crystal structure in either major, or minor amount. The common existence of manganese and iron oxides (+/- hydroxides) is common in nature (e.g. Hildebrand and Mosier, 1974; Siddiquie et al., 2015). Studied association in this work is relatively poor in many related mineral phases (e.g. coronadite, hollandite or manjiroite).

Cryptomelane is typical by a tunnel structure (so-called tunnel oxides - e.g. Pasero, 2005), which is made up of individual, twinned or wider MnO_6 octahedron chains, joined together through the edges into a mesh that closes the tunnels thus formed inside the structure (Biagoni et al., 2013). These tunnels can be occupied by water molecules and the previously mentioned cations (Na^+, K^+, Sr^{2+}, Ba^{2+} and Pb^{2+}). Water molecules occupy free positions in the canal site together with dominant K in the studied cryptomelane. In particular, the presence of water in cryptomelane confirms the calculation from WDS analyses (Table 1) and OH^- group is demonstrated by the Raman spectrum (Fig. 6). Length of hydrogen bond O-H...O, calculated according to an empirical formula of Libowitzky (1999), is ~ 2,47 Å.

Increased content of different cations (including trace elements) in oxides and hydroxides of Mn, is the result of their strong sorption abilities. For example, in the Silver Cliff site in Colorado, U.S.A., the cryptomelane structure is bearing 1 wt. % of silver (Ravikumar and Fuerstenau, 1997).

The iron ores (+/- cryptomelane) are typical with brecciated texture. The mineralization in the Dúbravica-Zolnica iron deposit is classified as the weathered, residual type (Slavkay et al., 2004). Cryptomelane in the case of this study represents the final (secondary) product of the primary minerals phases weathering. The manganese for the formation of the cryptomelane could be from two sources: (1) The Middle- to Upper Triassic dolomites, which can contain elevated Mn or Fe contents and occur in a close vicinity of the deposit (Polák et al., 2003). Manganese could be leached from these dolomitic rocks by the surface water, bringing it into the oxidation zone of the deposit. However, we suggest (2) the unspecified primary Mn minerals from already inaccessible parts of the deposit as the most probable sources of the manganese. Most likely, whey were hydroxides and oxides of manganese, because the carbonate rocks are not directly present in the deposit. These facts support an opinion (Hill and Forti, 1997) that at the surface pressures and temperatures the water soluble manganese ions (Mn^{2+} mobile form) oxidize to Mn^{3+} and Mn^{4+} ions (immobile form), which due to very low solubility of stable minerals accumulate at the top of weathering profiles of rocks and mineralized bodies.

Slight change in pH and Eh conditions during precipitation of Fe-Mn indicates cryptomelane, which precipitates at higher pH values, than iron minerals (Bouška et al., 1980). The potassium, which is located in the cryptomelane structure, is a product of chemical weathering, resp. the decomposition and subsequent transport of potassium feldspars, which are present in the deposit located in arkoses and sandstones.

Conclusion

The new occurrence of cryptomelane on the territory of the Slovakia was unambiguously confirmed by electron microanalyses and Raman spectroscopy. Finding the cryptomelane mineral extends our knowledge about the mineral forms of Mn in weathered Fe-oxide deposits, on an example of the Dúbravica-Zolnica deposit. In this contribution is presented one of the small number of published of Raman spectra of cryptomelane, and the length of the hydrogen bond O-H... O to ~ 2.47 Å was calculated. The empirical formula is $(K_{0.64}Na_{0.06}Ba_{0.02}Sr_{0.01}Ca_{0.01}Zn_{0.01}Co_{0.01})_{\Sigma 0.76}[(Mn^{4+}_{6.97}U^{6+}_{0.02}P_{0.01})_{\Sigma 7.00}(Mn^{3+}_{0.83}Fe^{3+}_{0.12})_{\Sigma 0.95}]O_{16.00}$.

Acknowledgements

The contribution was created owing to the financial support from the grant APVV-15-0050, VEGA 1/0650/15 and project ITMS 26210120024. Authors express their thanks to reviewers - Professors P. Uher and M. Košuth for their improvement of the original manuscript.

References

Baranchikov, A. E., Boytsova, O. & Ivanov, V. K., 2015: Synthesis of Nanocrystalline Birnessite and Cryptomelane by Microwave Hydrothermal Treatment. *Russ. J. Inorg. Chem., 60, 11, 1 419 – 1 424.*

Bergfest, A., 1951: The mining in Ľubietová on iron ores. II. part history of mining in Ľubietová. Manuscript. *Bratislava, SGIDŠ, not paged* (in Slovak).

Biagioni, C., Capalbo, C. & Pasero, M., 2013: Nomenclature tunings in the hollandite supergroup. *Eur. J. Mineral., 25, 85 – 90.*

Bouška, V., Jakeš, P., Pačes, T. & Pokorný, T., 1980: Geochemistry. *Prague, Academy, 555* (in Czech).

Bónová, K., Derco, J. & Hochmuth, Z., 2008: Mineralogical study of sediments from cave Skalistý potok (Slovak Krast). *Geogr. Cassoviensis, II, 1, 13 – 18.*

Dublan, L., Bezák, V., Biely, A., Bujnovský, A., Halouzka, R., Hraško, Ľ., Köhlerová, M., Marcin, D., Onačila, D., Scherer, S., Vozárová, A., Vozár, J. & Žáková E., 1997a: Geological map of Poľana, 1 : 50 000. *Bratislava, SGIDŠ.*

Dublan, L., Bezák, V., Biely, A., Bujnovský, A., Halouzka, R., Hraško, Ľ., Köhlerová, M., Marcin, D., Onačila, D., Scherer, S., Vozárová, A., Vozár, J. & Žáková E., 1997b: Explanatory notes to the geological map of Poľana 1 : 50 000. *Bratislava, SGIDŠ, 238.*

Fejdiová, O., 1980: The Lúžna Formation – formal lower Triassic litostratigraphy Unit. *Geol. Práce, Spr.*, *74, 95 – 101.*

Gao, T., Glerup, M., Krumeich, F., Nesper, R., Fjellvag, H. & Norby, P., 2008: Microstructures and Spectroscopic Properties of Cryptomelane-type Manganese Dioxide Nanofibers. *J. Phys. Chem. C., 112, 34, 13 134 – 13 140.*

Hill, C. A. & Forti, P., 1997: Cave minerals of the World. *Huntsville, National Speleol. Soc., 464.*

Hildebrand, F. A. & Mosier, E. L., 1974: Argentian Cryptomelane and Bromargyrite in Volcanic Rocks near Silver Cliff, Colorado. *Geol. Surv. Bull., 1 382 – C, 543 – 585.*

Jeleň, S., Háber, M., Andráš, P. & Stankovič J., 2006: Manganese minerals from the oxidation zone of Banská Štiavnica deposit. *In: Acta mineral. petrogr. (Szeged), 5, 52.*

Jirásek, J., Matýsek, D., Vaculíková, L. & Sivek, M., 2015: Hollandite and cryptomelane from Poniklá at Jilemnice, Czech Republic. *Bull. Mineral.-petrol. Dep. Nat. Mus. (Prague), 21, 1, 103 – 108* (in Czech).

Libowitzky, E., 1999: Correlation of O-H stretching frequencies and O-H…O hydrogen bond lengths in minerals. *Monatshefte Chem., 130, 1 047 – 1 059.*

Ľuptáková, J., Milovská, S., Biroň, A., Jeleň S. & Andráš P., 2012: Study of secondary minerals of abandoned Cu deposit Ľubietová-Podlipa (Slovakia). *In: Acta mineral. Petrogr. (Szeged), 7, 80.*

Maleňáková, A., Matýsek, D., Jirásek, J., Welser, P. & Zikeš, J., 2016: Cryptomelane from South Bohemia quartz veins. *Mineral: The world of minerals and precious stones, 24, 3, 269 – 271* (in Czech).

Pasero, M., 2005: A short outline of the tunnel oxides. *Rev. Mineral. Geochem., 57, 291 – 305.*

Petro, M., Ozdín, D. & Ferenc, Š., 2001: Metalogenetic of Ľubietová Zone and the adjacent part of the Hronské synclinory: Text Attachment to the Geological report. *Manuscript. Bratislava, Archive of SGIDŠ, 1 – 93* (in Slovak).

Polák, Ľ. & Vlasáč, J., 2017: Historical mining of iron ores between Poniky and Osrblie village (central Slovakia) I. *Mineral: The world of minerals and precious stones, 25, 2, 188 – 193* (in Slovak).

Polák, M., Filo, I., Havrila, M., Bezák, V., Kohút, M., Kováč, P., Vozár, J., Mello, J., Maglay, J., Elečko, M., Vozárová, A., Olšavský, M., Siman, P., Buček, S., Siráňová, Z., Hók, J., Rakús, M., Lexa, J., Šimon, L., Pristaš, J., Kubeš, P., Zakovič, M., Liščák, P., Žáková, E., Boorová, D. & Vaněková, H., 2003: Explanatory notes to the geological map of Starohorské vrchy Mts., Čierťaž Mts. and North part of Zvolen basin, 1 : 50 000. *Bratislava, SGIDŠ.*

Ravikumar, R. & Fuerstenau, D. W., 1997: Silver Sorption by Manganese Oxide. *Mater. Res. Soc. Proc., 31 – 39.*

Rojkovič, I., 2001: Early Paleozoic Manganese Ores in the Gemericum Superunit, Western Carpathians, Slovakia. *Geolines, 13, 34 – 41.*

Rojkovič, I., Ožvoldová, L. & Sýkora, M., 2003: Manganese mineralization near Šarišské Jastrabie village, Pieniny Klippen Belt, Western Carpathians, Slovakia. *Slovak Geol. Mag., 9, 51 – 64.*

Siddiquie, F. N., Alam, J. & Shaif, M., 2015: Occurrence of Manganese Ore Deposits and Their Mineralogy in Vizianagaram-Visakhapatnam Manganese Ores Belt (Andra Pradesh) India. *International J. Geosci., 6, 549 – 566.*

Slavkay, M., Beňka, J., Bezák, V., Gargulák, M., Hraško, Ľ., Kováčik, M., Petro, M., Vozárová, A., Hruškovič, S., Knésl, J., Knéslová, A., Kusein, M., Maťová, V. & Tulis, J., 2004: Mineral deposits of the Slovak Ore Mountains. *Bratislava, SGIDŠ,* 282 (in Slovak).

Kryptomelán $K(Mn^{4+}{}_7Mn^{3+})O_{16}$ z Fe ložiska Dúbravica-Zolnica (severné veporikum)

Témou príspevku je kryptomelán $K(Mn^{4+}{}_7Mn^{3+})O_{16}$ (člen hollanditovej superskupiny, coronaditovej skupiny), ktorý bol identifikovaný na základe Ramanovej spektroskopie (obr. 6) a elektrónovej mikroanalýzy (tab. 1). Minerál bol zistený na menej známom historickom železnom ložisku Dúbravica-Zolnica (obr. 1), ktoré sa nachádza v spodnotriasovom lúžňanskom súvrství v oblasti severného veporika v pohorí Poľana (Dublan et al., 1997a; Fejdiová, 1980). V minulosti malo ložisko v tejto oblasti väčší význam, pretože bolo dôležitým zásobovateľom 2 km vzdialenej vysokej pece v Ponickej Hute železnou rudou.

Na základe rozloženia povrchových dobývok sa dá usudzovať, že zrudnenie (*limonitické* rudy) tvorili bohatšie hniezdovité akumulácie. Počas posledného štúdia haldového materiálu sa zistili len goethit a *limonit*, ktoré pravdepodobne vznikli zvetrávaním hematitu meteorickými vodami (Slavkay et al., 2004). Posledné analýzy rudy sa vykonávali pravdepodobne v čase exploatácie ložiska v roku 1877. Uvádzajú, že obsah Fe_2O_3 v ťažených rudách bol 46,31 hm. %, Mn_3O_4 5,99 hm. % a P_2O_5 2,94 hm. % (Bergfest, 1951).

Minerál sa (spolu s Fe zrudnením) nachádza na puklinách a dutinách kremencov, arkóz a pieskovcov. Vytvára siete nepravidelných žiliek modrosivej až oceľovosivej farby, hrubých maximálne do 3 mm (v priemere do 1 mm; obr. 2) a botryoidné agregáty (obr. 3) oceľovosivej farby v maximálnom plošnom rozsahu 2 x 3 mm. Lesk je zemitý až matný, poprípade kovový. Textúra rúd je brekciovitá (obr. 4) a koloformná. V študovanom materiáli (vo výbrusoch) boli identifikované aj klasty kremeňa s výrazným undulóznym zhášaním vo veľkosti do 1,5 mm. Sú angulárne až subangulárne. Menej sú prítomné živce, zriedkavo sľudy. Ich veľkosť je do 0,3 mm. Matrix má väčšinou kremenný, poprípade sericitový charakter. Kryptomelán sa nachádza v asociácii s goethitom I. a II. generácie a *limonitom*. Goethit II často nahrádza kryptomelán (obr. 5) a goethit I je zas nahrádzaný kryptomelánom. Celkovo je však asociácia chudobná na prítomnosť iných príbuzných minerálov, ako sú napr. hollandit, coronadit alebo manjiroit.

Štúdiom chemického zloženia kryptomelánu (tab. 1) sa zistili v jeho štruktúre prímesi Co a Zn (do 0,01 a 0,02 *apfu*). Na katiónovej pozícii *A* je charakteristická prevaha draslíka (0,73 *apfu*) nad sodíkom (0,08 *apfu*), báriom (0,02 *apfu*) a stronciom (0,02 *apfu*), zistila sa aj prítomnosť Ca (0,02 *apfu*). Zaujímavý je aj zvýšený obsah Fe (0,22 *apfu*), U (0,02 *apfu*) a P (0,02 *apfu*) v pozícii M1/2. Empirický vzorec bol na základe elektrónovej mikroanalýzy (priemer 8 bodových analýz) stanovený takto: $(K_{0.64}Na_{0.06}Ba_{0.02}Sr_{0.01}Ca_{0.01}Zn_{0.01}Co_{0.01})_{\Sigma 0.76}[(Mn^{4+}{}_{6.97}U^{6+}{}_{0.02}P_{0.01})_{\Sigma 7.00}(Mn^{3+}{}_{0.83}Fe^{3+}{}_{0.12})_{\Sigma 0.95}]O_{16.000}$

Získané Ramanovo spektrum poskytlo informácie o prítomnosti rozličných pásov, ktoré sa pripisujú do rodiny mangánových oxidov (obr. 6). Spektrum veľmi dobre korešponduje s publikovanými hodnotami spektra kryptomelánu (Gao et al., 2008; Baranchikov et al., 2015). Ramanovo spektrum zobrazuje nízkofrekvenčné pásy pri ~ 182 cm^{-1} (translačný pohyb MnO_6 oktaédra), 282, 367 a 383 cm^{-1} (deformačná vibrácia Mn-O väzieb). Silné vysokofrekvenčné pásy sú pri ~ 508, 579 a 632 cm^{-1} a zodpovedajú symetrickým vibráciám atómov kyslíka vzhľadom na atómy mangánu pozdĺž oktaédrických reťazcov a valenčným vibráciám Mn-O väzieb v kolmom smere na dvojité reťazce oktaédrov MnO_6. Ostré pásy pri 579 a 632 cm^{-1} zároveň naznačujú dobre vyvinutú tetragonálnu sústavu kryptomelánu s intersticiálnym priestorom pozostávajúcim z tunelov (2 x 2). Pásy pri 1 393 a 1 414 cm^{-1} je možné priradiť k väzbe OH^-. Ostatné pásy v Ramanovom spektre, ktoré neboli priradené k žiadnym väzbám, sú výsledkom veľmi minoritných prímesí podieľajúcich sa na celkovom chemickom zložení kryptomelánu.

Pre kryptomelán je typická tunelová štruktúra (Biagioni et al., 2013), do ktorej môžu vchádzať molekuly vody napriek tomu, že jeho ideálny vzorec ju neobsahuje. To je aj prípad tejto štúdie kryptomelánu, do ktorého štruktúry vchádza zeolitová voda. Tá sa potvrdila elektrónovou mikroanalýzou aj Ramanovou spektroskopiou. Na základe prejavu OH^- väzieb v Ramanovom spektre bola vypočítaná dĺžka väzby O–H...O na ~ 2,47 Å (Libowitzky, 1999). Prítomnosť zeolitovej vody v jeho štruktúre však podľa platnej nomenklatúry hollanditovej superskupiny nie je podnetom na vyčlenenie nového minerálneho druhu (Ozdín et al., 2004).

Kryptomelán je finálny produkt zvetrávania primárnych mangánových minerálnych fáz, ktoré sa však v rámci tejto práce nezistili. Zdrojom mangánu mohli byť: a) stredno- až vrchnotriasové dolomity, ktoré môžu bežne obsahovať prímes mangánu. Z nich mohol byť mangán vylúhovaný povrchovou vodou, vďaka čomu sa mohol dostať do prostredia oxidačnej zóny ložiska a povrchovo blízkych partií; b) primárne minerály mangánu, ktoré sa nachádzali/nachádzajú v častiach ložiska, v súčasnosti neprístupných. Zdrojom draslíka prítomného v štruktúre kryptomelánu môžu byť arkózy a pieskovce, resp. chemické zvetrávanie živcov, z ktorých bol počas rozkladu draslík následne transportovaný. Ložisko má zvetrávací, reziduálny charakter (Slavkay et al., 2004).

Doručené / Received: 13. 11. 2017
Prijaté na publikovanie / Accepted: 19. 12. 2017

Mineralia Slovaca, 49 (2017), 177 – 184
Web ISSN 1338-3523, ISSN 0369-2086

The quality improvement of non-metallic raw materials by bioleaching

IVETA ŠTYRIAKOVÁ[1], ALEXANDRA BEKÉNIOVÁ[2] and DARINA ŠTYRIAKOVÁ[3]

[1]State Geological Institute of Dionýz Štúr, Regional center Košice, Department of Applied Technology of Raw Materials, Jesenského 8, 04001 Košice, Slovakia; iveta.styriakova@geology.sk
[2] Institute of Geotechnics Slovak Academy of Sciences, Watsonová 45, 040 01 Košice, Slovakia
[3]Institute of Geosciences, Faculty of Mining, Ecology, Process Control and Geotechnologies, Technical University of Košice, Park Komenského 15, 042 00 Košice, Slovakia

Abstract: The process of biological leaching is a simple and effective technology for quality improvement of non-metallics, which is possible to use either as a pretreatment of these raw materials before the electromagnetic separation for the increase of the yield at iron removal, or as an autonomous 1-3 months lasting treatment of non-metallics in the processes of discontinuous static leaching in the water environment. These processes were tested under laboratory conditions, applying the quartz sands from the deposits of Vyšný Petrovec, Šaštín and Plachtince, next the feldspar raw materials from localities of Liešťany, Vydrovo and Rudník, as well as the kaolin from the deposits of Horná Prievrana, Vyšný Petrovec and Rudník. The amount of removed iron was not directly proportional to the initial iron content in the natural samples**;** it was dependent on the mineralogical composition of the iron minerals and on the binding of Fe with the clays and silicate minerals, as well as on the grain-size of the iron minerals, the bioleaching conditions, and on the addition of chelating substances. The heterotrophic bacteria, growing in the presence of all non-metallic raw materials, were able to dissolve the iron. Quickly forming anaerobic conditions by bacteria for iron reduction and dissolution enable simple manipulation with the sample solution.

Presented simple comparison of laboratory bioleaching experiments for iron decrease applying the heterotrophic bacteria on non-metallics were conducted to explore the best economical way for non-metallic raw materials treatment with the elimination of conventional operations in the industrial scale. The laboratory experiments of the iron removal from the host industrial minerals were verified twice - during the *in-situ* conditions applying the quartz sand, where the unsterile climatic conditions were taken into consideration. At the *in-situ* bioleaching of the quartz sands, the changes of medium pH, oxygen and glucose concentration, as well as bioleaching time, were the important factors during iron removal.

Key words: non-metallic raw materials, kaolin, feldspars, quartz sands, bioleaching

Graphical abstract

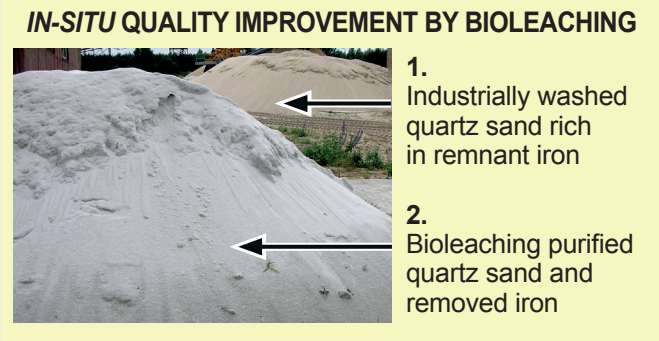

Highlights

- Removal of natural fine iron coatings from the surface impurities on silicate grains of non-metallic raw materials allows their industrial utilization
- The bioleaching of the non-metallic raw materials caused breaking of the bindings in the iron-silicate minerals and their purification
- This *in-situ* bioleaching purification process of quartz sands was verified the first time in Slovakia

Introduction

The non-metallic raw materials, such as carbonates and silicates, contain no energy source for the microorganisms to utilize. Such raw materials may be leached applying the heterotrophic bacteria and fungi, which require an organic source as a source of energy and carbon for their growth. Bioleaching of non-metallic raw materials and minerals may be used for the recovery of valuable metals from the low-grade ores and minerals, as well as for the beneficiation of raw materials (Jain and Sharma, 2004).

Industrial silicate-based minerals, such as kaolin, feldspars and quartziferous sands, often contain impurities that lower their economic value and hinder their application in the ceramic and paper industries. The main impurities are Fe(III)-oxides, because they lower the degree of whiteness, being an important factor related to the quality of the product (Veglio, 1997).

The chemical treatment methods are based on the leaching with mineral acids and treatment with reducing agents such as Na-dithionite and Al-sulphate, sulphur dioxide and Al-powder, or sulphur dioxide and Zn-powder. These bleaching methods are usually suitable for achieving a high degree of iron removal, but they are expensive, need complex operating conditions, and are environmentally hazardous (Mesquita et al., 1996).

The bioleaching is environmental friendly, it may lower operational cost and energy requirements. Heterotrophic bacteria have the potential for producing acidic metabolites that can solubilize oxide, silicate, carbonate and hydroxide minerals by reduction, acid attack, and complexation mechanisms (Jain and Sharma, 2004).

Naturally occurring silicates contain oxidic iron minerals as coatings on grains or impregnations in the matrix. The extent of iron removal from industrial silicate minerals depends on the mineralogy and distribution of iron in silicate rocks. For this reason, bioleaching studies with industrial minerals for their beneficiation have examined the kinetics of iron dissolution from the siliceous matrix (Veglio, 1997).

Heterotrophic bacteria production of organics by fermentation (Štyriaková et al., 1999), or reductive dissolution of Fe mineral phases from non-metallics (Štyriaková et al., 2003a) greatly accelerates the destruction of mica (Štyriaková et al., 2004, Štyriaková et al., 2003c) and smectite (Štyriaková et al., 2006b), or silicate matrix that is impregnated with iron minerals (Štyriaková et al., 2003a).

The purpose of the present study is to provide an overview of biochemical leaching of the non-metallics and to highlight the recent advances in application of this process for purification of industrial silicate minerals such as kaolin, feldspars and quartz sands.

Bioleaching

Bioleaching was tested under laboratory conditions on feldspar raw materials of localities Liešťany (F1), Vydrovo (F2), Rudník (F3), on kaolin from the deposits of Horná Prievrana (K1), Vyšný Petrovec (K2) and Rudník (K3), as well as on quartz sands of the ore Šaštín (Q1), Vyšný Petrovec (Q2) and Plachtince (Q3). *In-situ* bioleaching processes were attested by half-processing of quartz sands of the Šaštín deposit.

Laboratory bioleaching

The bioleaching experiments were carried out independently in 300 ml and 500 ml Erlenmeyer flasks containing 10 g powdered feldspar (F), 50 g quartz sands (Q) and 100 ml liquid medium and also 100 g kaolin (K) and 300 ml of liquid medium. The medium contained 2.0 g K_2HPO_4, 1.0 g $(NH_4)_2SO_4$, 0.1 g $CaCl_2$, 0.2 g NaCl, 0.085 g $NaNO_3$, 0.2 g urea and 0.1 g yeast extract, as well as 20 g of glucose per liter. The samples were inoculated with indigenous heterotrophic bacteria. The flasks were incubated under static conditions at 24 °C, with the contents being stirred to homogenize the solution prior to sampling and chemical analyses. After 10 minutes of centrifugation at 10 000 rpm, the culture solution was separated from the sample. The liquid supernatant was collected three times, always after the replacement of the culture solution during the bioleaching experiment. Appropriate abiotic controls were included in the experiments of article citations.

In-situ bioleaching

The *in-situ* bioleaching experiments were carried out with 13 tons of Q in fixed-basin container (volume 16.3 m^3), being filled with a leaching solution consisting of 7000 l of fresh surface water, supplemented with (per litre) 0.5 g NaH_2PO_4, 1.0 g $(NH_4)_2SO_4$ and 0.2 g NaCl. Moreover 20 g of technical-grade glucose A60 per litre media with 2mM Na_2EDTA was added into the container, too. The container was incubated under static ambient conditions for 3 months. The liquid phase was replaced four times with 7000 litres of fresh medium. The spent media (leachates) were sampled for iron analysis. Bioleaching experiments and analyses were conducted in duplicate, and the presented data are the averaged value of the measurements.

Laboratory bioleaching

Feldspar raw materials

Iron removal (Tab. 1) from feldspar ores by heterotrophic bacteria was investigated during 95 days of samples incubation. Three types of feldspar raw materials were used (F1) leucocratic granitoid; (F2) hydrolite granite and (F3) granite (Štyriaková et al., 2006a). The overall effect of batch bioleaching on Fe removal was different in these individual samples.

Granite was the most suitable feldspar raw material in iron removal by bioleaching. Despite the fact that Fe_2O_3 content in granite was two times higher than in samples F1 and F2, the effect of biological leaching on the sample F3 (Tab. 1) was manifested more expressively, up to 60 % decrease of Fe content in this raw material. It is postulated that Fe is not as tightly bound between grains or on the surface of silicate particles. The bioleaching of hydrolite granite and leucocratic granite was less effective and the decrease in the Fe content was about 22–35 %.

The amount of solubilized and removed iron from feldspar ores was not directly proportional to the initial Fe content in natural sample, because it was dependent on mineralogical composition of iron minerals and the dis-

Tab. 1
Comparison of iron content before and after bioleaching of feldspars raw materials.

Feldspar ores	Fe_2O_3 (wt.%) before bioleaching	Fe_2O_3 (wt.%) after bioleaching
F1	0.175	0.114
F2	0.198	0.129
F3	0.288	0.115

semination of iron minerals in silicate matrix. Although, the bioleaching released the Fe impurities from the silicate mineral matrix, additional chemical leaching with 0.1 M oxalic acid and subsequent magnetic separation allows to increase their iron removal. The chemical leaching applied after the bioleaching increased the iron concentration only negligible, up to 41 % and 25 % in the sample F1 and F2, respectively (Figs. 1, 2 and 3). The magnetic separation and the combination of bioleaching and magnetic separation decreased the content of independent particles of iron minerals and mica, which ensure the higher quality and white colour of raw materials. The whiteness of feldspar raw materials (mainly F1 and F3) was confirmed by smelting (Figs. 1 and 3) because the subsequent magnetic separation decreased the Fe content below to 69–75 % in the samples F1 and F3. The sample F2 did not contain the magnetic minerals. A low decrease in the Fe-content of the sample (F2) is a result of geological transformation of granite, which underwent the hydrothermal transformation – illitization up to kaolinization.

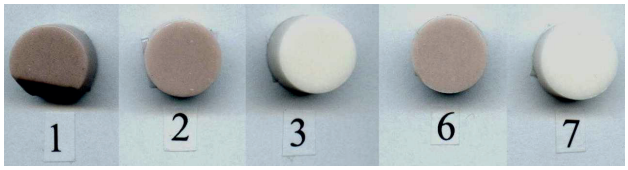

Fig. 1. Smeltings of the untreated sample F1 (1), bioleached sample (2), bio-chemical leached sample (6), bioleached and magnetic separated sample (3), bio-chemical leached and magnetic separated sample (7).

Fig. 2. Smeltings of the untreated sample F2 (10), bioleached samples (11), bio-chemical leached (14).

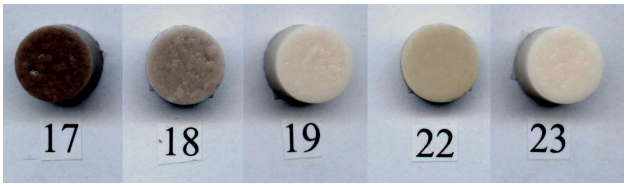

Fig. 3. Smeltings of the untreated sample F3 (17), bioleached sample (18), bio-chemical leached sample (22), bioleached and magnetic separated samples (19), bio-chemical leached and magnetic separated sample (23).

A dramatic increase in Fe, Si and K release was also observed due to the destruction of feldspars and Fe oxides in granitic eluvium by bacteria of *Bacillus spp.* (Štyriaková et al., 2003b). The results obtained in the laboratory conditions suggest that this bacterial genus, ubiquitous in silicate rocks, plays an important role in biochemical destruction of feldspars, as well as in the cycle and transformation of iron bearing minerals. Despite the decrease of distribution of fine-grained fraction, there was observed the increase in the value of the specific surface area of feldspar grains from 3.65 m^2/g to 4.82 m^2/g. This fact confirms the activity of bacteria of *Bacillus* genus in point corrosion of mineral grains suitable for the releasing of iron mineral disseminations in silicate matrix.

A summary of the iron dissolution results achieved by various investigators is given by Eisele and Gabby (2014). The large variation in results appears to be mainly due to (a) differences in the organisms used; (b) varying degrees of crystallinity of the iron minerals being dissolved; and (c) differing goals of the leaching process. Some of these studies are examining removal of iron contaminants from another material, some are specifically recovering iron as a product, and some are describing geochemical studies that are not attempting to maximize iron dissolution for industrial application at all.

Tab. 2
Comparison of iron content before and after kaolin bioleaching.

Kaolin	Fe_2O_3 (wt. %) before bioleaching	Fe_2O_3 (wt. %) after bioleaching
K1	0.92	0.53
K2	1.43	1.29
K3	0.69	0.55

Kaolin

Iron removal was investigated on three samples of kaolin raw material (K1, K2, K3) over 28 days of bioleaching (Tab. 2). The K1 sample of kaolin contains iron (0.92 wt.%), especially in the form of Fe hydroxides. The presence of Fe minerals was also identified by visible brown

colour of this material. However, the samples K2 and K3 contained iron, these materials were of white colour with high mica disseminations. Therefore it is suggested that substantial part of iron in the sample is bounded in the aluminosilicate lattice. The removal of structural Fe ions from K2 and K3 samples was not so efficient because only about 15–20 % of Fe_2O_3 was removed; however, from K1 sample 43 % of free iron was removed by bioleaching. The prolongation of bioleaching time from 1 month to 3 months and thus the longer production of organic acids and metal-complexing substances by *Bacillus* spp. caused the increase of iron removal from K3. After 3 months there was observed the 52 % extraction of Fe atoms from the octahedral position in mica, when Al removal was only about 2 % (Štyriaková et al., 2000).

The mica destruction was detected in kaolin and quartz sands samples by X-ray diffraction analysis and also by scanning electron microscopy (SEM). The SEM pictures show a different morphology in the boundary region of mica grains before and after the bioleaching (Fig. 4). The biological destruction of mica led to the development of illite, which was detected by energy-dispersion microanalysis (EDS). The illite development also caused the enrichment of the kaolin sample by fine-grained fraction. This effect is important for manufacturing of papier (Štyriaková et al., 2003c).

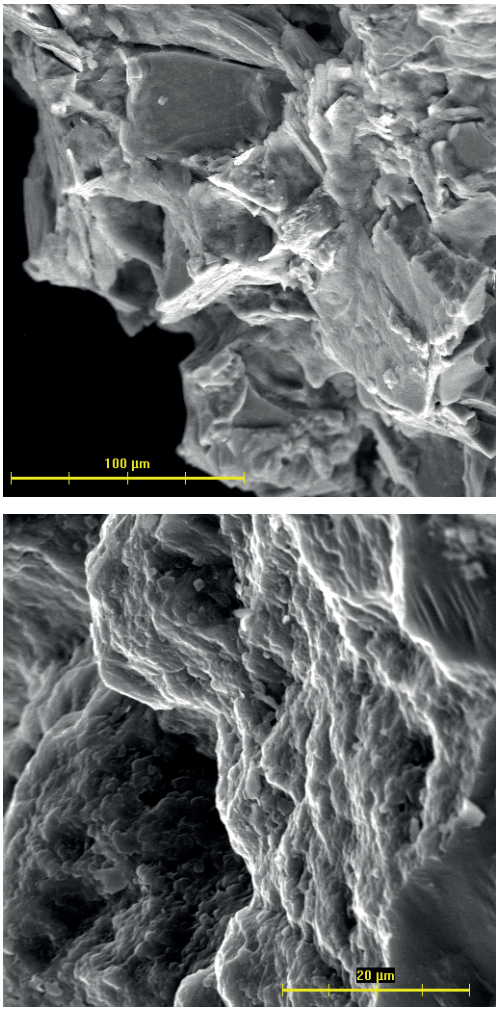

Fig. 4. SEM of border parts of mica before bioleaching (A) and after bioleaching (B).

The disordering of kaolinite structure has favourable effect on the iron removal, because the poorly ordered kaolinite sample KG2 provided better results in the iron extraction during the bioleaching (Mockovčiaková et al., 2008). The bioleaching did not cause significant changes in the major mineral compositions, but improved the degree of crystallinity.

More than 50 % of the iron impurities were removed from the china kaolin by bioleaching at a sugar concentration of around 5 % after 7 days of incubation. The increase of the whiteness index from 61 % to 82 % by bioleaching indicated that the quality of the kaolin sample was improved after the heating of bioleached sample to 1280 °C (Guo et al., 2010). In other study, the reduction of iron oxides contents, using the species *Aspergilus niger,* resulted in a removal of 43 % of Fe in the kaolin (Hosseini et al., 2007). The corresponding removal of iron was obtained also in the chemical leaching tests with 0.1 M oxalic acid at 100 °C for 90 min (Ambikadevi and Lalithambika, 2000).

The biobeneficiation methods, applied during the past two decades, were collected and divided into three categories, named as fungal leaching, bacterial leaching, and bioflocculation. Then, the last findings in each area were revealed, and the influence of effective parameters on both - the process efficiency and clay specifications - were described. Most of the involved studies have offered valuable knowledge about the technique, and have presented very promising results which are worthy of note and to continue in testing with a higher amount of material (Hosseini and Ahmadi, 2015).

Quartz sands

Naturally occurring quartz sands contain various iron and clay minerals, which are coating the quartz particles or impregnating the quartz surfaces. Three types of sand materials were used: (Q1) quartz sands; (Q2) kaolin sands and (Q3) glauconite sands. As can be seen from the results listed in Table 3, the extent of iron removal was the highest in sample Q1, where hematite covered quartz particles, than in the samples Q2 and Q3 with higher mica or glauconite contents. The 83 days lasting bacterial treatment resulted in a 60 %, 47 % and 30 % decrease of Fe content in Q1, Q2 and Q3 sample, respectively.

The sample Q3 is typically dominated by glauconite (10–12 %) over smectite (2–7 %). A part of glauconite has been removed by magnetic separation. Following the

bioleaching, the washing of Q3 resulted in up to 0.56 % decrease of Fe_2O_3 content in the sample Q3 with lower purification by bioleaching than in the sample Q1 or Q2 (Šuba and Štyriaková, 2015).

Tab. 3
Comparison of iron content before and after quartz sands bioleaching.

Quartz sands	Fe_2O_3 (wt. %) before bioleaching	Fe_2O_3 (wt. %) after bioleaching
Q1	0.32	0.13
Q2	0.36	0.19
Q3	1.03	0.72

The bioleaching processes in combination with other methods such as electromagnetic separation or elutriation can increase the iron removal from non-metallic raw materials, because the bioleaching is predominantly effective for the removal of surface layers of fine iron minerals. The lower depletion of iron in the sample Q2 due to the content of different mineral impurities was successfully treated with bioleaching and elutriation. In the process, poorly crystalline Fe-oxides, sealing siderite nodules, were released due to the bacterial action from the intergranular space of quartz sands. These Fe-oxides formed a fine-grained fraction with Fe-bearing minerals and the fine mica fraction, which were subsequently removed by elutriation process (Štyriaková et al., 2003a).

For the sample Q1, the bioleaching resulted in a 60 % decrease of the Fe content in the quartz sands and the subsequent two stages of magnetic separation decreased the Fe content in Fe_2O_3 from 0.13 % to 0.02 %. Thus the separated magnetic fraction was about 5 % from the untreated Q1 sample and 10 % from the bioleached sample (Štyriaková et al., 2007). Several experiments have recently confirmed that the bioleaching enhances the release of Fe minerals from silicate matrix and the yield of iron removal by magnetic separation.

The best leaching acid, used only in the chemical purification of iron impurities from the quartz sands, is H_3PO_4 under ultrasound irradiation, which can be compared with the other strong acids such as H_2SO_4, HCl and HF. The optimal leaching rate is up to 77 % at the temperature conditions of 80 °C, 10 % ratio of solid to liquid, and quartz sands size of 100 mesh for 120 min with ultrasound and conventional stirrings at 500 rpm (Zhang et al., 2012). The chemical purification with heating and stirring has increased the economic cost of the quality improvement process of non-metallic raw materials. The bioleaching process in combination with the physical processes (magnetic separation, elutriation, etc.) represents an alternative, eco-friendly and effective process for the purification of non-metallic raw materials.

The bioleaching running for three months makes the process less feasible than the chemical leaching. Application of the bioleaching would require much shorter duration - for example at least by 60 % for removal of Fe from the sample Q1. This is why the optimization applying AQDS, NTA, EDTA and other chelating agents proved to be useful. The addition of Na_2EDTA caused that the amount of totally dissolved iron was significantly higher than in case of other forms of chelators. NTA were partially less effective than Na_2EDTA in Fe dissolution from the samples, but more effective than Na_4EDTA or EDTA p.a. The changes in iron removal from the samples obtained during the laboratory bioleaching were used to assess the chelator effectiveness of the heterotrophic *in-situ* bioleaching process, because the bioleaching time was shorted from 4 months to 2.5 months in natural conditions (Štyriaková et al., 2010). Shelebolina (2004) stimulated iron-reducing bacteria by addition of the chelator, nitriloacetic acid (NTA), which was used to increase the bioavailability of Fe in clay and to intensify natural processes.

In-situ bioleaching

The laboratory experiments of quartz sand bioleaching were verified twice during the *in-situ* conditions in containers (Fig. 5A) without the using of big-bags in 2009 (Štyriaková et al., 2010) and second time in 2010 in containers, using the big-bags (Štyriaková et al., 2015), when the influence of unsterile climatic conditions and the application of big-bags was taken into consideration. The manipulation with quartz sands in big-bags was easier during the replacement of leachates for fresh medium. The composition of medium, its pH changes, oxygen concentration, presence of active bacterial species, granularity and the bounds of iron minerals, as well as the mineralogical composition of the industrial mineral, were the important factors of the *in-situ* bioleaching.

Under the first and second *in-situ* static bioleaching conditions, the initial oxygen content of 9–7 mg/l O_2 was consumed by microbial respiration to 0.09–0.08 mg/l O_2 within 6 days, indicating the formation of anaerobic environment. The value of the initial redox potential +180 mV decreased within 6 days to –150 mV, indicating the formation of reducing conditions. The bacterial growth has produced organic acids within 19 days of incubation of quartz sands in the presence of non-sterile bioleaching conditions, as the pH has decreased from 7 to 4. In leachates, the concentration of dissolved CO_2 was increased up to 730–1336 mg/l, because the heterotrophic bacteria fermented of organic source. The pH decrease was neutralized at each replacement of the medium. The temperatures of the media during the first bioleaching (June–August 2009) and the second bioleaching (July and September 2010), when the bioleaching was carried out, were reported in the range from 13 to 26 °C.

Application of a discontinuous process, in which the medium was exchanged after the maximum concentration of iron in solution had been reached, prevented the iron ions from the re-oxidation and precipitation. By this way there is possible to remove the iron from the quartz sand by *in-situ* bioleaching, though the negative effects of surrounding temperature changes and especially unsterile conditions must be eliminated by chemical additions. The investigation of the iron extraction concentration into liquid phase - the leachates - served especially for monitoring of bacterial activity and bioleaching time. The great volumes of leachates were changed in basins of a volume app. of 7000 l, but the exact measurements of solution exchanges were not performed. That is why the measurement of Fe_2O_3 concentration from the solid phase represented a conclusive background for the determination of the visual effect of bioleaching process (Fig. 5B).

The first and second bacterial pilot-plant bioleaching tests have decreased the iron content in Fe_2O_3 from 0.26 % to 0.13 %, being comparable with the results of laboratory bioleaching. The subsequent industrial magnetic separation decreased the Fe_2O_3 concentration to 0.08 %. The total decrease of iron content by up to 70 % was obtained under *in-situ* conditions. In the world, the pilot plant processes of quartz sands bioleaching were firstly held in Slovakia in 2009–2010.

Fig. 5. *In-situ* bioleaching in container (A) and the visual colour comparison of the heaps of industrially washed and bioleached quartz sands (B).

Conclusion

The naturally occurring non-metallic ores contain the unfavourable admixture of iron minerals, occurring in the form of coatings on grains or impregnations in the matrix. The study presents results of laboratory bioleaching of the non-metallic raw materials represented by feldspars, kaolin and quartz sands. The extent of iron removal was different and dependent on the mineralogy and distribution of iron in silicate matrix. The bioleaching process in iron removal has to be tested specifically at each type of non-metallic raw material, but the experimental treatment is needed to clarify the intensity of iron binding in different minerals and the feasibility to increase the bacterial iron removal by addition of nutrients and chelators. The laboratory experiments on iron removal were firstly verified twice during *in-situ* conditions on industrial mineral of quartz sands, taking the influence of unsterile climatic conditions into the consideration. The changes of medium pH, oxygen and glucose concentration, as well as bioleaching time represented the important factors during the iron removal in the *in-situ* bioleaching of the quartz sands. The bioleaching can be performed also on heaps, what is the future plan for development of this technology.

Acknowledgement

These works were supported by national projects from the Slovak Academy of Science under the contracts VEGA Nos. 2/5033/5 and 2/0109/11, as well as the Science and Technology Assistance Agency under the contracts Nos. APVV-0472-07 and APVT-51-006304. Authors express their thanks to Prof. Ivan Kraus and Dr. Z. Danková for improving the manuscript.

References

Ambikadevi, V. R. & Lalithambika, M., 2000: Effect of organic acids on ferric iron removal from iron-stained kaolinite. *Appl. Clay Sci., 16, 133 – 145.*

de Mesquita, L. M. S., Rodrigues, T. & Gomes, S. S., 1996: Bleaching of Brazilian kaolins using organic acids and fermented medium. *Miner. Engin., 9, 965 – 971.*

Eisele T. C. & Gabby, K. L., 2014: Review of reduction leaching of iron by anaerobic bacteria. *Mineral Processing & Extractive Metall. Rev., 35, 75 – 105.*

Hosseini, M. R. & Ahmadi, A., 2015. Biological benefication of kaolin: A review on iron removal. *App. Clay Sci., 107, 238 – 245.*

Jain, N., Sharma & D. K., 2004: Biohydrometallurgy for non-sulfidic minerals-a review. *Geomicrobiol. J., 21, 135 – 144.*

Mockovčiaková, A., Štyriaková, I., Škvarla, J. & Kozáková, I., 2008: Characterization of changes low and high defect kaolinite after bioleaching. *App. Clay Sci., 39, 202 – 207.*

Shelobolina, E. S., Anderson, R. T., Vodyanitskii, Y. N., Sivtsov, A. V., Yuretich, R. & Lovle, D. R., 2004: Importance of clay size minerals for Fe(III) respiration in a petroleum-contaminated aquifer. *Geobiology, 2, 67 – 76.*

Štyriaková, I., Štyriak, I. & Kušnierová, M., 1999: The release of sulphidic minerals from aluminosilicates by Bacillus strains. *Biohydrometallurgy and the environment toward the mining of the 21st century (Amils, R., Ballester, A., Eds.). Amsterdam, Elsevier, 587 – 596.*

Štyriaková, I., Štyriak, I., Kraus, I., Hradil, D., Grygar, T. & Bezdička, P., 2003a: Biodestruction and deferritization of quartz sands by Bacillus species. *Miner. Engin., 16, 709 – 713.*

Štyriaková, I., Štyriak, I., Galko, I., Hradil, D. & Bezdička, P., 2003b: The release of iron-bearing minerals and dissolution of feldspars by heterotrophic bacteria of Bacillus species. *Ceramics – Silikáty, 47, 20 – 26.*

Štyriaková, I., Štyriak, I., Nandakumar, M. P. & Mattiasson, B., 2003c: Bacterial destructon of mica during bioleaching of kaolin and quartz sands by Bacillus cereus. *World J. Microbiol. Biotechnol., 19, 583 – 590.*

Štyriaková, I., Bhatti, T. M., Bigham, J. M., Štyriak, I., Vuorinen, A. & Tuovinen, O. H., 2004: Weathering of phlogopite by Bacillus cereus and Acidithiobacillus ferrooxidans. *Can. J. Microbiol. 50, 213 – 219.*

Štyriaková, I., Štyriak, I., Malachovský, P. & Lovás, M., 2006a: Biological, chemical and electromagnetic treatment of three types of feldspar raw materials. *Miner. Engin., 19, 348 – 354.*

Štyriaková, I., Štyriak, I., Malachovský, P. & Hredzák, S., 2006b: Glass sand processing by biochemical leaching and magnetic separation. *Proceedings of XXIII International Mineral Processing Congress (G. Onal, N. Acarkan, M. S. Celik, F. Arslan, G. Atesok, A. Guney, A. A. Sirkeci, A. E. Yuce, K. T. Perek, Eds.), Vol. 2, Turkey, Istanbul, 933 – 938.*

Štyriaková, I., 2007a: Influence of chelators on iron solubilization from quartz and feldspars by bioleaching. *Advanced Material Research, 20 – 21, 87 – 90.*

Štyriaková, I., Štyriak, I. & Malachovský, P., 2007b: Nutrients enhancing the bacterial iron dissolution in the processing of feldspar raw materials. *Ceramics – Silikáty, 51, 202 – 209.*

Štyriaková, I., Štyriak, I., Malachovský, P., Večera, Z. & Koloušek, D., 2007c: Bacterial clay release and iron dissolution during the quality improvement of quartz sands. *Hydrometallurgy, 89, 99 – 103.*

Štyriaková, I., Jablonovská, K., Mockovčiaková, A., Bekéniyová, A., Štyriak, I., Kraus, I., Osacký, M. & Lovás, M., 2010: Dissolution of iron from quartz sands by basin bioleaching under static in-situ condition. *Hydrometallurgy, 104, 443 – 447.*

Štyriaková, I., Mockovčiaková, A., Štyriak, I., Kraus, I., Uhlík, P., Madejová, J. & Orolínová, Z., 2012: Bioleaching of clay and iron oxide coatings from quartz sands. *App. Clay Sci., 61, 1 – 7.*

Šuba, J. & Štyriaková, D., 2015: Iron minerals removal from different quartz sands. *Proc. Earth Planet. Sci., 15, 861 – 865.*

Veglio, F., 1997: Factorial experiments in the development of a kaolin bleaching process using thiourea in sulphuric acid solutions. *Hydrometallurgy, 45, 181 – 197.*

Zhang, Z., Li, J., Li, X., Huang H., Zhou, L. & Xiong, T., 2012: High efficiency iron removal from quartz sand using phosphoric acid. *Int. J. Mineral Processing, 114, 30 – 34.*

Zlepšovanie kvality nerudných surovín biolúhovaním

Proces biolúhovania patrí k nekonvenčným technológiám úpravy nerudných surovín, ktorý je možné využiť buď ako úpravu suroviny pred magnetickou separáciou na zvýšenie výťažnosti Fe, alebo ako samostatnú, 1 – 3-mesačnú úpravu nerudných surovín v procesoch diskontinuálneho statického lúhovania suroviny vo vodnom prostredí. Postupy biolúhovania boli odskúšané na troch typoch živcových surovín z lokalít Liešťany (F1), Vydrovo (F2) a Rudník (F3), na kaolínoch zo slovenských ložísk Horná Prievrana (K1), Vyšný Petrovec (K2) a Rudník (K3), ako aj na kremenných pieskoch ložísk Šaštín (Q1), Vyšný Petrovec (Q2) a Plachtince (Q3).

Pri prvom type granitoidnej horniny (F1) s obsahom živcov sa dosiahlo biologickým lúhovaním 35 % zníženie obsahu Fe, čo sa prejavilo viditeľnou zmenou belosti suroviny po tavení vzorky. Chemickým dolúhovaním vzorky s 0,1 M kyselinou oxálovou sa odstránilo ešte 6 % Fe. Nasledujúcou magnetickou separáciou uvoľnených častíc Fe minerálov, a hlavne sľúd po biologicko-chemickom lúhovaní F1, sa získala vysoko kvalitná surovina pre keramický priemysel s obsahom 0,046 % Fe_2O_3 s bielym výtavkom. Pri druhom type granitoidnej horniny (F2) sa kombinovaným biologicko-chemickým lúhovaním dosiahlo 25 % zníženie obsahu Fe, pričom magnetická separácia sa nerealizovala, pretože vzorka neobsahovala magnetické minerálne častice. Pri treťom type granitoidnej horniny (F3) sa biologické lúhovanie prejavilo 60 % znížením obsahu Fe v surovine. Organochemickým lúhovaním suroviny sa ešte odstránili 4 % Fe. Nasledujúcou magnetickou separáciou po biologicko-chemickom lúhovaní sa získala surovina s obsahom 0,061 % Fe_2O_3 a výtavky bielej farby, ktoré svedčia o vysokej kvalite suroviny po využití konvenčných a nekonvenčných spôsobov úpravy.

Pri biolúhovaní kaolínov bolo možné pozorovať aktivitu heterotrofných baktérií v deštrukcii sľúd a odstraňovaní železitých iónov z kryštálovej mriežky neusporiadaného kaolinitu. Z výsledkov biolúhovania kaolínov vyplynulo, že po mesačnom lúhovaní sú tieto baktérie schopné odstrániť 43 % voľného Fe obsiahnutého v amorfných formách oxyhydroxidov vzorky K1 a približne 10 % viazaného Fe v sľude po biolúhovaní kaolínov K2. Vzorka K1 s 0,92 % Fe_2O_3 mala červenú farbu, pretože obsaho-

vala voľné oxyhydroxidy Fe, ale vzorka K2 s obsahom 1,43 % Fe_2O_3 bola biela, pretože železo bolo viazané v sľudách. Amorfné formy Fe sú ľahšie extrahovateľné bakteriálnym lúhovaním ako viazané formy Fe v sľudách. V kaolínoch z Vyšného Petrovca (K2) sa pri predĺžení času lúhovania na 3 mesiace podarilo odstrániť 52 % viazaného Fe, pričom dochádzalo k deštrukcii sľúd a obohateniu vzorky o jemnozrnnejšie frakcie. Biotransformácia sľudy s fengitickým zložením na illit bola zachytená fotodokumentáciou rastrovacím elektrónovým mikroskopom s energiovo-disperznou analýzou po bakteriálnom lúhovaní separovaných vzoriek sľúd z ložiska Vyšný Petrovec. Ako je preukázané v publikáciách, baktérie druhov *Bacillus* spp. môžu znížiť obsah voľného Fe, ako aj viazaného Fe v sľude, ktorá má fengitické zloženie. Biologickým lúhovaním kaolínu z ložiska Rudník (K3) bolo možné znížiť obsah Fe_2O_3 približne o 20 % a pri kombinácii bakteriálneho lúhovania a magnetickej separácie bolo možné znížiť obsah Fe_2O_3 o 36 %, pričom vplyvom aktivity baktérií sa obohatila jemnozrnná frakcia a tým sa zvýšil index plasticity z 18 na 20 %.

Biolúhovaním kremenných pieskov ložiska Šaštín (Q1) v laboratórnych podmienkach sa odstránilo 60 % Fe a nasledujúcimi opakovanými laboratórnymi magnetickými separáciami sa zvýšilo celkové množstvo odstráneného železa z 0,13 na 0,02 % Fe_2O_3. REM odhalila nerovný povrch kremenných zŕn po bakteriálnom lúhovaní a EDS analýza potvrdila prítomnosť inklúzií ílových minerálov s obsahom Mg, Na a Fe, ktoré tvorili jemný povlak a impregnácie v kremennom matrixe. Baktérie svojou cielenou produkciou organických kyselín uvoľňovali ílové a železité minerály, pričom sa dosiahlo vybielenie povrchu kremenných častíc s formovaním jemnozrnnej frakcie. Röntgenovo-difrakčná analýza jemnozrnnej frakcie preukázala okrem hlavnej fázy kremeňa prítomnosť kaolinitu, smektitu a živcov. Z laboratórnych bakteriálne inokulovaných extrakčných štúdií po pridaní rozličných foriem chelátov EDTA (p. a., Na_4EDTA, Na_2EDTA), AQDS a NTA koncentrácia rozpusteného totálneho železa bola oveľa vyššia než biotická kontrola bez chelátov. To indikovalo, že železité minerály sa rýchlejšie bakteriálne rozkladali v prítomnosti chelátov. Pridanie Na_2EDTA však vykazovalo, že obsah totálne rozpusteného železa bol signifikantne vyšší než v prípade iných foriem chelatónov počas biolúhovania kremenných pieskov.

Potenciálna surovina kremenných pieskov z ložiska Vyšný Petrovec (Q2) po vyplavení ílových minerálov obsahovala železité minerály, ktoré zvyšovali koncentráciu železa v surovine. Technikou diskontinuálneho biolúhovania a plavenia bolo možné odstrániť podstatnú časť železitých minerálov. Hnedé minerálne zrná s veľkosťou 0,1 – 0,8 mm boli identifikované röntgenovo-difrakčnou analýzou, ktorá potvrdila polykomponentné minerálne zloženie vo forme sideritu, rutilu, anatasu, ferrihydritu a kaolinitu, s výnimkou kremeňa. Sideritové noduly sú cementované oxyhydroxidmi železa a tieto oxyhydroxidy tvoria aj povlaky na kremenných zrnách. V prvej fáze biolúhovania sa odstránili povlaky železitých minerálov z povrchu zŕn a v druhej fáze sa formovala hnedá jemnozrnná frakcia minerálnych častíc s veľkosťou menej ako 0,1 mm rozkladom sideritových nodúl s polykomponentným zložením. Táto jemnozrnná frakcia, ktorá obsahovala vysoký podiel železitých minerálnych častíc, bola odstránená z Q2 jednoduchým procesom plavenia. Biolúhovacie experimenty uskutočnené na kremenných pieskoch z ložiska Vyšný Petrovec potvrdili, že baktérie rodu *Bacillus* extrahujú Fe, Si a Al z kremenných pieskov a redukujú oxyhydroxidy Fe stmelené sideritom. Aplikáciou biologického lúhovania a plavenia bolo možné odstrániť 47 % Fe z kremenných pieskov, ktoré môžu slúžiť ako nerudná priemyselná surovina. Glaukonitický piesok (Q3) bol z pohľadu odstránenia železitých minerálov biolúhovaním najnevhodnejšou surovinou.

Kremenný piesok je potenciálna surovina pre sklársky priemysel, preto tieto laboratórne procesy biolúhovania boli prvýkrát overené v poloprevádzkových podmienkach Slovenska na kremennom piesku z ložiska Šaštín. Potvrdilo sa, že nesterilné podmienky *in-situ* nemali vplyv na dosiahnutie zhodného odstránenia nežiaducich povlakov železa ako v laboratórnych experimentoch. Dve veľkoobjemové nádrže (18 m^3) boli umiestnené v technologickom areáli LB MINERALS, a. s., každá nádrž bola naplnená 13 tonami priemyselne plaveného piesku v *big-bagoch*. V blízkosti bazénových nádrží boli umiestnené paletové nádrže potrebné na množenie a nasledujúcu inokuláciu baktérií a prípravu živných médií. Na_2EDTA bol v heterotrofnom biolúhovacom systéme najúčinnejší chelát, ktorý zamedzoval spätnú precipitáciu železa v roztoku. Potvrdilo sa to laboratórnymi prácami. V podmienkach *in-situ* bol proces odstraňovania železa z kremenných pieskov kombinovaný s prítomnosťou autochtónnych baktérií, ktorá nemala inhibičný vplyv na rozpúšťanie železa. Potvrdil to aj laboratórny test riedenia vzoriek autochtónnej kultúry.

Heterotrofné baktérie izolované z miest zvetrávania silikátových hornín a jazier produkujú organické kyseliny a siderofory v procesoch biolúhovania nerudných surovín. Je to spojené s rozpúšťaním jemných povlakov železa ako hlavnej nežiaducej prímesi týchto surovín. Proces biolúhovania prebieha v modifikovanom médiu s obsahom základných biogénnych prvkov, uhlíka a chelátov. Chemické dolúhovanie s 0,1 M kyselinou oxálovou sa môže uskutočniť v prípade, ak chceme skrátiť samotný proces biolúhovania. Magnetickú separáciu je možné využiť pred samotnou biologickou úpravou alebo po biologicko-chemickej úprave, ak surovina obsahuje vysoký podiel sľúd alebo samostatné odolné častice Fe-Ti minerálov.

Získané poznatky sú významné pri zlepšovaní kvalitatívnych vlastností tak živcov a kaolínov, ako aj kremenných pieskov používaných v keramickom a sklárskom priemysle. Reálne sa predpokladá, že využívanie bakteriálnej úpravy je v porovnaní s klasickými kombináciami technológií, magnetickou separáciou a flotáciou, ekonomicky a ekologicky výhodnejšie, a to najmä pri využití hnojív a odpadových nutričných zdrojov s obsahom uhlíka ako náhradného zdroja energie pre heterotrofné baktérie.

Doručené / Received: 24. 11. 2017
Prijaté na publikovanie / Accepted: 19. 12. 2017

Inštrukcie autorom

Etika publikovania, záväzná pri publikovaní v časopise Mineralia Slovaca: *www.geology.sk/new/mineralia_etika_publikovania*

1. Geovedný časopis Mineralia Slovaca publikuje scientometricky hodnotné recenzované pôvodné vedecké články s vysokým citačným potenciálom. V úvode príspevku musí autor jasne deklarovať, čím konkrétnym je jeho príspevok prínosný pre rozvoj geovied. Rešeršné štúdie sa publikujú len ojedinele.

2. Články na publikovanie (manuskripty) sa do redakcie zasielajú poštou (dva vytlačené exempláre a CD so všetkými súbormi v editovateľnej podobe) alebo e-mailom (editovateľné súbory a kompletná verzia vo formáte PDF).

3. Súčasne s článkom je potrebné redakcii poslať autorské vyhlásenie o originalite textu a obrázkov. Kópie obrázkov z iných publikácií musia byť legalizované získaním práva na publikovanie. Vyhlásenie musí obsahovať meno autora (autorov), akademický titul a trvalé bydlisko.

4. Rozsah manuskriptu na publikovanie je najviac 25 rukopisných strán (MS Word, Times New Roman, veľkosť písmen 12 bodov, riadkovanie 1,5) vrátane literatúry, obrázkov a vysvetliviek. V prípade veľkého odborného prínosu sú v ojedinelých prípadoch povolené aj dlhšie články.

5. Články sú publikované v angličtine alebo v slovenčine. Články v slovenčine musia obsahovať anglický preklad názvu, abstraktu, kľúčových slov, resumé a popisov k obrázkom a tabuľkám. Články písané v angličtine musia obsahovať slovenské resumé.

Text

1. Abstrakt stručne sumarizuje článok. Môže mať najviac 200 slov a nemá obsahovať citácie. Počet kľúčových slov je maximálne 6. Text má mať úvod, charakteristiku (stav) skúmaného problému, použitú metodiku, nové zistenia, ich interpretáciu, diskusiu, záver a zoznam literatúry. Východiskové údaje musia byť zreteľne odlíšené od interpretácií. V texte musia byť odvolávky na všetky použité obrázky a tabuľky.

2. Hierarchiu nadpisov v texte je potrebné vyznačiť ceruzkou na ľavom okraji strany manuskriptu: 1 – najvyššia, 2 – nižšia, 3 – najnižšia.

3. V texte sa uprednostňuje citácia v zátvorke, napr. (Dubčák, 1987; Hrubý et al., 1988), pred formou ... podľa Dubčáka (1987).

4. Pozícia obrázkov a tabuliek v texte sa označí. Nie je vhodné, aby text v editore MS Word obsahoval vložené obrázky, ale náhľadová verzia v pdf ich má obsahovať.

5. Grécke písmená treba identifikovať na ľavom okraji slovom (napr. sigma). Potrebné je odlišovať pomlčku od spojovníka. Symboly, matematické značky, názvy skamenelín a pod., ktoré sa majú vysádzať kurzívou, autor v rukopise podčiarkne vlnovkou.

Obrázky a tabuľky

1. Ilustrácie a tabuľky vysokej kvality bývajú publikované buď **na šírku stĺpca (81 mm), alebo strany (170 mm).** Optimálna veľkosť písma a čísiel v publikovaných obrázkoch je 2 mm. Články v slovenčine musia mať popisy v obrázkoch a tabuľkách v slovenčine, záhlavie tabuliek a texty pod obrázkami a tabuľkami sú v slovenčine a angličtine. Články v angličtine majú všetky texty v angličtine. **Maximálny rozmer ilustrácie a tabuľky vytlačený v časopise je 170 x 230 mm.** Väčšie (skladané) ilustrácie sú publikované len v ojedinelých prípadoch.

2. Pri počítačovej tvorbe obrázkov odporúčame používať programy s vektorovým zobrazením (Corel Draw, Adobe Illustrator a pod.). Čiary tzv. vlasovej hrúbky, softvérová alebo rastrová výplň plôch (napr. v Corel Draw) nie sú prípustné. Výplne v obrázkoch musia pozostávať zo samostatne vysádzaných objektov.

3. Ilustrácie vrátane fotografií musia obsahovať **grafickú mierku** v centimetrovej či metrovej škále, prípadne sa rozmer zobrazených objektov vyjadrí v popise obrázka. Mapy a profily musia mať aj **azimutálnu orientáciu** a jednotné vysvetlivky, ktoré sa uvedú pri prvom obrázku. Zoskupené obrázky, napr. fotografie a diagramy, sa uvádzajú ako jeden obrázok s jednotlivými časťami označenými písmenami (a, b, c atď.).

4. Pri zasielaní fotografií vo forme počítačových súborov (formáty JPG alebo TIF) sa požaduje rozlíšenie minimálne 600 DPI. Publikovanie farebných ilustrácií môže byť spoplatnené.

Literatúra

1. Minimálne 50 % citácií musí reprezentovať publikácie od roku 2000. V zozname literatúry sa v abecednom poradí uvádza len literatúra citovaná v danom článku.

2. Spôsob uvádzania literatúry v zozname literatúry

Knižná publikácia: Gazda, L. & Čech, M., 1988: Paleozoikum medzevského príkrovu. *Bratislava, Alfa, 155 s.*

Časopis: Vrba, P., 1989: Strižné zóny v metapelitoch. *Miner. Slov., 21, 135 – 142.*

Zborník: Návesný, D., 1987: Vysokodraselné ryolity. *In: Romanov, V. (ed.): Stratiformné ložiská gemerika. Špec. publ. Košice, Slov. geol. spol., 203 – 215.*

Manuskript: Radvanský, F., Slivka, B., Viktor, J. & Srnka, T., 1985: Žilné ložiská jedľoveckého príkrovu gemerika. Záverečná správa z úlohy SGR--geofyzika. *Manuskript. Spišská Nová Ves, archív Št. Geol. Úst. D. Štúra, 28 s.*

3. Pri článku viac ako dvoch autorov sa v texte cituje iba prvý autor s dodatkom et al., ale v zozname literatúry sa uvádzajú všetci.

Instructions to authors

Publication ethics, being obligatory for publishing in the journal Mineralia Slovaca: *www.geology.sk/new/mineralia_publikation_ethics*

1. Geoscientific journal Mineralia Slovaca publishes scientometrically valuable original peer-reviewed scientific articles with a high citation potential. In the introduction of each article the author(s) must clearly declare, which innovative data the paper brings for the development of geosciences. The retrieval studies are published only exceptionally.

2. The articles for publishing (manuscripts) must be sent to Editorial Office by post (two printed copies and CD with editable files), or by e-mail (editable files plus complete preview version in PDF format).

3. Simultaneously with the article the Editorial Office must receive the author´s proclamation that no part of the manuscript was already published and figures and tables are original as well. Copied illustrations from other publications must contain a copyright.

4. The extent of the manuscript for publishing is limited to 25 manuscript pages (MS Word, 12 points Times New Roman, line spacing 1.5) including figures, tables, explanations and references. In the case of contribution with a high scientific value, the longer manuscripts for publishing are exceptionally permitted.

5. Articles can be published in Slovak or English languages. The title, abstract, key words, shortened text (resumé), as well as description to figures and tables in Slovak articles are published also in English. Articles published in English contain Slovak resumé.

Text

1. Abstract briefly summarizing the article is limited to 200 words, no references are allowed. The maximum number of key words is 6. Text of the article has to contain the introduction, characterization (state) of investigated problem, applied methodology, obtained new data, discussion, conclusion and references. The obtained data must be distinctly separated from interpretations. All applied figures and tables must be referred in the text.

2. The hierarchy of headings in the manuscript must be indicated by a pencil note: 1 – highest level, 2 – lower, 3 – lowermost level.

3. The references in the text prefer parentheses, e.g. (Dubčák, 1987; Hrubý et al., 1988). The form "according to Dubčák (1987)" should be used only exceptionally.

4. Position of figures and tables must be indicated in the manuscript. Editable text of manuscript sent to editorial office must be without figures and tables, though the preview PDF has to contain them in a correct position.

5. Greek letter in the text must be identified at the left margin of the text (e.g. sigma). The text should strictly distinguish the dash from hyphen. Symbols, mathematic signs, names of fossils, etc., which should be printed in italics, must be underlined by the wavy line in the manuscript.

Figures and tables

1. The high quality figures and tables can be published either in **maximum width of column (81 mm) or page (170 mm).** The optimum size of letters and numbers in the camera-ready figure is 2 mm. Articles published in Slovak contain the Slovak descriptions in figures and tables, the tables headings and descriptions beneath figures and tables are in Slovak and English. English articles contain all texts in English. **Maximum dimension of figures and tables in the journal is 170 x 230 mm. Larger (fanfolded)** illustrations are published only exceptionally.

2. For figures drawing the editorial office recommends the vector graphics editors (Corel Draw, Adobe Illustrator, etc.). The very thin lines (hair lines), the pre-defined software or raster fillings of polygons (e.g. in Corel Draw) are not allowed. The filling must consist from separately set objects.

3. Each illustration including photographs must contain graphic (metric) scale, eventually the dimensions of visualized objects have to be stated in the describing text to figure. Maps and profiles must contain also the azimuth orientation, their detail explanations are stated at the first figure. Grouped figures, e.g. photographs and diagrams, are compiled as one figure with separate parts designated by letters (a, b, c, etc.).

4. The photographs sent as JPG of TIF files are required for having minimum 600 DPI resolution. Publishing of colour illustrations can be charged by a fee.

References

1. Minimum 50 % of referred works must represent contemporary publications after 2000. The references in alphanumeric order encompass only literature cited in the article.

2. Examples of referring:

Book: Gazda, L. & Čech, M., 1988: Paleozoic of the Medzev nappe. *Bratislava, Alfa, 155 p.*

Journal: Vrba, P., 1989: Shear zones in the metapelite complexes. *Miner. Slov., 21, 135–142.*

Anniversary volume: Návesný, D., 1987: High-potassium rhyolites. *In: Romanov, V. (ed.): Stratiform deposits of Gemericum. Spec. publ. Košice, Slov. geol. soc., 203–215.*

Manuscript: Radvanský, F., Slivka, B., Viktor, J. & Srnka, T., 1985: Vein deposits of the Jedľovec nappe of Gemericum. Final report from the project SGR-geophysics. *Manuscript. Spišská Nová Ves, Archive Št. Geol. Úst. D. Štúra, 28 p.*

3. The article with more than two authors is referred by the name of the first author with the amendment et al., but the list of references contains names of all authors.

Ďalšie informácie/Further information: mineralia.slovaca@geology.sk; zoltan.nemeth@geology.sk

OBSAH – CONTENT

PÔVODNÉ ČLÁNKY – ORIGINAL PAPERS

Dyda, M., Ružička, P. & Hain, M.
Crystal size distribution (CSD) of titanite inclusions in grossular from a calc-silicate rock in the Malé Karpaty Mts., Slovakia
Distribúcia kryštálových veľkostí (CSD) titanitových inklúzií v grosulári z vápenato-silikátovej horniny Malých Karpát, Slovensko

Kováčik, M. & Olšavský, M.
Obliakový materiál vrchnopaleozoických sedimentov hronika v Malých Karpatoch: petrogenetické a provenienčné otázky
Pebble-material of Hronic Upper Paleozoic sediments in the Malé Karpaty Mts. (Western Carpathians): petrogenetic and provenance aspects

Žecová, K.
Paleoecology of calcareous nannofossils from Paleogene formations of the Magura Unit in the Western Carpathians
Paleoekológia vápnitých nanofosílií z paleogénnych súvrství magurskej jednotky Západných Karpát

Gaál, Ľ., Németh, Z., Bella, P. & Koděra, P.
Caves in magnesite – a rare phenomenon of karstification: The case study from Slovakia
Jaskyne v magnezitoch – vzácny fenomén krasovatenia: príkladová štúdia zo Slovenska

Polák, Ľ., Vlasáč, J., Vrtiška, L. & Mikuš, T.
Cryptomelane, $K(Mn^{4+}_7Mn^{3+})O_{16}$, from the Dúbravica-Zolnica Fe deposit (North Veporic Unit, Slovak Republic)
Kryptomelán $K(Mn^{4+}_7Mn^{3+})O_{16}$ z Fe ložiska Dúbravica-Zolnica (severné veporikum)

Štyriaková, I., Bekéniová, A. & Štyriaková, D.
The quality improvement of non-metallic raw materials by bioleaching
Zlepšovanie kvality nerudných surovín biolúhovaním

Indexed / Abstracted / Accessed by SCOPUS and EBSCO
Indexované / abstraktované / sprístupňované databázami SCOPUS a EBSCO

www.geology.sk/mineralia